Application-oriented approaches to modeling and satellite-based monitoring of watershed sediment dynamics

Claire Beveridge

A dissertation

submitted in partial fulfillment of the

requirements for the degree of

Doctor of Philosophy

University of Washington

2020

Reading Committee:

Faisal Hossain, Chair

Alexander R. Horner-Devine

David Butman

Program Authorized to Offer Degree:

Civil & Environmental Engineering

University of Washington

Abstract

Application-oriented approaches to modeling and satellite-based monitoring of watershed sediment dynamics

Claire Beveridge

Chair of the Supervisory Committee:
Professor Faisal Hossain
Civil & Environmental Engineering

Global river sediment dynamics are dramatically being altered by humans in various ways, such as dam-building, deforestation, mining, and climate change. This is having major impacts on the environment and society, as sediment is vitally interconnected with water, food, energy, and ecological systems. In-situ monitoring of sediment is challenging and sediment data records are highly limited, especially in developing countries. Computational modeling and satellite remote sensing can support sediment management needs by providing sediment-related information at broad spatial and temporal scales. Considering this, researchers are frequently developing "use-inspired" tools and approaches for the modeling and monitoring of sediment dynamics, and the environment more broadly. However, use-inspired research does not always go on to become "user-ready," or directly integrated into societal application. This is largely because engagement between researchers and stakeholders is lacking. The main objective of this dissertation is to

assess how sediment dynamics research approaches of computational modeling and satellite remote sensing can be more effectively oriented towards watershed planning, management, engineering, and decision-making. First, a unique, interdisciplinary modeling approach was developed, combining state-of-the-art hydrologic and sediment transport modeling research methods. The model was tested in the Elwha River basin upstream of a former dam. The model produced accurate lifetime reservoir sedimentation volume estimates and other management-related outputs. Second, satellite remote sensing data was used to quantify changes in suspended sediment concentration (SSC) patterns due to widespread dam development in the 3S tributaries of the Mekong River Basin. Satellite data on nighttime lights and land cover helped to better explain SSC patterns. The capacities and limitations of satellite remote sensing to support sediment management were explored. Finally, a cloud-based, satellite remote sensing tool for monitoring SSC was co-developed with the Bangladesh Water Development Board. The aim of the tool was to support management of widespread riverbank erosion and riverbed accretion. The key strengths, weaknesses, and lessons learned in the stakeholder engagement process were highlighted. The two foundational strengths were a long-standing researcher-stakeholder partnership and stakeholder leadership. Overall, this dissertation demonstrates how to take sediment dynamics research tools from use-inspired to user-ready so that they effectively support growing societal needs.

TABLE OF CONTENTS

LIST OF FIGURES

LIST OF TABLES

ACKNOWLEDGEMENTS

I thank my advisor, Professor Faisal Hossain, for his strong mentorship and for his constant enthusiastic inspiration to cross the last mile and make an impact on the world. I thank Professor Erkan Istanbulluoglu for his strong mentorship and for his inspiration to think deeply and innovatively about addressing societal challenges. I'm grateful for how Erkan and Faisal pushed me beyond my intellectual comfort zone and always put their students first.

I thank my reading committee, Professor Alex Horner-Devine and Professor David Butman for their thoughtful and constructive feedback, refreshing encouragement, and generous time commitment. I thank my Graduate School Representative Professor Alison Duvall for her kind enthusiasm and generous time commitment.

I thank the current and former members of the SASWE and Watershed Dynamics Research groups. They have become like family, and always brought boundless support, creative ideas, and bright joy to our countless working hours together. I also thank the Hydrology & Hydrodynamics graduate students and Freshwater Initiative leaders for being amazing, encouraging, and energizing communities that always broadened my horizons.

I thank the Bangladesh Water Development Board for making Chapter 4 of this dissertation possible. Being able to collaborate with them was a dream come true. Their generosity, enthusiasm, support, and hospitality go unmatched.

I thank my mother, father, sister, and brother for their unwavering love, support, joy, and reminder of who I am. They are my greatest blessings and have been there for every one of life's mountaintops, low valleys, and wild paths in between. I also thank countless other family members, friends, professors, mentors, and peers/colleagues that have graciously supported me along the paths that got me to and through graduate school.

Above all, I give thanks and praise to my Lord Jesus Christ for the graces I received to accomplish this dissertation, and for the beauty of the journey.

I thank the following funding institutions for making this work possible:

- National Science Foundation (NSF) Graduate Research Fellowship Program– 3 years (Grant No. DGE-1762114).
- Office of Energy Efficiency and Renewable Energy, U.S. Department of Energy and the Hydropower Foundation (Award Number DE-EE0006506) – 2 quarters
- Department of the Interior Northwest Climate Adaptation Science Center- 2 quarters
- University of Washington (UW) Charles V. Tom and Jean C. Gibbs Endowed Presidential Fellowship in Environmental Engineering– 1 year
- UW Golder Fellowship, NASA Water Applied Science Program (grant NNX15AC63G), and Bangladesh Water Development Board –Bangladesh trip support

At the time of writing this, Chapter 2 has been published in *Journal of Advances in Modeling Earth System*, Chapter 3 has been published in *Journal of Hydrologic Engineering*, and Chapter 4 has been accepted and forthcoming in *Environmental Modelling and Software*. These chapters are:

Chapter 2:
Beveridge, C., Istanbulluoglu, E., Bandaragoda, C., & Pfeiffer, A. M. (2020). A Channel Network Model for Sediment Dynamics Over Watershed Management Time Scales. *Journal of Advances in Modeling Earth Systems*, 12(6), 1–29. https://doi.org/10.1029/2019ms001852

Chapter 3:
Beveridge, C., Hossain, F., & Bonnema, M. (2020). Estimating Impacts of Dam Development and Landscape Changes on Suspended Sediment Concentrations in the Mekong River Basin's 3S Tributaries. *Journal of Hydrologic Engineering*, 25(7), 1–14. https://doi.org/10.1061/(ASCE)HE.1943-5584.0001949

Chapter 4:
Beveridge, C., Hossain, F., Biswas, R. K., Haque, A. A., Ahmad, S. K., Biswas, N. K., Hossain, M. A., Bhuyan, M. A. (2020). Stakeholder-driven development of a cloud-based, satellite remote sensing tool to monitor suspended sediment concentrations in major Bangladesh rivers. *Environmental Modelling and Software*.

DEDICATION

For:

The people of Bangladesh whose livelihoods are impacted by riverbank erosion

&

The people of the Mekong River Basin whose livelihoods are impacted by ongoing dam development

&

The Lower Elwha Klallam Tribe whose livelihoods have been impacted by the Elwha dams

Chapter 1. INTRODUCTION

1.1 CHANGING RIVER SEDIMENT DYNAMICS

While human-induced global warming is a frequent topic of government discussions and media headlines, a broader yet under-appreciated human impact is that on global sediment fluxes (Syvitski & Kettner, 2011). Human activities such as deforestation, urbanization, agricultural development, and mining have increased sediment erosion and loads to streams by ~15% compared to pre-human levels. Simultaneously, ~25-30% of global sediment discharge is trapped in reservoirs, resulting a net reduction of sediment flux to the ocean (Syvitski, Vorosmarty, Kettner, & Green, 2005; Vörösmarty et al., 2003). However, these percentages were estimated over a decade ago, and in the past five to ten years have grown (Li et al., 2020). Human impacts are largely distributed in time and space due to different environmental settings and patterns of landscape development and dam implementation. With the expected ongoing dam construction and landscape development, the human imprint on sediment will only continue to increase (Dunn et al., 2019). Furthermore, climate change impacts such as melting glaciers, declining snowpack, and increasing extreme events (e.g., floods, droughts, landslides) are also changing the timing, size, and character (e.g., grain sizes) of river sediment loads.

These dramatic changes in sediment have major impacts on the environment and society, as sediment is significantly interconnected with water, food, energy, and ecological systems. Sediment forms and stabilizes riverbanks, floodplains, and deltas, where there are often fragile ecosystems and large human populations. Sediment provides vital aquatic habitat that supports biodiversity. Sediment transports nutrients that sustain fisheries and agriculture, which human livelihoods depend on. Thus, retention of sediment behind dams degrades downstream ecological

habitat, agriculture, and fisheries. It also leads to subsidence of deltas, which are already sinking due to sea level rise. Additionally, reservoir sedimentation decreases hydropower efficiency and dam lifespan, safety, and overall cost-effectiveness. Increased sediment loading from human activities and climate change can cause riverbed sediment accretion which can then lead to major flooding and riverbank erosion. This can further cause infrastructure damage, interrupt economic productivity, and put human lives and safety at risk. Sediment loading of unnatural volumes and grain sizes can also have adverse impacts on fisheries. Increased sediment loads and potential pollutants carried by human-impacted sediments can also degrade water quality and exceed water treatment system capacities.

Human impacts on sediment are posing a particular risk in economically-developing countries, where dam construction (Zarfl, Lumsdon, & Tockner, 2015) and landscape development are, generally, rapidly increasing. This has been evidenced by significant increases and decreases in suspended sediment loads of major rivers in developing countries (Li et al., 2020). In these countries, large populations live near water bodies are at heightened risk to reservoir sediment trapping, erosion, flooding, and water quality impacts. The livelihoods of these populations are also often directly tied to farming and/or fishing. Despite the vulnerability of these populations, they typically have little say in or gain from the dam and landscape development activities.

1.2 River sediment monitoring and modeling approaches

Along with the complications of anthropogenic impacts, there are inherent complexities in the monitoring, modeling, and understanding of sediment dynamics. Sediment dynamics entail supply, transport, and storage processes and feedbacks which are nonlinear, episodic, and often occurring over complex terrains (Wohl et al., 2015). The sediment yield at a single location and

moment integrates physical processes occurring over a broad range of spatial scales (e.g., grain-scale interactions on a channel bed; sediment production at the hillslope scale) and temporal scales (e.g., tectonics at millennial scale; river sediment storage at seasonal scale). Hence, research relating to sediment dynamics consists of diverse scientific and engineering fields that analyze Earth systems on different spatial and temporal scales, such as geology, fluid mechanics, and water resources engineering. The research aims, approaches, and spatial and temporal scales of interest of these research fields do not always synergize with each other nor with water resources managers and decision-makers.

What further inhibits understanding of sediment dynamics is the limited accessibility and consistency of in situ sediment monitoring records. Less than 10% of the world's rivers have openly available sediment data (Syvitski, 2003). In the USA, where there are over 23,000 US Geological Survey gaging stations, only 1,640 sites (<8%) have over 10 years of suspended sediment concentration (SSC) data and 9 sites (<1%) have over 50 years of data (Wohl et al., 2015). In developing nations, suspended sediment records are often less common and held proprietary by stakeholders (Syvitski, 2003; D. E. Walling & Fang, 2003). Bedload measurements throughout the world are rare. Furthermore, different in situ monitoring methods are used in different places which makes comparison between global river basins challenging. Reasons for these sediment monitoring limitations are that in situ sediment sampling is time-consuming, expensive, complicated, and can be difficult in terms of when (e.g., during floods) and where (e.g., remote alpine areas) sampling can be conducted. Even at locations where long records of sediment data are available, it is often unreasonable to extrapolate beyond the time and location a sample is collected considering the variability of sediment supply and transport dynamics in watershed.

With these deficiencies of in situ sediment monitoring, the understanding and management of sediment dynamics can be largely supported by computational modeling and satellite remote sensing. Modeling and satellite remote sensing can provide sediment predictions at broad spatial and temporal scales, which supports watershed sediment planning, management, engineering, and decision-making. Modeling and satellite remote sensing also can help to determine how and to what extent humans are influencing the natural sediment flow regime in a watershed. This is critical for determining how to locally manage infrastructure and natural resources in ways that minimize adverse impacts on the environment and society (e.g., conducting reservoir sediment flushing similar to natural sediment flow patterns). Technological advancements such as cloud-based, high-performance computing and big data storage enhance the accessibility of sediment models and satellite remote sensing.

Computational models integrate and simulate the theoretical physical processes, interactions, and feedbacks that govern sediment dynamics across a watershed. Of strong relevance to management are "source-to-sink" sediment models which integrate sediment storage, transport, and storage dynamics throughout a watershed. These models can provide spatially distributed, short-and long-term projections of sediment yields at high resolutions. Thus, source-to-sink models allow for holistic understanding of watershed processes and sediment yields and can support management needs (e.g., predicting reservoir sedimentation, guiding stream restoration). A challenge with watershed sediment models is that they often have significant input data and computational requirements, which, as previously mentioned, can be highly limited, especially in developing nations and other resource-limited regions.

While computational models can simulate and predict watershed processes, earth-observing satellites can monitor what is actually occurring in the interconnected environmental

and human systems over broad spatial and temporal scales. There is a diversity of freely-available satellite-derived data products that are relevant to watershed sediment dynamics. For example, satellites can monitor precipitation, land use/land cover, river planform, SSC, and delta extent. Records can extend as far back as multiple decades, and thus can fill gaps in which on-the-ground observations were not recorded. This is especially valuable in transboundary watersheds where environmental data sharing and communication on water resource management are limited. Satellite remote sensing products are also often available on a short turnaround from acquisition, which supports prompt decision-making. Satellite remote sensing products are becoming more accessible by cloud-based platforms that allow for satellite data acquisition and high performance computation at no or limited costs to end-users (e.g., Google Earth Engine, Planet). Satellite-based observations related to sediment and water quality will become more available with proposed satellite missions (e.g., SWOT, ECOSTRESS). With the abundance of data consistently being measured across the globe, satellite remote sensing directly helps to overcome limitations of in situ monitoring and modeling. Satellite observations also help to holistically understand the dynamic, increasing impacts that humans are having on sediment dynamics, which models can rarely predict, and point in situ sediment measurements cannot fully reveal.

1.3 ENVIRONMENTAL RESEARCH AND SOCIETY

Clearly, the technologies of computational modeling and satellite remote sensing offer promising opportunities to support sediment management in the face of growing global challenges. Considering this, researchers are frequently developing “use-inspired” tools and approaches for the modeling and monitoring of sediment dynamics and, more broadly, the environment. This use-inspired research integrates innovative science, engineering, and technology to address

socially-relevant questions. The outcomes are often scientifically-sound strategies to improve environmental planning, management, engineering, and decision-making. However, use-inspired research does not always go on to become "user-ready," or directly integrated into societal application and decision-making (Hossain, 2015; Hossain et al., 2014c; McIntosh et al., 2011; Prados et al., 2019). This situation is analogous to two standalone mountains, one symbolizing research and the other symbolizing society. In between the mountains is a desolate "valley of death" (National Research Council, 2000), as research outcomes often perish before making it to society for uptake (Figure 1.1). The crux is that research tools cannot cross the valley and go from use-inspired to user-ready on their own. Researchers must take their innovations, descend from their mountain, and journey across the valley with stakeholders.

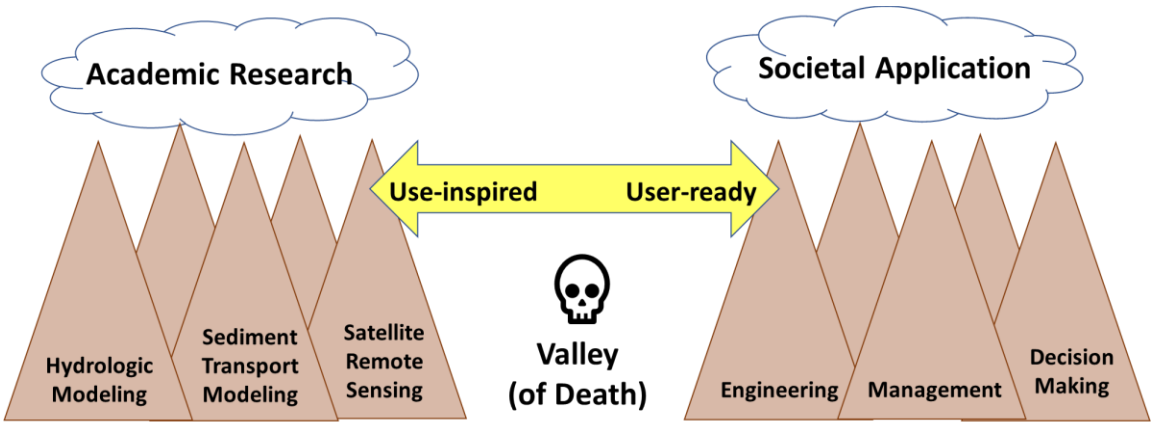

Figure 1.1. Analogy for disconnection between research and society

However, stakeholder engagement has not traditionally been considered a responsibility of science and engineering researchers. Thus, researchers rarely have the training and incentive to take this step. Researchers are typically highly specialized in a certain field of science or engineering, are rigorously trained to use the scientific method, and driven to advance their career by publishing journal articles. While these facets are undoubtedly important, stakeholder engagement goes far beyond them. It entails effectively co-developing and transferring a locally-

relevant and management-oriented tool that stakeholders can own and build long-term capacity from. The needs, constraints, and capacities of stakeholders are not just in the science and engineering realms, but formed by—and is sometimes overwhelmingly driven by– the complexities of politics, power, economics, and culture. Researchers are often disconnected from these broader realities in conducting use-inspired research. Furthermore, researchers often develop use-inspired tools that are far from user-friendly, and accessible only to others that share their high degree of specialization, which excludes most stakeholders.

Despite these reasons for the persistent valley of death, there are promising opportunities to bring the valley into life. Interdisciplinary, socially-relevant, public participatory, and policy-oriented environmental research is a growing emphasis of research institutions. The US Senate recently proposed the "Economic Frontier Act" which would support technology transfer from research to society (Gwynne, 2020). The world is becoming increasingly connected, allowing researchers and stakeholders to easily collaborate from across the world. Barriers to high performance computing as well as data access and sharing are being lowered with the development of cloud computing and storage. Earth observing satellites continue to be launched which collected a plethora of data that is becoming increasingly accessible with web-based platforms. The opportunities can bear fruit however must be intentionally and properly oriented to take research from use-inspired to user-ready.

1.4 RESEARCH OBJECTIVES

The main objective of this dissertation is to assess how research approaches to understanding watershed sediment dynamics—particularly computational modeling and satellite remote sensing—can be more effectively oriented towards watershed planning, management, engineering, and decision-making. This objective is explored from two

interconnected perspectives: One is a scientific and computational perspective of integrating research approaches and developing tools. The other is a stakeholder engagement perspective of transferring tools and technologies to end-users. Specific objectives are:

Develop and test a watershed network model for predicting sediment yields at time and space scales relevant to watershed planning and management in the Elwha River Basin.

Apply satellite remote sensing techniques to analyze the impacts of dam development and landscapes changes on SSC in the 3S tributaries of the Mekong River Basin.

With stakeholders, co-develop a cloud-based, satellite remote sensing tool to monitor SSC and support engineering and management of river erosion and accretion in major Bangladesh rivers.

1.5 APPROACH

These objectives are addressed in three core chapters. **Chapter 2** (published as Beveridge, Istanbulluoglu, Bandaragoda, & Pfeiffer, 2020) describes the development and application of a mountainous watershed network model for estimating source-to-sink sediment dynamics. The model combined state-of-the-art interdisciplinary research approaches, such as forcing from a physically-based hydrologic model. The sediment model was demonstrated in the Elwha River Basin of Washington, upstream of the former Glines Canyon dam. The model was evaluated based on its ability to predict the known volume of sediment that accumulated in the dam over its lifespan. Chapter 2 highlights the theoretical and computational advancements needed for network sediment models to better address societal needs. **Chapter 3** (published as Beveridge, Hossain, and Bonnema 2020), evaluates using long-term satellite remote sensing records to monitor seasonal changes in river SSC patterns due to widespread dam implementation and landscape changes. The study was conducted in 3S tributaries of the Mekong River Basin, where rapid dam development has been occurring over the past two decades and is expected to

continue. Chapter 3 gives practical insights on the capacity of satellite remote sensing to capture rapidly evolving human impacts on watershed sediment dynamics, which is particularly valuable in transboundary and resource-limited nations. **Chapter 4** (in review as Beveridge, Hossain, Biswas, et al., 2020) describes stakeholder-driven development of a cloud-based, satellite remote sensing tool for monitoring SSC of major water bodies in Bangladesh. The study was conducted in collaboration with the Bangladesh Water Development Board, which is interested in using this system to support engineering and management of river erosion and accretion. Chapter 4 highlights the key strengths, weaknesses, and lessons learned in the stakeholder engagement process, particularly to support early-career researchers in conducting user-ready research. **Chapter 5** concludes this dissertation.

Chapter 2. A CHANNNEL NETWORK MODEL FOR SEDIMENT DYNAMICS OVER WATERSHED MANAGEMENT TIME SCALES

Note: This chapter has been published mostly in its current form in the *Journal of Advances in Modeling Earth Systems* (Beveridge, Istanbulluoglu, et al., 2020).

Abstract: A mountain watershed network model is presented for use in decadal to centurial estimation of source-to-sink sediment dynamics. The model requires limited input parameters and can be effectively applied over spatial scales relevant to management of reservoirs, lakes, streams, and watersheds (1-100 km^2). The model operates over a connected stream network of Strahler-ordered segments. The model is driven by streamflow from a physically-based hydrology model and hillslope sediment supply from a stochastic mass wasting algorithm. For each daily time step, segment-scale sediment mass balance is computed using bedload and suspended load transport equations. Sediment transport is partitioned between grain size fractions for bedload as gravel and sand, and for suspended load as sand and mud. Bedload and suspended load can deposit and re-entrain at each segment. We demonstrated the model in the Elwha River Basin, upstream of the former Glines Canyon dam, over the dam's historic 84-year lifespan. The model predicted the lifetime reservoir sedimentation volume within the uncertainty range of the measured volume (13.7-18.5 million m^3) for 25 of 28 model instances. Gravel, sand, and mud fraction volumes were predicted within measurement uncertainty ranges for 18 model instances. The network model improved the prediction of sediment yields compared to at-a-station sediment transport capacity relations. The network model also provided spatially and temporally distributed information that allowed for inquiry and understanding of the physical

system beyond the sediment yields at the outlet. This work advances cross-disciplinary and application-oriented watershed sediment yield modeling approaches.

2.1 INTRODUCTION

In September 2014, the largest dam removal in history was completed with the removal of two dams along the Elwha River, located in Washington State's Olympic National Park (Figure 2.1). This historic record was attributed, in part, to the combined volume of sediment impounded behind the two dams, ~21 million m^3 (Magirl et al., 2015; Randle, Bountry, Ritchie, & Wille, 2015). The massive volume of sediment to be released upon dam removal posed major challenges to the removal strategy and uncertainties in the future ecosystem recovery. The scrutiny of reservoir sediment impacts in the Elwha watershed (e.g., Downs et al., 2009; Randle et al., 2015; J. A. Warrick et al., 2015) illuminates how critical sediment management is in all phases of a dam's life-cycle —design, construction, operations and maintenance, and removal. In each stage, miscalculating reservoir sediment yields can have dramatic consequences on a system's storage capacity, hydropower production, operations, maintenance, costs, safety, and ecosystem impacts. However, most methods used in dam planning and operations do not adequately represent the complex sediment dynamics of river and reservoir systems (United States Society on Dams, 2015). Existing methods are especially deficient in steep mountainous regions, where a large portion of global hydropower dams are existing or planned (Lehner et al., 2011; Zarfl et al., 2015).

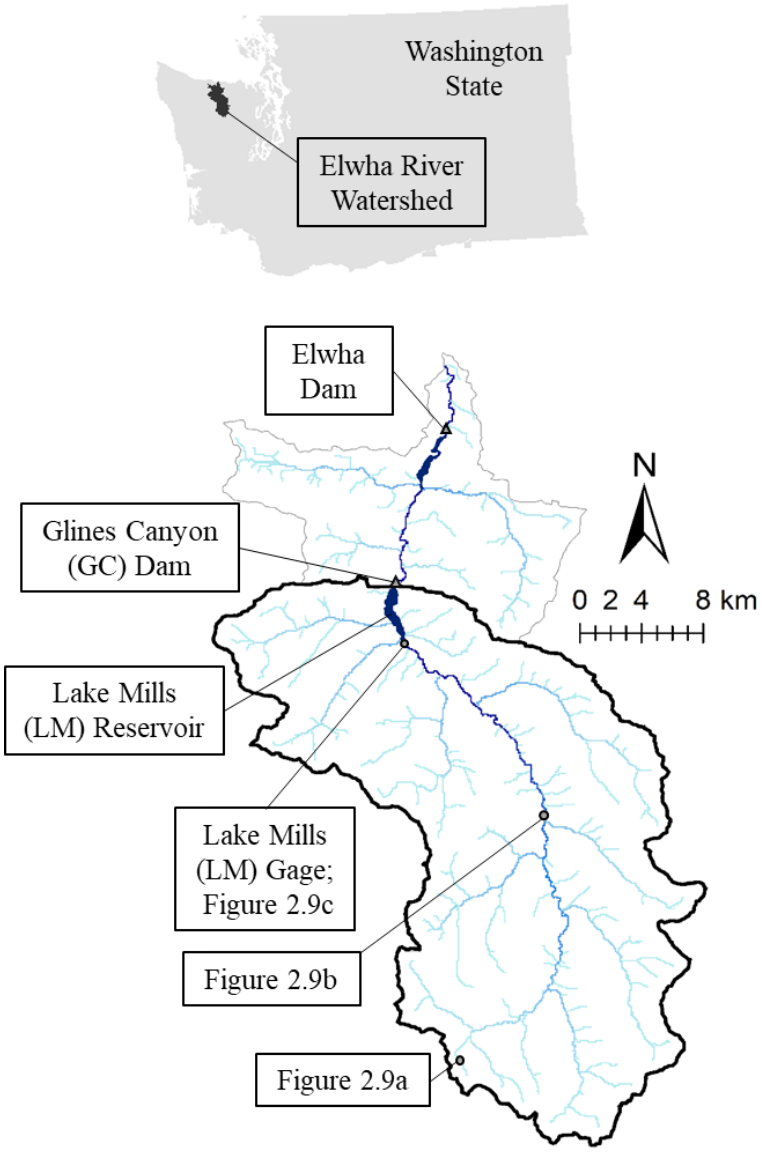

Figure 2.1. Map of Elwha River watershed in Washington State, USA.

Study area of the Glines Canyon Dam Tributary is outlined in black.

Methods commonly used for watershed management and the planning and design of water infrastructure do not adequately integrate the spatial and temporal variations in watershed sediment dynamics over typical infrastructure lifespans (~40 to 100 years). For example, the common approach of empirical at-a-station sediment rating curves uses streamflow and sediment data collected at a single location and for a limited temporal frequency and extent. As a result,

peak flow magnitudes that dominate sediment yields and sediment resulting from land management and disturbances may not be adequately represented. The prediction of hillslope sediment supply is often from simple empirically-based methods such as the Universal Soil Loss Equation (USLE; Wischmeier & Smith, 1978) and its variants (e.g., Revised USLE; Renard et al., 1991). However, these approaches were developed for agricultural fields and are poorly suited for mountainous watersheds (Shen et al., 2009; United States Society on Dams, 2015). They also have limited sediment transport mechanisms (e.g., sheet or rill erosion) and only provide mean annual sediment yields. More sophisticated mechanistic models are used such as Water Erosion Prediction Project (WEPP; Flanagan & Nearing, 1995), designed for rural agricultural watersheds, or HEC-6 (Hydrologic Engineering Center, 1993), designed for scour and deposition in rivers and reservoirs. However, these models do not account for climate variability and extremes, lack the holistic representation of source-to-sink geomorphic processes, and often require estimation of numerous unknown parameters (United States Society on Dams, 2015).

Watershed network sediment routing models developed for academic research purposes, on the other hand, are typically developed to investigate domain-specific questions (e.g., fluvial sediment transport, hillslope geomorphology). However, they often lack adequate representation of complexity in other process domains (e.g., distributed hydrology) as well as space and time scale considerations that are relevant to watershed planning and management. The seminal work of Benda and Dunne (1997b, 1997a) demonstrated a stochastic sediment input routine to drive sediment routing and storage in channel networks using spatially homogeneous rainfall. Studies by Czuba et al. (2017) and Schmitt et al. (2018a, 2018b; 2016) have further advanced understanding on the network-scale connectivity of sediment sources and sinks. Various other

sediment routing models have had sophisticated representations of mixed-size bedload transport such as the network model of Czuba (2018), the network model of Gasparini et al. (2004), The Unified Gravel-Sand (TUGS) model (Cui, 2007), and Morphodynamics and Sediment Tracers in 1D (MAST-1D) model (Lauer et al., 2016). However, each of these modeling frameworks lacks integration of both bedload and suspended load as well as advanced representation of either hillslope input, distributed hydrology, or long-term watershed sediment yields.

2.1.1 *A channel network model for sediment dynamics*

Predicting sediment balances in mountainous watersheds requires mechanistic understanding of the intermittency and magnitudes of sediment flux into the channel network and propagation of sediment as it interacts with the river channel. There is disconnect between methods and models used to predict sediment yields for water management and engineering applications and those used for researching fluvial fluxes, forms, and patterns and their linkage to climate and environmental change. Considering these limitations, we developed a parsimonious channel network sediment model to address two key research questions:

1. How can domain-specific research approaches to modeling network sediment dynamics be combined to predict watershed sediment yields over temporal and spatial scales relevant to planning and management?

2. What improvements does a network-scale sediment routing model provide compared to at-a-station based transport estimates in predicting reservoir sediment yields?

Our new model connects processes of hillslope sediment supply with fluvial sediment deposition, accumulation, and transport routed across watershed network channel segments. Two novel attributes of our model are that (1) it simulates both bedload and suspended load transport, partitioned between gravel, sand, and mud fractions; and (2) the streamflow forcing is from a

physically-based distributed hydrology model. The network sediment transport is driven by intermittent mass wasting events represented by a stochastic arrival process, run independently for watershed area above each network segment. The network sediment model operates on a daily time step and outputs annual sediment yields for each segment.

The network sediment model's novel attributes as well as its temporal and spatial scales are relevant to dam and watershed management needs. Predictions of distributed fluvial sediment transport capacity can help, for example, to identify stream reaches where river management (e.g., erosion mitigation) and frequent in situ monitoring may be needed. Predictions of annual sediment fluxes can help with short-term watershed planning and operations. For example, understanding the annual movement of bedload can inform whether channel bed gravel is sufficiently replenished for optimal fish habitat. Modeling of both bedload and suspended load is valuable since they both impact river ecology, geomorphology, and infrastructure, however often in different ways. Streamflow forcing from an advanced hydrologic model is critical for to capturing the spatial and temporal complexity of watershed sediment dynamics. This is particularly valuable in watersheds with complex topography and climatology, where sediment dynamics are not adequately represented by simplified hydrologic relationships (e.g., streamflow as a function of contributing area).

This paper introduces our new network sediment routing model and its implementation in the Elwha River watershed upstream of the Glines Canyon dam. An ensemble of 28 model experiments was conducted over the 84-year dam lifespan using historic meteorological forcing data. Historic hydrologic, sediment transport, and reservoir sedimentation data were also used to parameterize, calibrate, and validate the model. Three model parameters were systematically varied in the model experiments. We also compared the network model performance in

predicting lifetime reservoir sedimentation to the traditional approach of at-a-station sediment rating curves. We tested both empirical and physically-based approaches to developing these sediment rating curves and streamflow duration curves.

2.1.2 *Chapter outline*

In the text that follows, Section 2.2 describes the network sediment model processes as well as the methods and rationale used in developing them. Details are included on the model framework, stochastic hillslope sediment supply, suspended load and bedload transport equations, hydrologic forcing, and model experiments. Section 2.2 also describes the development and application of the sediment rating curve approaches. Section 2.3 describes the Elwha River watershed background, historic hydrologic and sediment data, hydrologic model input data, empirical sediment rating curves, and measured reservoir sedimentation estimates. Section 2.4 provides the results and discussion for the hydrologic forcing model, sediment rating curves, and network sediment model. Section 2.5 provides the paper summary and conclusions. The supplementary material provides further details on the development and of the network model and rating curves. A complete list of notations used throughout the paper is at the end of this text. The sediment model code is written in Python programming language. It is publicly available online along with the data used in this study at github.com/cbev/network_sediment_model.

2.2 METHODS

An overview of the network sediment model processes follows (Section 2.2.1) and details of model processes are in subsequent sections (Sections 2.2.1.1 to 2.2.2.3). This is followed by discussion of the bedload transport formula performance (Section 2.1.3) and the hydrologic forcing model implementation (Section 2.2.4). Then, the testing of the network sediment model

with 28 model instances is described (Section 2.2.5). In the network model testing, three parameters were systematically varied. These parameters were the hillslope sediment production rate ($rate_d$) and fractions of sand (λ_{ss}) and mud (λ_{ms}) on the channel bed surface that are available for suspended load transport. These parameters are described in their respective sections (Section 2.2.1.1 and 2.2.1.2). Finally, we present our approach for using sediment rating curves to predict lifetime reservoir sediment yields in order to compare them to network model outputs (Section 2.2.6).

2.2.1 *Network model framework*

Our sediment model (Figure 2.2) connects processes of hillslope sediment supply with fluvial sediment transport and deposition across a Strahler-ordered channel network. Each segment has geomorphic and fluvial state attributes treated as either static or dynamic. Static attributes of each segment are stored in the geomorphic and fluvial state matrix and include segment Strahler order number o_j; segment length l_j; average segment slope S_j; average segment width W_j computed from hydraulic geometry (Section 2.2.2.1); downstream segment number ds_j; total contributing area $CA_{T,j}$; local contributing area $CA_{L,j}$; representative channel bed grain sizes $D_{mean,j}$, $D_{gb,j}$, $D_{s,j}$, $D_{50,j}$, and $D_{90,j}$ (Section 2.2.2.2); and channel bed grain roughness $n_{g,b}\,(H_{50})_j$ (Section 2.2.2.3). Dynamic attributes of each segment include the volumes of sediment incoming, outgoing, stored on the channel bed, and bedload transport capacity (Table 2.1a). These sediment volumes are classified according to their grain size and transport mode i (Table 2.1b). The channel bed volumes are used to compute the dynamic bed surface fractional proportions of gravel F_{gb}; sand F_s; and sand and silt (i.e., non-gravel size sediments) F_{ssm}. Dynamic segment attributes are updated in each daily timestep in conjunction with the segment-scale sediment mass balance.

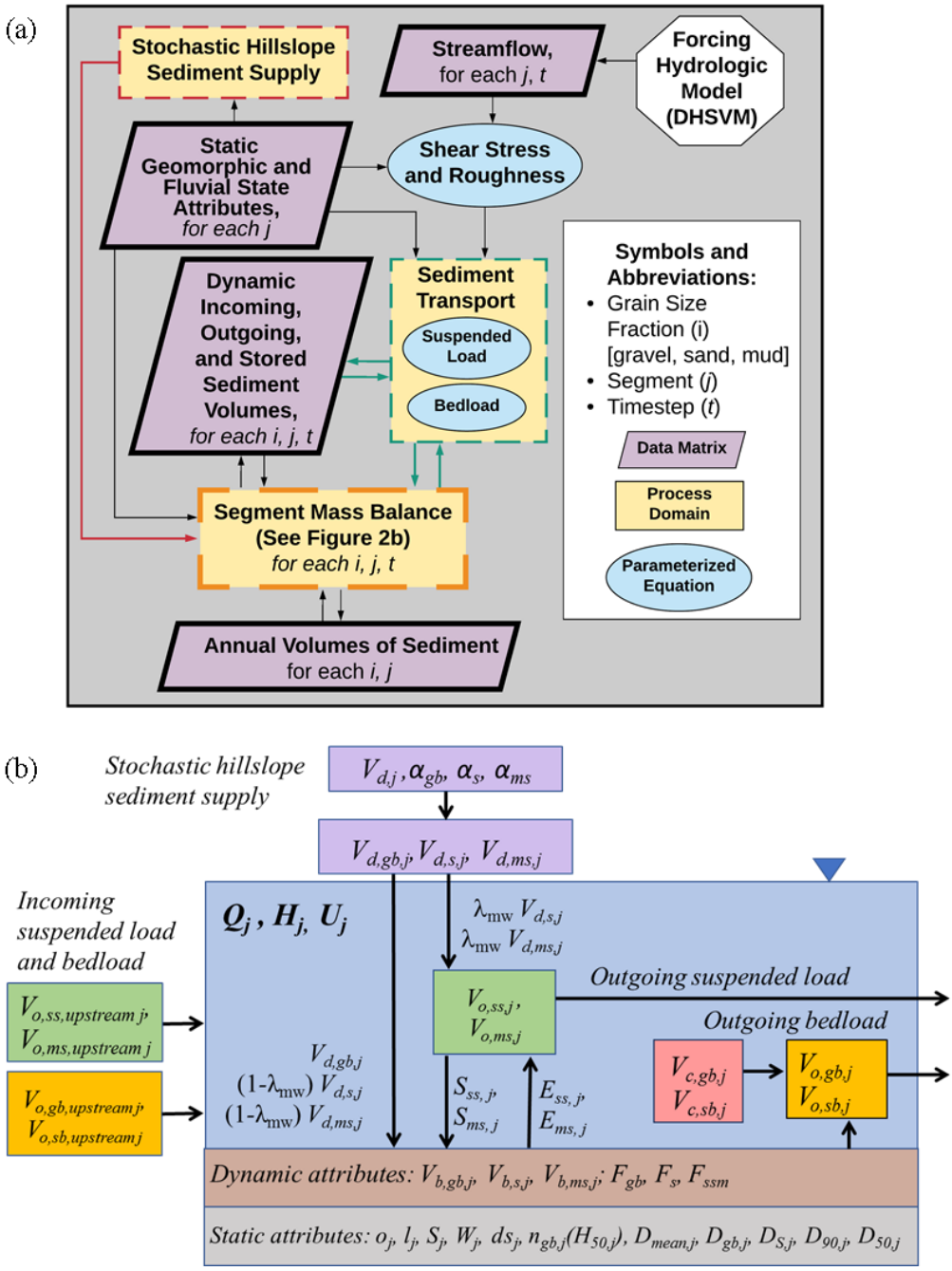

Figure 2.2. Conceptual diagrams of network sediment model workflow.

(a) Linkage between model processes, key equations, and segment-based data matrices.

(b) Schematic of a segment longitudinal profile with sediment mass balance components.

For each daily timestep, a sequence of model processes is conducted at each segment.

The processes start at segments with a Strahler order of one and continue downstream to the highest order. The initial model process step is the sediment supply component, which is a simple algorithm that emulates stochastic mass wasting (Section 2.2.1.1). If mass wasting occurs for a given timestep, a sediment volume sourced from the segment's local contributing area is transferred into the channel. The partitioning of the deposited volume between gravel, sand, and mud is based on model parameters (α_{gb}, α_{s}, α_{ms}). Fractions of sand and mud in the deposit go directly into suspension based on a model parameter (λ_{mw}). The entire fraction of gravel and remaining fraction of sand in the deposit are added onto the channel bed. In addition, sediment volumes transported out of segments directly upstream (if the segment order is greater than one) are added into the suspended sediment column or onto the channel bed.

Next, suspended load (Section 2.2.1.2) and bedload (Section 2.2.1.3) transport are estimated for the volumes of sediment in suspension and on the channel bed. The transport processes are driven by streamflow outputs from a distributed hydrology model (Section 2.2.4). Hydraulic geometry relationships are also used to compute the transport formula variables of streamflow velocity $U_{j,t}$, streamflow depth $H_{j,t}$, and grain shear stress $\boldsymbol{\tau_{g,j,t}}$. Suspended load transport, partitioned between sand and mud volumes, is computed based on models by Patil et al. (2012) and Abad et al. (2008). Bedload transport capacity, partitioned between gravel and sand volumes, is computed from a modified, two-fraction version of the Wilcock and Crowe (2003) formula.

2.2.1.1 Stochastic hillslope sediment supply

In this study, the primary purpose of the stochastic hillslope sediment supply component is to be a perpetual sediment driver for testing the network sediment routing. The two main premises of the sediment supply forcing component are: the Olympic Mountains are in erosional steady-state

(Montgomery & Brandon, 2002) with a constant denudation rate; and most fluvial sediment is supplied by threshold-dependent and episodic mass wasting events such as landslides, gullying, and debris flows (Warrick et al., 2011; Buffington & Woodsmith, 2003). In the algorithm, the probability that each segment *j* will have a mass wasting event is from an exponential distribution (e.g., Stark & Passalacqua, 2014):

$$\boldsymbol{f\left(t_{L,j}; \frac{1}{\bar{t}_L}\right) = \frac{1}{\bar{t}_L}\ \exp\left(-\frac{t_{L,j}}{\bar{t}_L}\right)} \qquad (2.1)$$

In (2.1), $t_{L,j}$ is the time lag between mass wasting events for each segment and $\boldsymbol{\bar{t}_L}$ is the mean time lag for the entire network. After each mass wasting event, $t_{L,j}$ is reset for the respective segment. When a mass wasting event occurs, the sediment volume deposited in the segment is the amount that has generated over the preceding lag time $t_{L,j.}$ The generation rate of the sediment volume deposit depends on the local contributing area of each segment $CA_{L,j}$ and a constant soil production $rate_d$. Hence, the total mass wasting deposit volume $V_{d,j}$ is

$$\boldsymbol{V_{d,j} = rate_d\ CA_{L,j} t_{L,j}} \qquad (2.2)$$

This is an approximate model to provide intermittent sediment supply to channel segments controlled by soil production. In any given year there could be more than one mass wasting event or no event. This level of detail for sediment input is deemed sufficient for this study as our focus is on the network sediment routing model. The total mass wasting volume is divided into proportions of gravel, sand, and mud (i= *gb, s, ms*) based on multipliers of α_{gb}, α_s, and α_{ms} which collectively sum to 1 (i.e., $\alpha_{gb}V_{d,j} = V_{d,gb,j}$; $\alpha_s V_{d,j} = V_{d,s,j}$; $\alpha_{ms}V_{d,j} = V_{d,ms,j}$; $V_{d,gb,j} + V_{d,s,j} + V_{d,ms,j} = V_{d,j}$) (Figure 2.2). From the proportions of sand and mud in the deposit volume, a fraction is directly added into the suspended load of the segment based on the multiplier of λ_{mw} ($\lambda_{mw}V_{d,s,j}$, $\lambda_{mw}V_{d,ms,j}$). These sand and mud volumes from the mass wasting deposit are added to the incoming fluvial suspended load volumes from the segment(s) immediately upstream. These

suspended load volumes can potentially be transported further downstream based on suspended load transport computations (Section 2.1.2). The mass wasting deposit fractions of sand and mud that were not directly added to the suspended load ([1-λ_{mw}]$V_{d,s,j}$, [1-λ_{mw}]$V_{d,ms,j}$) along with the entire mass wasting deposit volume of gravel are added to the channel bed ($V_{b,s,j}$, $V_{b,ms,j}$, $V_{b,gb,j}$). The channel bed also contains gravel, sand, and mud volumes from the previous timestep as well as incoming fluvial bedload volumes from the segment(s) immediately upstream. Hence, the changes in suspended load volume ($\boldsymbol{\Delta V_{o,j}}$) and channel bed sediment volume ($\boldsymbol{\Delta V_{b,j}}$) following a hillslope mass wasting event are:

$$\Delta(V_{o,ss,j} + V_{o,ms,j}) = \lambda_{mw}\left[V_{d,s,j} + V_{d,ms,j}\right] \quad (2.3)$$

$$\Delta\left(V_{b,gb,j} + V_{b,s,j} + V_{b,ms,j}\right) = V_{d,gb,j} + (1 - \lambda_{mw})\left[V_{d,s,j} + V_{d,ms,j}\right] \quad (2.4)$$

The parameters $\boldsymbol{rate_d}$, $\boldsymbol{\bar{t}_L}$, α_{gb}, α_s, α_{ms}, and λ_{mw} are user-specified and network model results are sensitive to their values. However, there is limited published research to derive their values from, therefore values were selected largely based on scientific reasoning and model performance. We varied $rate_d$ based on values published for the study area soil denudation rates (0.18-0.22 mm/year; Sections 2.2.5 and 2.3.1). We set $\boldsymbol{\bar{t}_L}$ to be constant at 20 years based on an average landslide return interval for upland catchments in the North Cascades (Strauch, Istanbulluoglu, & Riedel, 2019) which are similar to the Olympic Mountains. Additional parameters that we kept constant were λ_{mw} at 0.10 and α_{gb}, α_s, α_{ms} each at 0.33. We chose these values since the parameters are empirical and the model performed strongly for these values in the study area.

2.2.1.2 Suspended load transport

For each daily timestep, volumes of suspended load (sand and mud) can enter a segment from hillslope mass wasting ($\boldsymbol{\Delta[V_{o,ss,j} + V_{o,ms,j}]}$, (2.3)) and the segments immediately upstream

$V_{o,ss,upstream\,j}$ and $V_{o,ms,\,upstream\,j}$ (Figure 2.2). The depth-averaged concentration of sand and mud in the water column $C_{ssm,\,j}$ (kg/m^3) is computed using the suspended load volumes, modeled streamflow volume $\boldsymbol{V_{w,j}}$, water density ρ, and ratio of sediment to water density sg (2.65), as

$$C_{ssm,j} = sg \cdot \rho \cdot (\Delta[V_{o,ss,j} + V_{o,ms,j}] + V_{o,ss,upstream\,j} + V_{o,ms,upstream\,j})/V_{w,j} \quad (2.5)$$

Then, based on C_{ssm} and other local conditions, in-channel settling and erosion of suspended sand and mud may occur prior to suspended sediment transport out of the segment. We made the simplifying assumption that suspended load transport is in local equilibrium and therefore the local settling and erosion rates are from equilibrium transport (Kondolf & Piégay, 2003).

Settling and erosion formulae are based on the network model framework of Patil et al. (2012) and equations in Abad et al. (2008). However, in the suspended load erosion rates of these formulae, we incorporate three additional multipliers of $\lambda_{ss,}$ λ_{sm}, and F_{ssm}. These multipliers implicitly account for shielding of sand and mud on the channel bed by gravel and were necessary for preventing anomalously high suspended sediment transport rates. The multipliers λ_{ss} and λ_{ms} account for the fractions of sand and mud, respectively, on the channel bed that are erodible (i.e., in the active surface layer). The multiplier λ_{ss} also accounts for the fraction of sand on the bed surface that has a small enough diameter to be transported as suspended load. The multipliers λ_{ss} and λ_{ms} are user-specified and network model results are sensitive to their values. However, there is limited published research to derive their values from. In the model testing for this analysis (Section 2.2.5), we varied values of λ_{ss} and λ_{ms} selected based on scientific reasoning and model performance. The multiplier F_{ssm} accounts for shielding of sand and mud by gravel on the bed surface. It is updated prior to the computation of suspended load as

$$F_{ssm,j=}(\boldsymbol{V_{b,s,j}} + \boldsymbol{V_{b,ms,j}})/(\boldsymbol{V_{b,gb,j}} + \boldsymbol{V_{b,s,j}} + \boldsymbol{V_{b,ms,j}}) \quad (2.6)$$

Following Abad et al. (2008), we approximate the net rate of change in suspended sand as E_{ss} - S_{ss} where E_{ss} is the potential suspended sand erosion rate and S_{ss} is the potential suspended sand settling rate (both in kg/m^2/s). The approximation of S_{ss} is

$$\boldsymbol{S_{ss} = v_{ss} \cdot \frac{C_{ssm}}{INT(Z_R)}} \qquad (2.7)$$

In (2.7), v_{ss} is the *ss* settling velocity (m/s), Z_R is the Rouse number, and $INT(Z_R)$is the integral of the suspended load concentration profile in the water column. For v_{ss}, we use the following expression (Camenen, 2007)

$$\boldsymbol{v_{ss} = \frac{v}{D_{ss}}\left[\sqrt{\frac{1}{4}\left(\frac{A}{B}\right)^{2/m} + \left(\frac{4}{3}\frac{D_{ss*}^3}{B}\right)^{1/m}} - \frac{1}{2}\left(\frac{A}{B}\right)^{1/m}\right]^m} \qquad (2.8)$$

In (2.8), v is the kinematic viscosity of water (10^{-6} m^2/s), and A, B, and m are the calibration coefficients for natural sand material (Julien, 1995), which are 24, 1.5, and 1, respectively. D_{ss*} is the dimensionless particle diameter defined as

$$\boldsymbol{D_{ss*} = D_{ss}\left(\frac{(sg-1)g}{v^2}\right)^{1/3}} \qquad (2.9)$$

In (2.9), g is the acceleration of gravity. The definition of Z_R is $\frac{v_{ss}}{k \cdot u_*}$, where k is the dimensionless von Kármán constant (0.41) and u_* is shear velocity $u_* = (\tau_g/\rho)^{0.5}$. We use the following numerical approximation for $INT(Z_R)$ (Abad and Garcia, 2006)

$$\boldsymbol{INT(Z_R) = \frac{1}{C_0 + C_1 \cdot Z_R + C_2 \cdot Z_R^2 + C_3 \cdot Z_R^3 + C_4 \cdot Z_R^4 + C_5 \cdot Z_R^5 + C_6 \cdot Z_R^6}} \qquad (2.10)$$

In (2.10), the coefficients C_0, C_1, C_2, C_3, C_4, C_5, and C_6 are 1.1038, 2.6626, 5.6497, 0.3822, –0.6174, 0.1315, and –0.0091, respectively. These coefficient values are for a boundary layer thickness to streamflow depth ratio (z_b/H) of 0.05 (see Abad and Garcia (2006) for details). The approximation of E_{ss} is

$$\boldsymbol{E_{ss} = \mathbf{Min}\{\lambda_{ss} \cdot F_{ssm} \cdot v_{ss} \cdot \frac{A_E Z_u^5}{1+\frac{A_E Z_u^5}{0.3}} \cdot sg \cdot \rho,\ \ \lambda_{ss} \cdot F_{ssm} \cdot V_{b,s,j}\}} \qquad (2.11)$$

The first equation in (2.11) follows Garcia & Parker (1991) with two multipliers we have added (λ_{ss} and F_{ssm}). The empirical model testing parameter λ_{ss} was varied between 0.010 and 0.030, which were the end members of the range that performed strongly in the study area. The second equation in (2.11) is the constraint for available sand on the bed surface that can be transported as suspended load. In (2.11), A_E is $1.3 \cdot 10^{-7}$ and $\boldsymbol{Z_u}$ is

$$\boldsymbol{Z_u = \alpha_1 \cdot \frac{u_* Re_p^{\alpha_2}}{v_{ss}}} \qquad (2.12)$$

Here, Re_p is the Reynolds number for sediment, defined as $\boldsymbol{Re_p = \frac{v_{ss} D_{ss}}{v}}$. The coefficients α_1 and α_2 depend on Re_p as (α_1, α_2) = (1, 0.6) for Re_p >2.36 and (α_1, α_2) = (0.586, 1.23) for Re_p <2.36.

The settling of mud (S_{ms}) and erosion of mud (E_{ms}) (both in kg/m^2/s) are modeled following the approach described in Patil et al. (2012). Each depends on the grain shear stress, τ_g, relative to the critical shear stress of mud, $\tau_{c,ms}$. We calculate $\tau_{c,ms}$ as (Mitchener & Torfs, 1996)

$$\boldsymbol{\tau_{c,ms} = 0.015 \cdot \left(\rho_{b,f} - \rho\right)^{0.73}} \qquad (2.13)$$

In (2.13), $\boldsymbol{\rho_{b,f}}$ is the bulk density of mud (or fine sediment) on the bed. Settling of mud occurs when $\tau_g < \tau_{c,ms}$, and is computed using the falling velocity of mud v_{ms} as

$$\boldsymbol{S_{ms} = \left(1 - \frac{\tau_g}{\tau_{c,ms}}\right) \cdot v_{ms} \cdot C_{ssm}} \qquad (2.14)$$

$$\boldsymbol{v_{ms} = 0.08 \cdot \frac{C_{vm}^{1.65}}{\left(C_{vm}^2 + 3.5^2\right)^{1.88}}} \qquad (2.15)$$

In (2.15), the constant C_{vm} depends on C_{ssm} as C_{vm}=0.15 for $C_{ssm} \leq 0.15$, C_{vm} =2.11 for C_{ssm}>2.11 and C_{vm}= C_{ssm} for 0.15<C_{ssm}≤2.11 (Hwang, 1989).

Erosion of mud occurs when $\tau_g > \tau_{c,ms}$ and is computed as

$$\boldsymbol{E_{ms} = \mathbf{Min}\{\lambda_{ms} \cdot F_{ssm} \cdot e_0 \cdot \left(\frac{\tau_g}{\tau_{c,sm}} - 1\right), \lambda_{ms} \cdot F_{ssm} \cdot V_{b,ms,j}\}} \quad (2.16)$$

In (2.16), e_0=0.2•10^{-3} kg/m^2/s. The empirical model testing parameter λ_{ms} was varied between 0.025 and 0.075, which were the end members of the range that performed strongly in the study area. The second equation of (2.16) is the constraint for available mud on the bed surface that can be transported as suspended load.

Hence, the outgoing suspended sediment load volume changes (m^3) are the sum of the erosion and settling rates of sand and mud

$$\boldsymbol{\Delta(V_{o,ss,j} + V_{o,ms,j}) = \begin{cases} (E_{ss,j} - S_{ss,j} - S_{ms,j}) \cdot L_j \cdot W_j \cdot \Delta t/(sg \cdot \rho), & \tau_g < \tau_{c,ms} \\ (E_{ss,j} - S_{ss,j} + E_{ms,j}) \cdot L_j \cdot W_j \cdot \Delta t/(sg \cdot \rho), & \tau_g > \tau_{c,ms} \end{cases}}$$

(2.17)

The subsequent channel bed volume is updated as

$$\boldsymbol{\Delta(V_{b,s,j} + V_{b,ms,j}) = (S_{ms,j} - E_{ms,j}) + (S_{ss,j} - E_{ss,j})} \quad (2.18)$$

2.2.1.3 Bedload transport

Bedload transport capacity is computed for gravel and sand using a modified version of the Wilcock & Crowe (2003) bedload transport formula, which is further described below. The gravel and sand bedload volumes transported out of each segment are the minimum of the bedload transport capacity and channel bed volume. The gravel and sand bed volumes consist of the sediment remaining from the previous timestep, deposited from hillslope mass wasting ($\boldsymbol{\Delta[V_{b,gb,j} + V_{b,s,j}]}$, (2.4)), and transported from the segments immediately upstream ($V_{o,gb,upstream\ j}$, $V_{o,sb,\ upstream\ j}$) (Figure 2.2). The bed surface grain size fractions of gravel, sand, and mud are computed using these volumes as well as the suspended sand and mud that are on the bed from hillslope mass wasting ($\boldsymbol{\Delta[V_{b,ms,j}]}$, (2.4)) and preceding suspended sediment transport

computations ($\boldsymbol{\Delta}[\boldsymbol{V_{b,s,j}} + \boldsymbol{V_{b,ms,j}}]$, (2.18)). We make the simplifying assumption that the bed surface grain size fractions of gravel (F_{gb}) and sand (F_s) are the same as the gravel and sand volume proportions on the bed (i.e., the bed is well-mixed), and thus are computed as

$$F_{gb,j} = \boldsymbol{V_{b,gb,j}} / (\boldsymbol{V_{b,gb,j}} + \boldsymbol{V_{b,s,j}} + \boldsymbol{V_{b,ms,j}}) \quad (2.19)$$

$$F_{s,j} = \boldsymbol{V_{b,s,j}} / (\boldsymbol{V_{b,gb,j}} + \boldsymbol{V_{b,s,j}} + \boldsymbol{V_{b,ms,j}}) \quad (2.20)$$

While the proportions of gravel and sand on the channel bed can change, we make the simplification that their median grain sizes are assumed constant for each segment. These simplifications for the bed surface grain size distribution neglect active layer dynamics in which bedload transport and grain size sorting is restricted to the bed surface layer (e.g., Gasparini et al., 2004; Czuba 2018).

Wilcock & Crowe (2003) is a commonly used surface-based bedload transport formula for mixtures of sand and gravel. The formula computes the transport rate for each grain size fraction *i* on the channel bed surface as

$$\boldsymbol{q_{bi}} = \frac{\boldsymbol{W^*_i F_i u_*^3}}{(\boldsymbol{sg-1})\boldsymbol{g}} \quad (2.21a)$$

$$\boldsymbol{W^*_i} = \begin{cases} \boldsymbol{0.002\phi^{7.5}} & \boldsymbol{\phi < 1.35} \\ \boldsymbol{14\left(1 - \frac{0.894}{\phi^{0.5}}\right)^{4.5}} & \boldsymbol{\phi \geq 1.35} \end{cases} \quad (2.21b)$$

$$\boldsymbol{\phi} = \boldsymbol{\tau_g / \tau_{ri}} \quad (2.21c)$$

For each grain size on the channel bed surface, q_{bi} is the volumetric bedload transport rate per unit channel width [m^2/s]; W_i* is the dimensionless bedload transport parameter; F_i is the fraction of the grain size on the bed surface; τ_{ri} is the reference shear stress, or the value of τ_g at which W_i* is equal to a reference value of 0.002 (Parker & Klingeman, 1982; Wilcock, 1997). Calculation of τ_{ri} using Wilcock & Crowe (2003) is

$$\frac{\tau_{r_i}}{\tau_{r_{mean}}} = \left(\frac{D_i}{D_{mean}}\right)^{b} \quad (2.22a)$$

$$b = \frac{0.67}{1+\exp\left(1.5 - \frac{D_i}{D_{mean}}\right)} \quad (2.22b)$$

$$\tau^*_{r_{mean}} = 0.021 + 0.015\exp(-20\,F_S) \quad (2.22c)$$

$$\tau^*_{r_{mean}} = \frac{\tau_{r_{mean}}}{(sg-1)\rho g D_{mean}} \quad (2.22d)$$

Here, D_i is the median grain diameter for each i; $\tau_{r_{mean}}$ is the reference shear stress (τ_{ri}) for the mean grain size on the bed surface D_{mean}; and $\tau^*_{r_{mean}}$ is the dimensionless $\tau_{r_{mean}}$. Finally, the bedload transport capacity volume [m^3] for each fraction $V_{c,i,j}$ is calculated as

$$V_{c,i,j} = q_{b,i,j} W_j \Delta t \quad (2.23)$$

The Wilcock & Crowe (2003) equations (2.21a-c, 2.22a-d) can be applied over an extensive, multi-fraction grain-size distribution to highly resolve multiple transport rates. However, given the uncertainty in the grain size distribution of the channel bed and sediment supply across the study area river network, we used a simplified two-fraction approach. A two-fraction approach, which only differentiates between sand (i=*sb*) and gravel (i=*gb*), has been used effectively in literature (e.g., Wilcock & Kenworthy, 2002; Gasparini et al., 2004). We compared Wilcock & Crowe (2003) in its multi-fraction form (with i for 16 grain size bins) and the two-fraction form (i=*sb*, *gb*) using data from the study area, and the difference in results was trivial. Hence, in our model framework, the Wilcock & Crowe (2003) equations are applied in a two-fraction form which we label hereinafter as W&C-2F.

The volumes of bedload transported as gravel and sand, respectively, are assumed to be the bedload transport capacity (2.23) unless constrained by the volume available on the bed. This is computed as

$$\Delta(V_{o,gb,j} + V_{o,sb,j}) = \mathbf{Min}\{V_{c,gb,j}, V_{b,gb,j}\} + \mathbf{Min}\{V_{c,sb,j}, V_{b,s,j}\} \quad (2.24)$$

The subsequent channel bed volume is updated as

$$\boldsymbol{\Delta\left(V_{b,gb,j}+V_{b,s,j}\right)=-\mathbf{Min}\left\{V_{c,gb,j},V_{b,gb,j}\right\}-\mathbf{Min}\left\{V_{c,sb,j},V_{b,s,j}\right\}} \quad (2.25)$$

2.2.2 *Network model initialization*

Channel width, streamflow depth, bed surface grain size diameters, bed grain roughness, and grain shear stress of each segment are parameterized based on observations collected at a single location in the study area watershed. This location, Lake Mills (LM) gage, and its observations are described in Section 2.3.2, however are referred to in this section.

2.2.2.1 Hydraulic geometry

At-a-station hydraulic geometry relationships for LM gage of depth H_{LM} and velocity U_{LM} of streamflow Q_{LM} were developed using the standard approach of power regression. The functions contain empirically-derived coefficients (a_H, a_U) and exponents (b_H, b_U) (Table 2.1) and have the following form:

$$\boldsymbol{H_{LM}=a_H Q_{LM}^{b_H}} \quad (2.26)$$

$$\boldsymbol{U_{LM}=a_U Q_{LM}^{b_U}} \quad (2.27)$$

Table 2.1. Notation for categories of (a) sediment volumes and (b) grain size/transport modes tracked for each segment and timestep in the watershed network model

a)

Notation (V_i)	Segment volume description	Sediment grain sizes/ transport modes (i, Table 1b) tracked
V_b	channel bed	gb, s, ms
V_c	bedload transport capacity	gb, sb
V_o	transported out	gb, sb, ss, ms
V_d	deposited by mass wasting event	gb, s, ms

b)

Notation (i)	Grain size	Transport Mode
gb	gravel	bedload
sb	sand	bedload
ss	sand	suspended load
s	sand	bedload (sb) + suspended load (ss)
ms	mud (silt/clay)	suspended load

The LM gage was in a wide bedrock canyon and observations of channel width W_{LM} had little variation with streamflow. Therefore, we set the LM gage channel width to be constant at the median value of measurements, 41.6 m.

Following Czuba (2018), we scaled streamflow depth H and channel width W for each segment relative to those at LM gage (H_{LM} and W_{LM}) along with the total contributing areas of LM gage $CA_{T,LM}$ and respective segment $CA_{T,j}$. We used typical exponents for downstream hydraulic geometry scaling (Leopold & Maddock, 1953; Park, 1977).

$$\boldsymbol{W_j = W_{LM}\left(\frac{CA_{T,j}}{CA_{T,LM}}\right)^{0.5}} \qquad (2.28)$$

$$\boldsymbol{H_j = H_{LM}\left(\frac{CA_{T,j}}{CA_{T,LM}}\right)^{0.4}} \qquad (2.29)$$

Per (2.28), channel width varies across the channel network; however, since width is locally constant, it does not vary with streamflow. Per (2.29), channel depth also varies across

the channel network; and, per (2.26), depth varies with changes in streamflow. Rectangular cross sections were assumed throughout the channel network and model duration. Thus, streamflow velocity for each segment was computed for each daily timestep by dividing streamflow with the product of depth and width. The hydraulic radius of segments were approximated as the depth.

2.2.2.2 Grain sizes

The approaches for modeling shear stress and bedload transport require the characterization of representative grain sizes on the channel bed surface including the median D_{50}, 90th percentile D_{90}, mean D_{mean}, median gravel D_{gb}, and median sand D_S. To assign fixed grain sizes of D_{50}, D_{90}, D_{mean}, and D_{gb} for each channel segment, we modified approaches of Pfeiffer & Finnegan (2017), Snyder et al. (2013), and Barry et al. (2004). We assumed a constant bankfull Shields stress $\boldsymbol{\tau^*_{bf}}$ for each segment j and solve for grain size at each segment based on its predicted $\boldsymbol{\tau^*_{bf}}$. We began with the equation for bankfull Shields stress,

$$\boldsymbol{\tau^*_{bf} = \rho g H_{bf} S / [(\rho_s - \rho) g D_{50}]} \qquad (2.30)$$

In (2.30), we substituted bankfull depth $H_{bf,j}$ with (29); substituted D_{50} with $D_{x,j}$, which can be $D_{50,j}$, $D_{90,j}$, $D_{mean,j}$, or $D_{gb,j}$; and substituted $\boldsymbol{\tau^*_{bf}}$ with $\boldsymbol{\tau^*_{bf,x}}$ which can be $\boldsymbol{\tau^*_{bf,50}}$, $\boldsymbol{\tau^*_{bf,90}}$, $\boldsymbol{\tau^*_{bf,mean}}$, or $\boldsymbol{\tau^*_{bf,gb}}$ (corresponding to the respective $D_{x,j}$). Then, we rearranged (30) with these substitutions as

$$\boldsymbol{\tau^*_{bf,x}}\left[\frac{(\rho_s-\rho) C A_{T,LM}^{0.4}}{\rho H_{bf,LM}}\right] = \frac{C A_{T,j}^{0.4} S_j}{D_{x,j}} \qquad (2.31)$$

In (2.31), it is assumed that the bracketed term as well as $\boldsymbol{\tau^*_{bf,50}}$, $\boldsymbol{\tau^*_{bf,90}}$, $\boldsymbol{\tau^*_{bf,mean}}$, and $\boldsymbol{\tau^*_{bf,gb}}$ were each respectively constant across all channel segments (Pfeiffer & Finnegan, 2017). Thus, we computed the four $\boldsymbol{\tau^*_{bf,x}}$ values at the LM gage using known grain size data from the

site ($D_{50,LM}$, $D_{90,LM}$, $D_{mean,LM}$, and $D_{gb,LM}$, Section 2.3.2). Then, we rearranged (2.31) to solve for grain sizes at each segment in the network ($D_{50,j}$, $D_{90,j}$, $D_{mean,j}$, $D_{gb,j}$) as

$$\boldsymbol{D_{x,j} = \frac{CA_{T,j}^{0.4}\, S_j}{\tau^*_{bf,x}\left[\frac{(\rho_s-\rho)CA_{T,LM}^{0.4}}{\rho H_{bf,LM}}\right]}} \qquad (2.32)$$

Values in the denominator of (2.32) were constant across all segments in the network. Values in the numerator of (2.32) are functions of topography that were assumed as static for each respective segment. Hence, $D_{50,j}$, $D_{90,j}$, $D_{mean,j}$, and $D_{gb,j}$ can conveniently be computed for each segment.

We assumed D_S was constant for all segments and therefore equal to the value computed at the LM gage (Section 2.3.2). This is justified since sand grain collisions are viscously dampened and therefore not subject to abrasion during downstream transport (Jerolmack & Brzinski, 2010).

2.2.2.3 Shear stress and surface roughness

The model sediment transport equations we used depend on grain shear stress τ_g, which is the fraction of boundary shear stress τ that acts only on sediment grains (rather than woody debris, etc.). To isolate grain shear stress from boundary shear stress, we considered the channel roughness n. Channel roughness similarly has a fraction of grain roughness n_g that is due to bed grains only and thereby relevant to sediment transport. Channel roughness is typically expressed from Manning's equation as $n=H^{2/3}S^{1/2}U^{-1}$, which can be rearranged as $H=(nU)^{3/2}S^{-3/2}$. Following Wilcock et al. (2009), this expression for H can be substituted into the equation for boundary shear stress, $\tau=\rho gHS$. Then, to compute τ_g, n can then be replaced with n_g. This resulted in

$$\boldsymbol{\tau_{g,j} = \rho g\left(n_{g,j}U_j\right)^{3/2}S_j^{1/4}} \qquad (2.33)$$

For our model, we developed an approach for computing grain roughness based on published formula and empirical findings. There are many empirical models for directly computing grain roughness, however they were developed across variety of site conditions and therefore each may or may not be relevant to a given application. From the studies of Rickenmann & Recking (2011) and Wang & Dawdy (2014), we obtained nine equations for computing grain roughness in gravel-bedded streams that are either widely used or represent a low or high degree of complexity (Section S.1.2 of Beveridge, Istanbulluoglu, et al., 2020). We computed grain roughness using LM gage observations in each of the nine equations and found that the computed grain roughness was nearly constant with streamflow depth in each equation. The computed grain roughness values from the nine equations fell in a narrow range of 0.022-0.027 (median of ~0.024). This median value is most closely represented by the equation of Bray (1979) $n_{g,b}$ which is

$$\boldsymbol{n_{g,b}} = \frac{\mathbf{0.113}\, \boldsymbol{H^{1/6}}}{\mathbf{1.26 - 2.16 \log_{10}(D_{90}/H)}} \qquad (2.34)$$

When we use equation (2.34) and compare predicted bedload by the W&C equation given fixed bed substrate size as observed at the Lake Mills gage site with bedload measurements (Section 2.2.3 below) the W&C under (over) estimate bedload in low (high) flows. Total roughness computed from Manning's equation and LM gage observations (of depth, slope, and velocity) showed significantly more variability with streamflow depth compared to grain roughness. The range of total roughness was 0.04 to 0.15 and a depth weighted mean $\bar{\boldsymbol{n}}$ was ~0.079. The computed variability of $n_{g,b}$ is a lot smaller (range: 0.022-0.027). We argue that this mismatch in bedload could be a result of disparity between the variation of estimated total n from observations and the calculated $n_{g,b}$ from (2.35).

An alternative approach to estimating $n_{g,b}$ is proposed that scales the variability of Manning's total roughness with depth to the magnitude of grain roughness computed from (2.34) (Section S.1.2 of Beveridge, Istanbulluoglu, et al., 2020)). We label this scaling relationship as $n_{g,E}$ (*E* for the Elwha watershed), and compute it as

$$\boldsymbol{n_{g,E,j} = n_{*,j}\, x\, n_{g,b}(H_{50})_j} \qquad (2.35)$$

In (2.35), $n_{g,b}\,(H_{50})_j$ is from (2.34) evaluated at the median flow depth, $H_{50,j}$ (which is computed using (2.29) with H_{LM} of the median streamflow discharge Q_{50} from (2.26)). Thus, $n_{g,b}\,(H_{50})_j$ is a static attribute for each segment. $\boldsymbol{n_*}$ is Manning's total roughness *n* normalized by $\boldsymbol{\bar{n}}$. Computing $\boldsymbol{n/\bar{n}}$ is only plausible where there are a broad range of observations available (in our case, at LM gage). So, we conducted a power regression for $\boldsymbol{n_*}$ as a function of flow depth using LM gage observations, emulating an at-a-station hydraulic geometry relationship for normalized roughness, as

$$\boldsymbol{n_{*,j} = c_{n_g} H_j^{d_{ng}}} \qquad (2.36)$$

We assume that the coefficient ($\boldsymbol{c_{n_g}}$) and exponent ($\boldsymbol{d_{n_g}}$) are constant throughout the network (Table 2.2). Hence, in the model, we used the static attribute of $\boldsymbol{n_{g,b}(H_{50})_j}$, computed from (2.26), (2.29), and (2.34), along with $\boldsymbol{n_{*,j}}$ computed from (2.36) to calculate $n_{g,E,,j}$ with (2.35). Then, $n_{g,E,,j}$ is substituted for $n_{g,j}$ in (2.33) to compute $\tau_{g,j}$.

Table 2.2. Empirically-derived coefficients (a_H, a_U, c_{ng}) and exponents (b_H, b_U, d_{ng}) for at-a-station hydraulic geometry relationships at the Lake Mills Gage.

Equation No.	Variables	Values	No. of Observations	Regression r^2
2.26	a_H, b_H	0.24, 0.41	28	0.93
2.27	a_U, b_U	0.10, 0.58	28	0.96
2.36	c_{ng}, d_{ng}	1.08, -0.44	22	0.77

2.2.3 *Lake Mills gage bedload formula performance*

Our parameterizations of the W&C-2F formula for computing bedload discharge showed strong performance when compared to observations at LM gage. The performance of the W&C-2F formula with grain roughness parameterization by Bray (1979) ($n_{g,b}$, (2.34)) and our empirically-developed formula ($n_{g,E,}$ (2.35)) is demonstrated in Figure 2.3. Replacing $n_{g,b}$ with $n_{g,E}$ improves the bedload discharge predictions r^2 from 0.44 to 0.51. This improvement is largely due to improved predictions at higher bedload discharge values (>~10^{-5} m^2/s), where the $n_{g,b}$ parameterization overestimated bedload discharge. Since median to high sediment discharges dominate long-term yields, we used the $n_{g,E}$ (rather than $n_{g,b}$) grain roughness parameterization in our network sediment model. We tested both grain roughness parameterizations ($n_{g,E}$ and $n_{g,b}$) in our sediment rating curve analyses (Section 2.6).

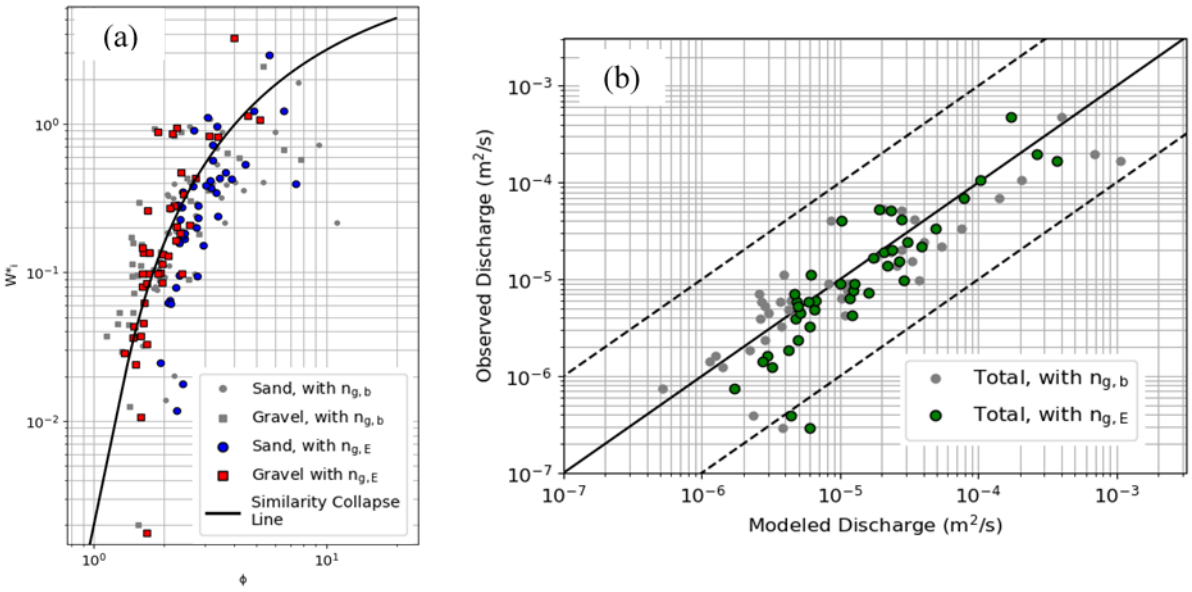

Figure 2.3. Bedload discharge from W&C-2F at Lake Mills gage.

(a) Similarity collapse of gravel and sand fractions. (b) Observed versus modeled total bedload discharge. Solid line is the 1:1 line and dashed lines are 1 order of magnitude beyond 1:1 line.

2.2.4 *Hydrologic forcing*

Our sediment network model uses streamflow inputs defined at the upstream node of each segment of the channel network, for each daily timestep. The streamflow inputs are from the Distributed Hydrology Soils Vegetation Model (DHSVM) (Wigmosta, Vail, & Lettenmaier, 1994). DHSVM is an open-source distributed, physically-based hydrology model that combines spatially explicit characteristics of a watershed with meteorological forcing data. DHSVM has been extensively applied in the Pacific Northwest (e.g., Wigmosta et al., 1994; Cuo et al., 2011; Frans, 2015; Mauger et al., 2016; Murphy, 2017; Sun et al., 2018; Bandaragoda et al., 2019).

To derive the study area soil depth grid and channel network topology, we used open source research software specifically developed for setting up DHSVM (PNNL, 2018). Soil depths were assigned based on local elevation and combined curvature variables within a specified a soil depth range. Segment attributes were assigned by DHSVM following channel network extraction. Historical meteorological forcing data was disaggregated from a daily timestep to three-hour timestep and incoming longwave and shortwave radiation and relative humidity were estimated. This was done using the Mountain Microclimate Simulation Model algorithms (Thornton & Running, 1999) as implemented in Bohn et al. (2013).

DHSVM was run in the study area at 30 m grid cell spatial resolution and three-hour timestep from years 1915-2011 (97 years). Streamflow was output at each segment at the three-hour timestep, and then aggregated to daily streamflow predictions. We calibrated DHSVM with a one-at-a-time method to fit the modeled streamflow outputs to observations at LM gage for water years 2006 and 2007. We limited the calibration to a computationally inexpensive approach based on parameters known to be sensitive for DHSVM (Kelleher, C., Wagener, T., McGlynn, 2015). We focused on adjusting the soil texture and depth parameters (final

parameters in Table S.2 of Beveridge, Istanbulluoglu, et al., 2020), as they had the strongest influence (compared to other parameters) on the modeled hydrographs. However, the input soil texture data in the study area is relatively low resolution (three generic soil classes), which could limit model performance where physically based soil parameterization is significant. We evaluated the DHSVM performance during the remaining (non-calibration) periods of streamflow observations periods (water years 1994-1998, 2004-2005 and 2004-2011).

2.2.5 *Network model instances*

We tested our model performance and calibrated parameters by comparing model outputs to observations of bedload and suspended load at LM gage. In this paper we present and ensemble of 28 model instances (unique parameter sets) from varying three model parameters within limited ranges. We varied the hillslope sediment production rate ($rate_d$) as 0.18, 0.20, and 0.22 mm/year. We varied the fractions of sand (λ_{ss}) and mud (λ_{ms}) on the channel bed surface that are available for transport as 0.010, 0.015, 0.025, and 0.030 for λ_{ss}, and 0.025, 0.050, and 0.075 for λ_{ms}. These are the plausible ranges of parameter values we see as realistic for the study site conditions. Thus, we limited our simulations to show the cumulative sediment accumulation for the study period to this given parameter combination.

We conducted a single model spin-up run to establish the initial quasi-equilibrium conditions of the channel bed for all segments (Cui, Parker, Braudrick, Dietrich, & Cluer, 2006). This spin-up run and each of the 28 model instances were run over 97 years (1915-2011) at a daily timestep. We evaluated model outputs for the 84 years (1927-2011) that the dam in the study area existed.

The reservoir is not explicitly incorporated into the network model. However, there are model network segments that overlay the former reservoir surface and dam which we used to

estimate the final total reservoir sedimentation. We summed the channel bed sediment volumes ($V_{b,i,j}$) for segments overlaying reservoir surface ($j \in$ reservoir surface) at the final timestep (t_{final}) along with summing the sediment volumes transported out of segments ($V_{o,i,j}$) crossing over the GC dam ($j \in$ GC dam) throughout the model evaluation period. Suspended sediment was multiplied by the empirical reservoir trap efficiency *rte*. Sediment volumes were converted from sediment in transport (with density ρ_s) to deposited (bulk) sediment in LM using the bulk densities of fine ($\rho_{b,f}$) and coarse ($\rho_{b,c}$) sediments. In equation form, lifetime reservoir sedimentation is as follows

$$\left[\sum_{\substack{j\in \textbf{reservior}\\ \textbf{surface},}} \left(\boldsymbol{V_{b,g,j}} + \boldsymbol{V_{b,s,j}}\right)_{t=t_{final}} + \sum_{j\in dam} \sum_{t=0}^{t=t_{final}} \left(\boldsymbol{V_{o,gb,j}} + \boldsymbol{V_{o,sb,j}}\right)_t\right] \cdot \frac{\rho_s}{\rho_{b,c}} + \tag{2.37}$$

$$\left[\sum_{\substack{j\in \textbf{reservoir}\\ \textbf{surface},}} \left(\boldsymbol{V_{b,m,j}}\right)_{t=t_{final}} + \sum_{j\in dam} \sum_{t=0}^{t=t_{final}} \boldsymbol{rte} \cdot \left(\boldsymbol{V_{b,ss,j}} + \boldsymbol{V_{b,ms,j}}\right)_t\right] \cdot \frac{\rho_s}{\rho_{b,f}}$$

2.2.6 *Lake Mills gage sediment rating curve testing*

We developed lifetime reservoir sedimentation predictions using the traditional approach of at-a-station sediment rating curves and streamflow duration curves in order to compare to network model outputs. We tested two forms of sediment rating curve equations, regression and physically-based, driven by two forms of streamflow duration curves, measured and modeled, at the LM gage. We compared the lifetime reservoir sedimentation predicted by the rating curves to our network model outputs. The two streamflow duration curves for the LM gage were constructed using: (i) the extent of complete water year observations available at LM gage; and (ii) model outputs from DHSVM over the 84-year dam lifespan. The regression sediment rating curve equations were bedload and suspended load equations developed from streamflow and sediment observations by Curran et al. (2009) (Section 2.3.4). The two physically-based sediment rating curve equations are W&C-2F (equations 2.21a-c and 2.22a-d) for bedload. The

two equations use grain shear stress computed from the two different roughness parameterizations tested in this study ($n_{g,b}$ and $n_{g,E}$; Section 2.2.2.3). For these two bedload rating curves, we also used parameterizations for the LM gage streamflow depth, streamflow velocity, channel width, and channel bed grain sizes presented in previous sections. The channel bed gravel and sand fractions were assumed constant at values computed using the Lake Mills channel bed grain size distributions (Section 2.3.2). Since pre-dam removal measurements of the LM gage local channel slope were not available, we used pre-dam removal Lidar data from Entrix (2009) to estimate the slope as 0.005 (Section S.1.1 of of Beveridge, Istanbulluoglu, et al., 2020).

We integrated the four daily sediment rating curves (one suspended load and three bedload) with both daily streamflow duration curves (measured and modeled) to compute the mean annual sediment loads. Then, we multiplied the annual loads by the reservoir lifespan to get the lifetime reservoir sedimentations. We used observations of LM gage suspended load grain size fractions to develop a linear equation which approximated the proportions of sand (coarse sediment) and silt (fine sediment) in the suspended load as a function of streamflow (Section S.1.3 of Beveridge, Istanbulluoglu, et al., 2020). As with the network model outputs (Section 2.2.5), we adjusted suspended load yields using the reservoir trapping efficiency and converted the transported sediment volumes to deposited sediment volumes using the bulk densities of fine and coarse sediments.

2.3 BACKGROUND OF STUDY AREA

2.3.1 *Elwha watershed regional setting*

The Elwha River watershed model study domain (Figure 2.1) spans the 636 square kilometer (km) watershed upstream of the former Glines Canyon (GC) dam, a 64 m tall concrete arch dam

located 21.6 km upstream of the Elwha River mouth. The GC dam construction was completed in 1927 and removal began in 2011, a project lifetime of ~84 years. The GC dam's reservoir, Lake Mills (LM), had the capacity for 50 million m^3 of storage at the time of construction (East et al., 2015). The study area is within the Olympic National Park, which is protected forested land with minimal human impacts aside from the former dam and reservoir, hiking trails, campsites, and historic homesteads.

The Elwha watershed has a maritime climate with dry summers and wet winters. The watershed elevation ranges from sea level to 2,250 m and mean annual precipitation ranges from 1,400 mm at low elevations to 5,600 mm at high elevations. Precipitation is predominantly rain at elevations below ~1,200 m, but in upper elevations is largely dominated by snow in the winters (Duda et al., 2011). There are small glaciers (total area of <2.1 km^2) in the headwaters of the Elwha watershed that have been rapidly retreating since 1980 (Pelto, 2018). The 5^{th}, 50^{th}, and 95^{th} percentile daily flows at LM gage are 8.9 m^3/s, 29 m^3/s, and 92 m^3/s (USGS, 2016) Geologically, the study area lies within the Olympic Subduction Complex, which is primarily composed of metasedimentary phyllites and schists (Warrick et al., 2011). The Olympic Mountains are considered to be in tectonic steady-state, although rock uplift rates vary spatially across the mountain range (Montgomery & Brandon, 2002). In the Elwha watershed, estimated denudation rates over geologic time range from ~0.3 mm/year at the coast to ~0.6 mm/year in the mountainous uplands (Batt et al., 2001; Brandon et al., 1998). Within the study area, the estimated modern erosion rate is ~0.18 mm/year (Brandon et al. 1998). At the headwaters, uplift rates and the dominant erosional processes that include debris flows, rockfalls, and shallow and deep landslides strongly influence the steep slopes and channel morphology (Warrick et al. 2011). The rapid erosion processes occur mostly during storm events and supply the majority of

sediment to headwater valleys (Buffington & Woodsmith, 2003). The Elwha River is broadly classified as a gravel-bedded river and alternates between narrow bedrock canyons and wider alluvial reaches for much of its length. This alternating boundary composition leads to differential sediment transport behavior along the river (Randle et al., 2015).

2.3.2 *Streamflow, sediment, and channel geometry data*

The streamflow, sediment, and channel geometry measurements used in this study were collected by the United States Geological Survey (USGS) at USGS gaging station number 12044900, Elwha River above Lake Mills (hereinafter referred to as LM gage) (Figure 2.1). The LM gage was located in a bedrock canyon approximately 400 m upstream of LM and 4.3 km upstream of GC dam (Curran et al., 2009). The LM gage drainage area of 513 km^2 is ~81% of the GC dam drainage area. The LM gage is the only long-term gaging station that existed upstream of the GC dam, with data collected from March 1994 to November 2015. Data were collected at LM gage by the USGS as part of their nationwide water monitoring program (USGS, 2016) and for special studies done in anticipation of dam removal (Childers et al., 2000; Curran et al., 2009). The temporal extent and number of samples for streamflow, channel geometry, bedload, channel bed/gravel bar surface distribution, and suspended sediment observations that were used in our study are summarized in Table 2.3.

Table 2.3. Summary of data collected at Lake Mills gage by USGS that was used in this study.

Parameter Description	Date Range and Frequency	No. of obs.	Reference
Streamflow Discharge and Channel Geometry			
Streamflow discharge and mean velocity; channel width, mean depth, cross-sectional area	3/25/1994 – 4/27/1994; Intermittent	11	Childers et al. (2000) (Table 2a)
Streamflow discharge and mean velocity; channel width, mean depth, cross-sectional area	5/11/1994 – 10/13/2011; Intermittent	80	USGS (2016)
Streamflow discharge	3/26/1994 – 5/31/1998, 2/18/2004 – 9/30/2011; Daily	3911	USGS (2016)
Bedload Discharge			
Bedload discharge, streamflow discharge, grain size distribution (0.5 mm - 64 mm)	4/8/1994-7/26/1994; Intermittent	19 (74 across transect)	Childers et al. (2000) (Table 2a)
Bedload discharge, streamflow discharge, grain size distribution (0.5 mm - 64 mm), channel width	11/1/1994-10/15/1997; Intermittent	23 (82 across transect)	Curran et al. (2009) (Appendix C)
Channel bed/Gravel Bar Surface Distribution			
Wetted channel bed sediments	4/9/1994	1 sample (5 across transect)	Childers et al. (2000) (Table 8)
Gravel bar surface	6/21/1994	2	Childers et al. (2000) (Table 9a)
Suspended Sediment Concentration and Discharge			
Suspended sediment concentration and discharge, streamflow discharge, percent sand and silt/clay, sand grain size distribution	3/25/1994-6/21/1994; Intermittent	30	Childers et al. (2000) (Table 4a)
Suspended sediment concentration, Streamflow discharge	4/11/1996-7/31/1997; Intermittent	7	USGS (2016)
Suspended sediment concentration and discharge, streamflow discharge	10/5/1994 – 12/11/1997; Intermittent	39	Curran et al. (2009) (Appendix A)
Suspended sediment concentration and discharge, streamflow discharge, percent sand and mud	11/2/2005 - 11/6/2006; Intermittent	13	Curran et al. (2009) (Table 1)

The observed grain size distributions of the channel bed and one gravel bar were used for computing the model parameters for LM gage channel bed grain diameters ($D_{50,LM}$, $D_{90,LM}$, $D_{mean,LM}$, $D_{gb,LM}$, $D_{S;}$ Section 2.2.2.2) and fractions ($F_{S,LM}$, $F_{gb,LM}$). The bedload discharge grain size distributions were also used to evaluate the channel bed parameters. Each of the 42 bedload discharge observations consisted of multiple samples across the channel transect, totaling to 156 samples. Grain size distributions were measured for all 156 samples and their distribution curves are shown in Figure 2.4. Similarly, the channel bed surface observation consisted of five samples across the channel transect and their distribution curves are shown in Figure 2.4. The grain size distribution curves for the two gravel bars are also included in Figure 2.4. In computing the channel bed grain size parameters, we included all five channel bed surface observations and the one downstream gravel bar observation. We excluded the one upstream gravel bar sample as an outlier since its distribution is relatively coarse compared to the channel surface, downstream gravel bar, and bedload grain size distributions. We interpolated the representative grain sizes and fractions for each respective sample, and then took the average of the six samples as the model parameter. The final model parameters are D_S of 0.93 mm, $D_{50,LM}$ of 9.7 mm, $D_{mean,LM}$ of 12.5 mm, $D_{gb,LM}$ of 13.2 mm, $D_{90,LM}$ of 27.5 mm, $F_{S,LM}$ of 0.37, and $F_{gb,LM}$ of 0.63.

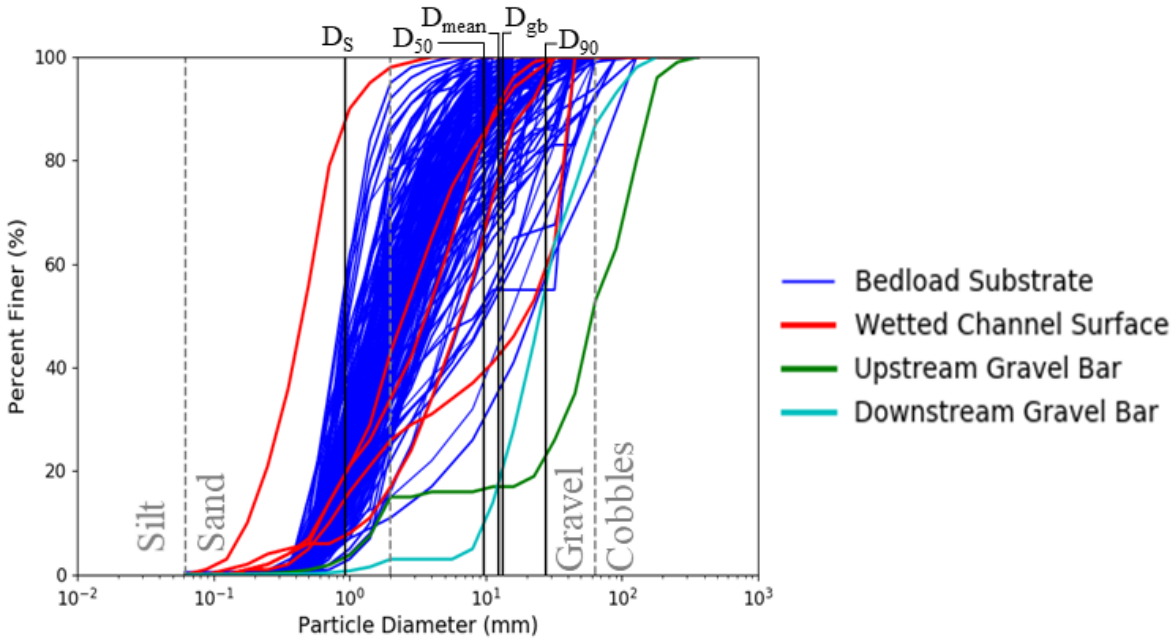

Figure 2.4. Grain size distributions of bed material observations at the Lake Mills gage reach.

We used suspended load grain size distribution data at the LM gage to estimate the median suspended sediment grain size to be 0.25 mm. The corresponding streamflow, suspended sediment load, and suspended sediment grain size distribution data were also used to develop the empirical relationship for predicting the proportion of sand and mud in suspended sediment load as a function of streamflow (Section S.1.3 of Beveridge, Istanbulluoglu, et al., 2020).

2.3.3 *Hydrologic forcing model input data*

The DHSVM input data were a 30 m digital elevation model (DEM) of the Puget Sound region of Washington from Finlayson et al. (2000); soil texture data from NRCS STATSGO2 (Soil Survey Staff, 2016); and vegetation data from the USGS National Land Cover Database 2011 edition (USGS, 2014). We determined the soil depth range from STATSGO2 data and manual calibration to be 0.75 m-3 m. We also specified a minimum channel initiation source area of 1 km^2. We obtained this by developing a slope-area plot with the watershed DEM and estimating the transition from hillslope to fluvial regime to be at a drainage area of ~1 km^2 (Figure S.4 of

Beveridge, Istanbulluoglu, et al., 2020); for background see Montgomery & Dietrich, 1994; McNamara et al., 2006; and Montgomery & Foufoula-Georgiou, 1993). The stream network of the study area includes 293 channel network segments ranging from lengths of 0.042 to 6.68 km.

For the meteorological forcing of DHSVM, we evaluated various gridded historical meteorological datasets (Livneh et al., 2013; Livneh et al., 2015; Salathé et al., 2014; Daly et al., 1994; Skamarock et al., 2008; Kalnay et al., 1996) using open source automated retrieval, preprocessing, and visualization software (Phuong et al., 2019). We compared the datasets to observations of temperature and precipitation in the Elwha watershed, and checked that annual precipitation from the gridded datasets in the LM gage tributary was greater than annual streamflow from observations for the LM gage. The Salathé et al. (2014) dataset best matched observations however it only spanned years 1950-2010, which does not cover the lifespan of the GC dam. Only the Livneh et al. (2013) dataset covered the GC dam lifespan, encompassing data for years 1915-2011. Hence, we developed a hybrid product of the Salathé et al. (2014) and Livneh et al. (2013) datasets (Section S.3 of Beveridge, Istanbulluoglu, et al., 2020) at 1/16 degree spatial resolution (~ 6km grid size) and daily temporal resolution.

2.3.4 *Empirical sediment rating curves and reservoir sedimentation volume estimates*

In our testing of sediment rating curves for estimating reservoir sedimentation, we used sediment rating curve equations from Curran et al. (2009) as the regression-based equations. Curran et al. (2009) developed bedload (Q_B, Mg/day) and suspended load (Q_S, Mg/day) rating curves along with a streamflow (Q, m^3/s) duration curve using USGS LM gage data through 2008. For our study, we developed an updated daily streamflow duration curve from the complete USGS LM gage daily streamflow record (Table 2.3). The sediment rating curve equations from Curran et al. (2009) were developed using empirical ordinary least squares regression, resulting in

$$Q_B = 1.13 \cdot 10^{-2} \cdot Q^{2.41} \quad \text{(no. of observations=44, } r^2\text{=0.77)} \quad (2.38)$$

$$Q_S = 1.08 \cdot 10^{-5} \cdot Q^{4.0} \quad \text{(no. of observations=52, } r^2\text{=0.92)} \quad (2.39)$$

Suspended sediment data collected during water years 2006 and 2007 were also used in Curran et al. (2009) to estimate the mean reservoir trap efficiency of LM to be 0.86. Data from these two years is representative of average streamflow conditions (within 14%; Curran et al., 2009), thus we used this reservoir trap efficiency in our study as a reasonable average estimate. However, we expect that the trap efficiency would vary with changing streamflow and reservoir storage ratios, therefore this static trap efficiency based on two years of data can be considered a limitation of the study.

The LM sedimentation volume at the time of the GC dam removal was estimated by Randle et al. (2015) to be $16.1 \pm 2.4 \cdot 10^6$ m^3. The LM sedimentation composition was also estimated by Randle et al. (2015) to be 44% fine sediment (silt, clay <0.062 mm) with a bulk density of 1.13 g/cm^3; and 56% coarse sediment (sand, gravel, cobble >0.062 mm) with a bulk density of 1.71 g/cm^3. These bulk densities were used in our computations for reservoir sedimentation (2.27) and suspended load transport of mud (2.13).

2.4 RESULTS AND DISCUSSION

2.4.1 *Hydrologic forcing model*

The hydrologic forcing model performance, which was assessed using the Nash-Sutcliffe model efficiency (NSE; Nash & Sutcliffe, 1970) and coefficient of determination (r^2), was acceptable at the monthly and annual timescales but weak at the daily timescale. The NSE is a common metric used to assess the predictive power of hydrologic models. Its value can range from <0 to 1. Generally, a hydrologic model with NSE > 0.5 for a monthly timestep is considered acceptable (Moriasi et al., 2007). The NSE and r^2 over the DHSVM hydrologic model calibration period

(water years 2006-2007) for daily flow were 0.53 and 0.57 and for monthly flow were 0.67 and 0.71. The NSE and r^2 over the evaluation period (water years 1994-1998, 2004-2005 and 2004-2011) for daily flow were 0.30 and 0.43 and for monthly flow were 0.50 and 0.53. The NSE and r^2 over the evaluation period for annual flow were 0.84 and 0.85.

The model performed poorly in predicting extremely high and low streamflows, but performed stronger for moderate, higher frequency flows. The model also overpredicted snow accumulation in most water years. Thus, modeled flow was generally lower than observations in cold months and higher than observations in warm months (i.e., snowmelt period). For flows of 2-40% exceedance probability (EP), the predictions were up to 26% greater than observations. For flows of 40-90% EP the predictions were up to 36% lower than observations. For flows over 90% EP (i.e., extremely low flows) the model predictions were poor, however model performance at extremely low flows has minimal impact on sediment transport predictions. Peak flow magnitudes (~<2% EP) were underrepresented by up to 54%, which thereby misrepresented peak sediment yields.

The limitations in the model performance are primarily attributed to the meteorological forcing data (Section S.3 of Beveridge, Istanbulluoglu, et al., 2020). The gridded meteorological datasets we used are generally more appropriate for capturing the average regional climatology rather than isolated extreme events. The datasets are gridded at a relatively low resolution (~6 km) compared to the scale of complexities in the terrain and hydroclimatology of the Elwha watershed. They largely misrepresented the regional temperature and precipitation lapse rates (Minder, Mote, & Lundquist, 2010). They also did not adequately capture regional atmospheric river events (Neiman, Ralph, Wick, Lundquist, & Dettinger, 2008) that are expected to be responsible for large, short pulses of streamflow and sediment discharge. Future improvements

in gridded hydrometeorology datasets are expected to significantly improve hydrology model performance, especially for >2% EP flood events and snow accumulation.

2.4.2 *Sediment load estimates from rating curves at Lake Mills gage*

Lifetime reservoir sediment yields predicted from at-a-station sediment rating curves driven by measured streamflow were primarily influenced by suspended load yields and peak streamflow discharges (Figure 2.5; Table 2.4, top section). The rating curve total reservoir sediment yields exceeded the measured range largely because the rating curves do not take sediment supply limitations into account. At ≤2% exceedance probability (EP), the suspended load rating curve exceeded the bedload discharge rating curves (Figure 2.5 inset). Similarly, rating curve suspended load yields dominated the total reservoir sedimentation predictions (suspended load yield was 73-84% of total yield) and caused the rating curve predictions to largely exceed measurements (Table 2.4, top section). Most of the suspended load rating curve yield was mud, which exceeded the measured reservoir mud fraction estimate (upper end of range) by 51%. The sand fraction of the suspended load rating curve yields was towards the upper end of the measured reservoir sand volume estimate (measured reservoir sand estimate was bedload and suspended load combined). Also at ≤2% EP, bedload yield predictions from the equation of W&C-2F with $n_{g,b}$ were highest followed by predictions from the regression equation and then W&C-2F with $n_{g,E.}$ (Figure 2.5 inset). Similarly, rating curve total reservoir sediment yields followed the order of the bedload rating curves at peak flows (Table 2.4, top section). The rating curve predictions of gravel from W&C-2F with $n_{g,b}$ exceeded the measured reservoir gravel fraction estimated range while the W&C-2F with $n_{g,E}$ prediction was below the estimated range.

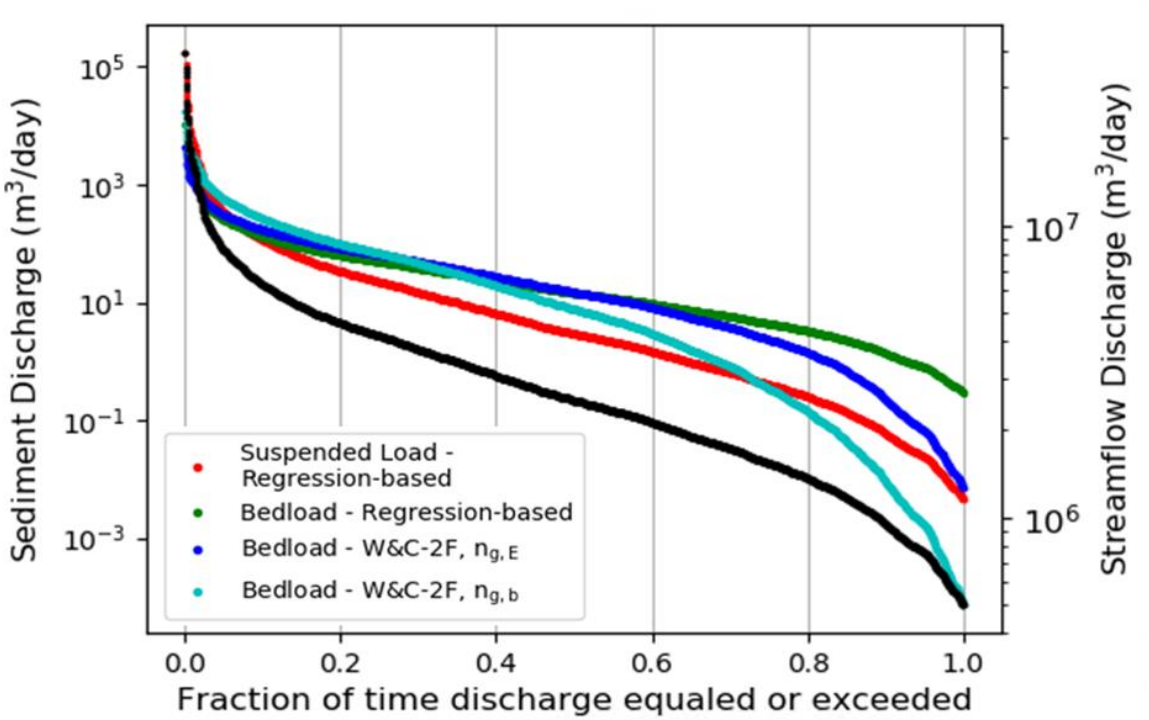

Figure 2.5. Daily measured streamflow duration curve (black curve; right side y-axis) and corresponding at-a-station sediment rating curves (red, green, blue, and cyan curves; left side y-axis) for Lake Mills gage.

Table 2.4. Lifetime reservoir sedimentation volume predictions from at-a-station sediment rating curves at Lake Mills gage using measured and modeled streamflow

Description	**Reference**	**Total Load** (10^6 m^3)	**Bedload** (10^6 m^3)		**Suspended Load** (10^6 m^3)		**% coarse**
			Gravel	**Sand**	**Sand**	**Mud**	
Measured estimate (Randle et al., 2015)		*16.1 (13.7-18.5)*	*3.0 (2.4-3.6)*[1]	*6.0 (4.7-7.3)*[1]		*7.0 (5.6-8.4)*	*56*
Measured streamflow duration curve							
Regression-based[2]	Curran et al. (2009)	23.7	3.9		7.1	12.7	46
W&C-2F n_E	Wilcock & Crowe (2003) (bedload); Curran et al. (2009) (suspended load)	23.5	1.7	2.0	7.1^2	12.7^2	46
W&C-2F n_b		27.2	3.8	3.6	7.1^2	12.7^2	53
Modeled streamflow duration curve							
Regression-based[2]	Curran et al. (2009)	12.0	3.7		2.8	5.5	54
W&C-2F n_E	Wilcock & Crowe (2003) (bedload); Curran et al. (2009) (suspended load)	12.4	1.9	2.3	2.8^2	5.5^2	56
W&C-2F n_b		16.0	3.9	3.9	2.8^2	5.5^2	66

Notes

1. In Randle et al. (2015), the "coarse fraction" consisting of boulders, cobble, gravel, and sand were reported together as $9.0 \pm 1.9 \times 10^6$ m^3. It was also reported that 1/3 of the coarse fraction was boulders, gravel and cobbles and 2/3 was sand. In this table, we report the result of applying these fractions to the estimated coarse fraction volume as well as the error range ($\pm 1.9 \times 10^6$ m^3).
2. Suspended load predictions are from the regression-based approach but are added to the bedload predictions in order to compared to the total predicted lifetime sediment load.

Table 2.5. Network model parameterizations and reservoir sedimentation volume results for 28 model instances. Instances are primarily grouped by rated, with λ_{ss}, and λ_{ms} systematically increased in each group of rated. Volumes in bold and gray are within the uncertainty range of measured estimates for reservoir sedimentation.

Instance	**rate$_d$**	**λ_{ss}**	**λ_{ms}**	**Total Gravel (10^6 m^3)**	**Total Sand (10^6 m^3)**	**Total Mud (10^6 m^3)**	**Total Sediment (10^6 m^3)**	**% coarse**
Measured Estimate (Randle et al., 2015)				**3.0 (2.4-3.6)**	**6.0 (4.7-7.3)**	**7.0 (5.6-8.4)**	**16.1 (13.7-18.5)**	**56**
1	0.18	0.010	0.025	**2.7**	4.3	**6.6**	13.6	52
2	0.18	0.015	0.025	**3.1**	**4.7**	**5.8**	**13.7**	57
3	0.18	0.030	0.025	**2.5**	4.3	**6.4**	13.2	52
4	0.18	0.030	0.075	**2.4**	3.8	**5.9**	12.1	51
5	0.20	0.010	0.025	**3.5**	4.6	**7.0**	**15.1**	54
6	0.20	0.010	0.050	**3.5**	**5.1**	**6.4**	**15.1**	57
7	0.20	0.010	0.075	**3.5**	**4.7**	**7.2**	**15.3**	53
8	0.20	0.015	0.025	**3.3**	**5.3**	**6.6**	**15.1**	57
9	0.20	0.015	0.050	**3.3**	**5.2**	**6.5**	**15.0**	57
10	0.20	0.015	0.075	**3.3**	**5.2**	**6.5**	**15.0**	57
11	0.20	0.025	0.025	**2.8**	**4.7**	**7.2**	**14.7**	51
12	0.20	0.025	0.050	**2.8**	4.5	**7.0**	**14.4**	51
13	0.20	0.025	0.075	**2.7**	4.6	**7.2**	**14.5**	50
14	0.20	0.030	0.025	**2.7**	4.6	**7.2**	**14.4**	50
15	0.20	0.030	0.050	**2.7**	4.6	**7.0**	**14.3**	51
16	0.20	0.030	0.075	**2.8**	**4.8**	**7.5**	**15.1**	50
17	0.22	0.010	0.025	3.7	**5.1**	**7.8**	**16.6**	53
18	0.22	0.010	0.050	3.7	**5.6**	**6.9**	**16.2**	57
19	0.22	0.010	0.075	**3.6**	**5.1**	**7.7**	**16.3**	53
20	0.22	0.015	0.025	**3.4**	**5.2**	**8.1**	**16.7**	51
21	0.22	0.015	0.050	**3.4**	**5.7**	**7.1**	**15.8**	58
22	0.22	0.015	0.075	**3.4**	**5.2**	**8.0**	**16.6**	52
23	0.22	0.025	0.025	**3.0**	**5.2**	**8.1**	**16.3**	50
24	0.22	0.025	0.050	**3.0**	**5.1**	**7.8**	**15.9**	51
25	0.22	0.025	0.075	**2.9**	**4.9**	**7.6**	**15.3**	51
26	0.22	0.030	0.025	**2.8**	**5.0**	**7.9**	**15.7**	50
27	0.22	0.030	0.050	**2.9**	**5.5**	**6.9**	**15.2**	55
28	0.22	0.030	0.075	**2.9**	**5.2**	**8.1**	**16.2**	50

Lifetime reservoir sediment yields predicted from the at-a-station sediment rating curves driven by modeled streamflow (Figure 2.6; Table 2.4, bottom section) were 50-59% lower than the yields from curves driven by measured streamflow. The rating curve total reservoir sediment yield was within the measured range when bedload was computed using W&C-2F with $n_{g,b}$., however lower than the measured range for the other two cases (regression and W&C-2F with $n_{g,E}$). The lower rating curve sediment yields are mainly because suspended load rating curve peak values from modeled streamflow are substantially less than those from measured streamflow. As previously discussed (Section 2.4.1), the hydrologic forcing model substantially underpredicted peak flows. The yield from the suspended load rating curve using modeled streamflow had mud and sand fraction volumes below the measured reservoir mud and sand volume estimates (Table 2.4, lower portion). The yields from the bedload rating curve using modeled streamflow marginally changed compared to those driven by measured streamflow, and rating curve gravel yields were again outside the ranges estimated from measurements. Overall, the limitations and uncertainties in using the streamflow rating curve and at-a-station sediment rating curves were consistent with their known limitations (e.g., Vaughan et al., 2017). This verified the need for our network model approach incorporating distributed sediment supply and transport dynamics.

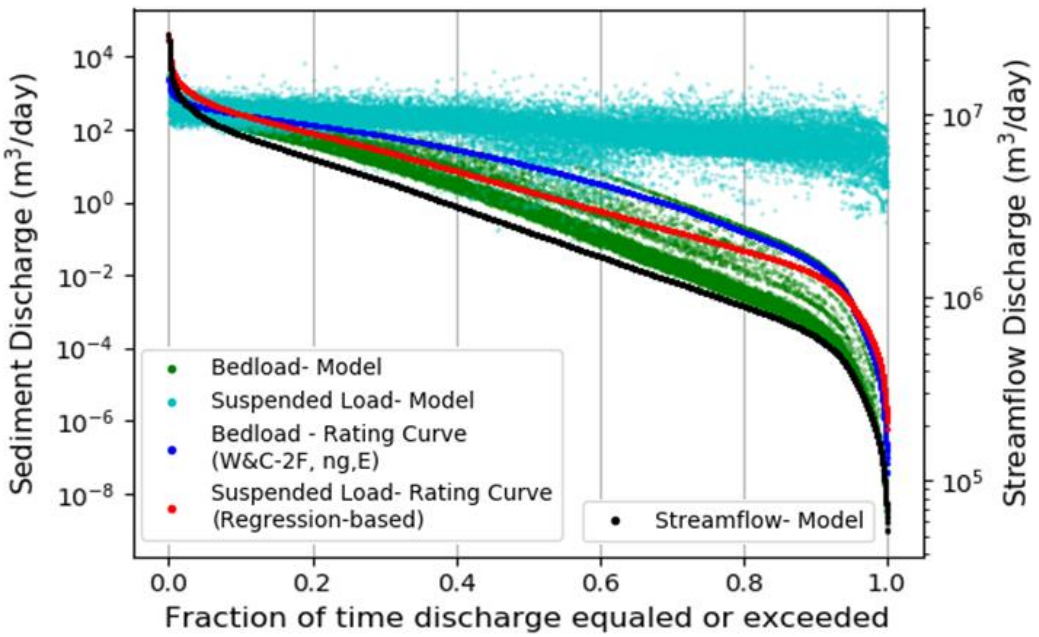

Figure 2.6. Daily modeled streamflow duration curve (black line; right side y-axis) and corresponding at-a-station sediment rating curves (blue and red curves; left side y-axis) for Lake Mills gage. Also shown are network model sediment outputs (green and cyan dots, left side y-axis) plotted against corresponding modeled streamflow exceedance probability for daily outputs at the network segment containing Lake Mills gage.

2.4.3 *Network Sediment Model*

2.4.3.1 Predicted volumes of lifetime reservoir sedimentation and model parameterization

Overall the results showed that the network model performance in predicting the measured total reservoir sedimentation and its estimated grain size volume fractions (particularly gravel and mud) was superior compared to the at-a-station sediment rating curves. Along with these improved sediment yields, the network model provided spatially and temporally distributed information allowing for inquiry and understanding of the physical system beyond the sediment yields at the outlet. Of the 28 network model instances, 25 were within the uncertainty range of the measured total reservoir sedimentation ($13.7 \cdot 10^6$ m^3-$18.5 \cdot 10^6$ m^3; Randle et al., 2015) (Table 2.5; Figure 2.7). The remaining three instances were within 12% of the lower end of the

measured uncertainty range. The model-predicted mud volumes all fell within the uncertainty range of the measured reservoir mud fraction estimate ($5.6 \cdot 10^6$-$8.4 \cdot 10^6$ m^3). The model-predicted gravel volumes mostly fell within uncertainty range of the measured reservoir gravel fraction estimate ($2.4 \cdot 10^6$-$3.6 \cdot 10^6$ m^3), except two which were within 1% of the range. The model-predicted sand volumes mostly fell within the uncertainty range of the measured reservoir sand fraction estimate ($4.7 \cdot 10^6$-$7.3 \cdot 10^6$ m^3). However, all the model-predicted sand volumes fell below the estimated sand fraction ($7.0 \cdot 10^6$ m^3) and eight were below the estimated uncertainty range. Seven of the low sand predictions were within 9% of the uncertainty range and one was 19% lower.

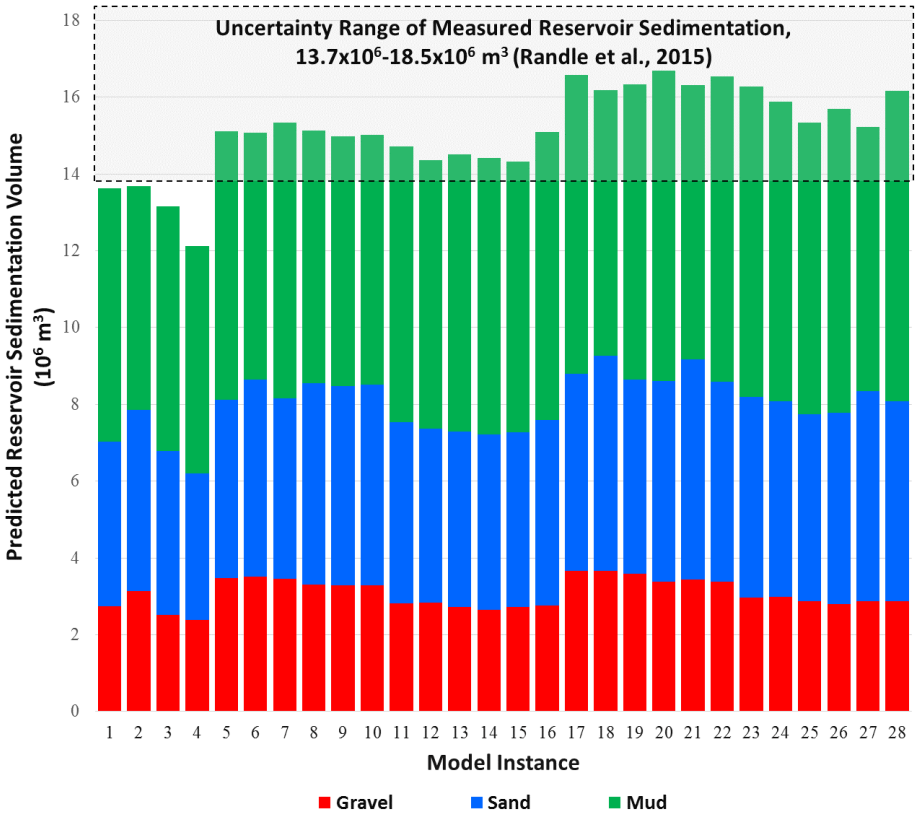

Figure 2.7. Network model lifetime reservoir sedimentation volume predictions of the 28 model instance. Model instance numbers correspond to Table 2.5.

As expected, the model-predicted total reservoir sedimentation volumes generally correlated with the soil production rates in the hillslope mass wasting algorithm ($rate_d$; Table 2.5). The three model predictions below the measured total volume all had a soil production rate of 0.18 mm/year and had the lowest modeled sand fraction volumes. Although in our limited sensitivity analysis we did not vary the mass wasting deposit grain-size composition (α_{gb}, α_s, α_{ms}), average frequency ($\bar{t_L}$), and sand and mud fractions directly added into suspension (λ_{mw}), their constant values were important to model performance. Further research is needed to provide guidance on the mass wasting deposit parameter value estimation and/or improved model representation of the relevant physical processes.

The network model performance was also sensitive to parameterizations that dictated suspended load: λ_{ss}, λ_{ms} and F_{ssm} in the suspended load equations and λ_{mw} in the mass wasting algorithm. The order of magnitudes for λ_{ss}, $\lambda_{ms,}$ and λ_{mw} prevented suspended sediment transport from being anomalously high. Without the four parameters (i.e., setting them all equal to one), the model essentially transported all suspended load as soon as it was supplied to the watershed. This caused nearly all sand to be transported as suspended load and thus the bedload consisted of nearly all gravel. This, furthermore, led to excessive gravel accumulation on shallow-sloped channels and caused the model to underpredict the gravel deposited in the reservoir. Although the volumes of sand and mud deposited in the reservoir fell within the estimated uncertainty ranges without incorporation of these four parameters (λ_{ss}, λ_{ms}, λ_{mw}, F_{ssm}), the overall model processes and results were physically unrealistic. An increase in λ_{ss} correlated with a decrease in the gravel fraction of the predicted reservoir sedimentation volume (Table 2.5). There was not a clear pattern in the model results from varying λ_{ms}, suggesting that this parameter is relatively insensitive in the range we used and could be tested more broadly in future work.

2.4.3.2 Interannual reservoir sedimentation variability

In addition to the prediction of lifetime reservoir sedimentation volume, reservoir operations and maintenance can also benefit from the understanding of interannual sediment loads and their correlation with streamflow. This is helpful, for example, in predicting ongoing reservoir storage loss and developing reservoir sediment flushing routines. Here, we discuss interannual sediment and streamflow yields from model instance 23 as an example of model performance. We use model instance 23 for these and subsequent results sections (2.4.3.3 and 2.4.3.2) since instance 23 was one of the strongest performing predictions of the modeled reservoir sedimentation volumes. For model instance 23, the range of variability in interannual total sediment loads was ~2.1 times the mean, and in the grain size fraction volumes was 1.7-3.6 times the respective means (Figure 2.8). Patterns of annual magnitude of streamflow and total sedimentation volume were poorly correlated (r^2=0.19). Correlation between gravel volumes and the other fractions were poor (r^2=0.27 for sand, r^2=0.11 for mud); however, correlation between sand and mud fractions were strong (r^2=0.84). The cases with poor correlation were reasonable considering the network model's distributed and stochastic nature of sediment supply as well as the time-lag in sediment transport of different grain size fractions throughout the watershed.

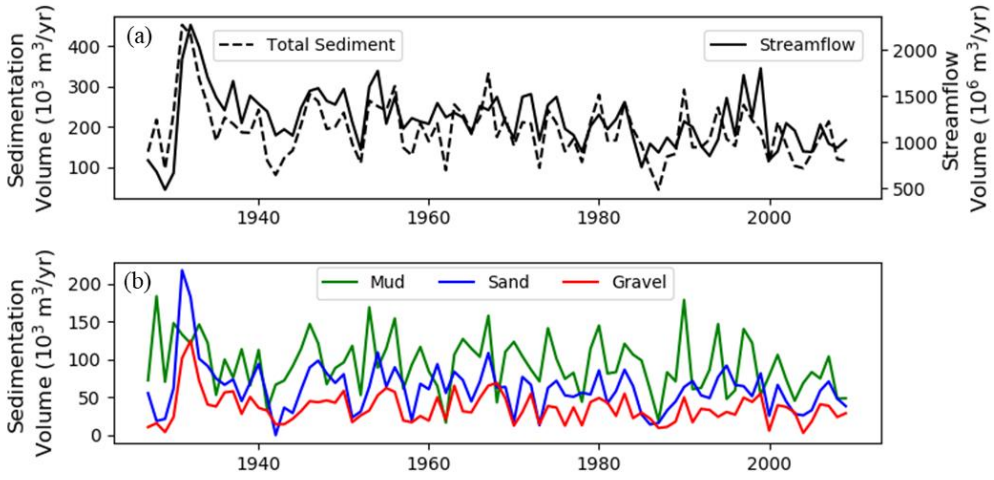

Figure 2.8. Predicted annual reservoir inflows for model instance 23.

(a) Total sedimentation (left y-axis) and streamflow (right y-axis) volumes. (b) Mud, sand and gravel sedimentation volumes.

The predicted annual inflow volumes of streamflow and sediment were:

- total sediment: mean of $190 \cdot 10^3$ m^3, range of $44 \cdot 10^3$ - $450 \cdot 10^3$ m^3 ($406 \cdot 10^3$ m^3 difference)
- gravel: mean of $36 \cdot 10^3$ m^3, range of $3 \cdot 10^3$ -$130 \cdot 10^3$ m^3 ($127 \cdot 10^3$ m^3 difference)
- sand: mean of $62 \cdot 10^3$ m^3, range of 0-$220 \cdot 10^3$ m^3 ($220 \cdot 10^3$ m^3 difference)
- mud: mean of $94 \cdot 10^3$ m^3, range of $17 \cdot 10^3$ -$180 \cdot 10^3$ m^3 ($163 \cdot 10^3$ m^3 difference)
- streamflow: mean of $1{,}245 \cdot 10^6$ m^3, range of $486 \cdot 10^6$ -$2{,}275 \cdot 10^6$ m^3 ($1{,}789 \cdot 10^6$ m^3 difference)

2.4.3.3 Sediment rating curve comparison at Lake Mills gage

Suspended load from the network model was driven by suspended sediment supply rather than the hydrologic forcing. Compared to the suspended sediment rating curve driven by modeled streamflow (Figure 2.6), the network model suspended sediment predictions at LM gage are dramatically less sensitive to streamflow. It is notable that at peak streamflow (~<2% EP),

suspended load from the network model did not steeply increase as the suspended load rating curve from the regression-based equation. This is because the network model accounts for sediment supply limitations.

As expected, the network model bedload predictions were sensitive to the hydrologic forcing (Figure 2.6) due to the dependence of the W&C-2F equations on shear stress. The scatter in the network model bedload predictions relative to the bedload rating curve is largely due to the difference in gravel and sand fractions on the channel bed. The bed fractions evolve in the network model however not in the bedload rating curve. We expect that more advanced representation of channel geomorphic conditions in network model (e.g., dynamic slope and grain sizes, advanced active layer dynamics) would further reflect the dynamicity of bedload.

2.4.3.4 Network sediment dynamics

In watershed management, spatial and temporal understanding of network-wide sediment dynamics is also valuable in addition to long-term yields. For example, identifying locations and time periods of high sediment supply and/or transport can help in planning more effective monitoring and mitigation measures. To serve this interest, our network sediment model allows for intercomparison of sediment dynamics for different segments, years, grain size fractions, and sediment volumes (Figure 2.9, example of model instance 23). Our ability to analyze network-wide model behavior also allowed us to verify that the simulated sediment transport and storage dynamics were physically realistic and reflected the geomorphology of the study area as it has been described in previous studies (e.g., Warrick et al., 2011).

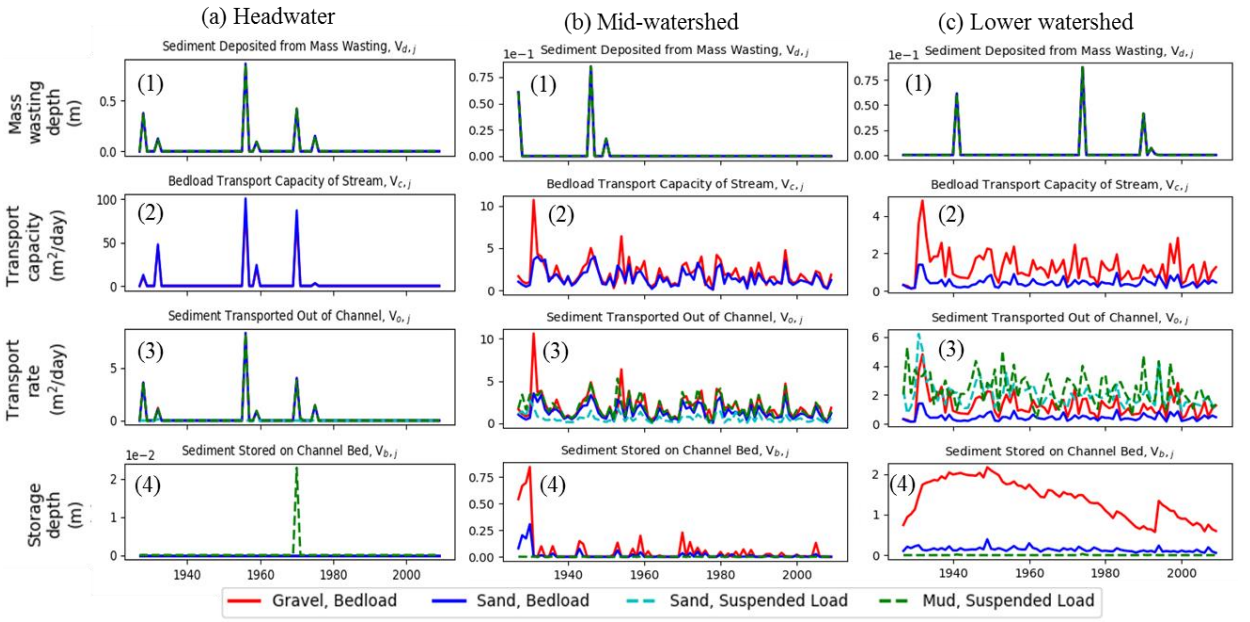

Figure 2.9. Plots of annual sediment volumes for network model instance 23 at three segments in the study area channel network: (a) headwater; (b) mid-watershed; (c) lower watershed. The locations of the segments are indicated in Figure 2.1.

The stochastic nature of the model's mass wasting algorithm is reflected in the mass wasting volume depth and frequency at different channel segments (Figure 2.9, row 1). The differences in suspended load and bedload behavior (e.g., supply and transport limitations) at a given location and over time and space are reflected in the bedload transport capacity (Figure 2.9, row two), volumes transported out (Figure 2.9, row three), and volumes stored on the bed (Figure 2.9, row four). Mass wasting deposit volumes (i.e., sediment supply) are conserved in the volume transported out and/or stored on the bed at each respective segment. Sediment volumes transported out of segments show that the relative magnitude of suspended load sand and mud increased relative to bedload gravel and sand moving downstream (Figure 2.9, from a to c). Thus, the model captured how suspended load transported relatively rapidly with streamflow and compounded in higher order streams. Bedload, on the other hand, transported relatively slowly

and was more often stored on the channel bed, particularly in low slope reaches of the channel network. Sediment volumes stored on the channel bed showed that the bed—primarily its gravel fraction—was generally more dynamic moving downstream, and bedrock streams (i.e., no sediment stored on the channel bed) were more common in upper reaches. There was little channel bed storage of mud which suggested that mud was largely supply-limited. By contrast, bed storage of gravel and sand varied in time and space, showing that these larger grain size fractions varied between being supply- and transport- limited.

2.4.3.5 Primary model limitations and future work recommendations

Because of the partial transport limitations of gravel and sand (Section 4.3.4), we expect that their model-predicted volumes would have been closer to their measured sedimentation estimates (i.e., higher) if the forcing hydrology model had improved representation of peak streamflow events (Section 4.1). The multipliers we incorporated into the suspended sediment modeling approach to represent gravel shielding and grain size partitioning of sand on the bed ($\lambda_{ss,}\ \lambda_{ms,}\ F_{ssm}$) as well as the entrainment from mass wasting processes (λ_{mw}) were significant simplifications of the physical processes. However, these factors were critical to producing suspended load predictions at the LM gage that were not anomalously high compared to observations (Section 4.3.1). The need for these multipliers highlights future work opportunities to improve upon our relatively simplistic approach of combining bedload and suspended load dynamics at the network scale as well as the partitioning of sand transport between bedload and suspended load. This future work would need to encompass improved process representation of their combined deposition, storage, erosion, and transport dynamics. Additional processes not included in our model that could be incorporated in future work would be accounting for the lateral exchange between sediment in the channels and floodplains (e.g., Lauer et al., 2016) as well as the channel bed active surface layer (e.g., Gasparini et al., 2004; Czuba, 2018).

The stochastic sediment supply algorithm was valuable for emulating the steady-state erosion and episodic mass wasting events of the study area. However, our model representation of network sediment supply was a first order approximation which can be improved with process-based hillslope mechanisms. These improvements include spatially explicit parameterizations for hillslope mass wasting (e.g., Benda, Lee; Dunne, 1997a; Czuba et al., 2017; Strauch et al., 2018) and additional sediment supply processes such as erosion. From a management perspective, it would also be beneficial to demonstrate the locations of dominant sediment supply as well as the connectivity of the hillslope sediment supply deposits to downstream sinks (e.g., Czuba, 2018; Schmitt et al., 2016, 2018b, 2018a).

2.5 CONCLUSIONS

Our watershed network sediment modeling approach and findings address an unmet need in applied engineering and management of predicting sediment yields in mountainous watersheds. Our model was developed by integrating empirical datasets with modeling approaches from hydrology, geomorphology, and sediment transport research fields. Compared to at-a-station sediment rating curves, our network model showed strong improvement in predicting short- and long-term reservoir sediment yields as well as understanding spatial and temporal dynamics of watershed sediment processes.

The two key novelties of our network sediment modeling approach were (1) combining bedload and suspended load transport modeling and (2) using streamflow forcing from a physically-based distributed hydrology model. We also incorporated a simplified stochastic, semi-distributed hillslope mass wasting algorithm which can be replaced by process-based hillslope input mechanisms. In taking these unprecedented steps to network sediment modeling, we illuminated both synergies and gaps in modeling physical processes that are critical to

watershed sediment yields over engineering and management timescales. We demonstrated the particular needs for improved understanding and modeling of (1) landslide sediment deposit volume-frequency, grain size fraction distributions, and the immediate fate of each grain size fraction (e.g., deposited on channel bed, transported in suspension); (2) combined bedload and suspended load transport dynamics; (3) improved partitioning of sand between bedload and suspended load; and (4) hydrologic modeling of peak flow events. These improvements would likely help to address the underprediction of sand in the network model. Improvements would also reduce the uncertainty due to the simplifying model parameters that we introduced in modeling suspended load (λ_{ss}, λ_{sm}, λ_{mw}, F_{ssm}). We intend to motivate and inform future work in these specific research areas as well as interdisciplinary network sediment modeling approaches. These advances can further serve applied engineering and management needs for better understanding of watershed sediment yield predictions under increasing environmental change.

Acknowledgements

This work presented in this paper was funded by: The National Science Foundation (NSF) Graduate Research Fellowship Program under Grant No. DGE-1762114; The Office of Energy Efficiency and Renewable Energy, U.S. Department of Energy, under Award Number DE-EE0006506 and the Hydro Research Foundation (HRF); and The Department of the Interior Northwest Climate Adaptation Science Center (NWCASC) through a graduate fellowship to the first author. Co-authors (Istanbulluoglu, Bandaragoda, Pfeiffer) acknowledge funding from NSF ICER 1663859. Any opinions, findings, and conclusions or recommendations expressed in this material are those of the authors and do not necessarily reflect the views of the NSF, the NWCASC, the HRF, nor the United States Government and any of its agencies.

The authors thank Christopher Curran, Andy Ritchie, Amy East, and Jonathan Warrick from USGS for providing data and further information about the Elwha watershed. The authors also thank Joanna Crowe Curran and David Gaeuman for their advice on bedload transport modeling. Finally, the authors thank Rafael Schmitt and anonymous reviewers whose comments have greatly improved this manuscript.

Notation

$\boldsymbol{a_H}$	empirically-derived hydraulic geometry constant for calculating *H*
$\boldsymbol{a_U}$	empirically-derived hydraulic geometry constant for calculating *U*
$\boldsymbol{b_H}$	empirically-derived hydraulic geometry exponent for calculating *H*
$\boldsymbol{b_U}$	empirically-derived hydraulic geometry exponent for calculating *U*
$\boldsymbol{c_{n_g}}$	empirically-derived constant for calculating n_g
C_{ssm}	depth-averaged concentration of *ss* and *ms* in water column [ML^{-3}]
CA_L	local contributing area of a segment *j* [L^2]
CA_T	total contributing area of a segment *j* [L^2]
$\boldsymbol{d_{n_g}}$	empirically-derived exponent for calculating n_g
ds	downstream segment of a given *j*
D_{gb}	median grain size of *gb* on channel bed surface [L]
D_i	median grain size of *i* on channel bed surface [L]
D_{mean}	mean grain size on channel bed surface [L]
D_{ss}	median Q_S grain size [L]
D_{ss*}	dimensionless D_{ss}
D_S	median grain size of sand (*ss* and *sb*) on channel bed surface [L]
$D_{x,j}$	represents D_{50}, D_{90}, D_{mean}, or D_{gb} in equation 2.33 [L]

D_{50}	median (50^{th} percentile) grain size on channel bed surface [L]
D_{90}	90^{th} percentile grain size on channel bed surface [L]
E_{ms}	erosion rate of mud (*ms*) [$ML^{-2}\ T^{-1}$]
E_{ss}	erosion rate of suspended sand (*ss*) [$ML^{-2}\ T^{-1}$]
F_i	proportion of *i* on the channel bed surface
F_{gb}	proportion of gravel (*gb*) on the channel bed surface
F_s	proportion of sand (*s*) on the channel bed surface
F_{ssm}	proportion of sand and silt (*s* + *ms*) on the channel bed surface
g	acceleration due to gravity [LT^{-2}]
gb	gravel (bedload) grain size fraction
H	streamflow depth [L]
H_{bf}	bankfull H [L]
H_{50}	median H of a segment [L]
i	grain size fraction and mode of transport classification
$INT(Z_R)$	integral of the Q_S concentration profile in the water column
j	channel network segment
k	von Kármán constant, 0.41
l	segment length [L]
ms	mud (suspended load) grain size fraction
n	channel roughness
$\bar{\boldsymbol{n}}$	depth-weighted mean of n
$\boldsymbol{n}_*$	n normalized by $\bar{\boldsymbol{n}}$, also computed generically by equation 2.38
n_g	channel grain roughness

$n_{g,b}$	n_g computed from equation of Bray (1979) (equation 2.36)
$n_{g,E}$	n_g developed in this study (for Elwha watershed) (equation 2.37)
o	segment Strahler order number
q_{bi}	bedload transport rate of i per unit width [L^2T^{-1}]
Q	streamflow discharge [L^3T^{-1}]
Q_B	bedload discharge [L^3T^{-1}]
Q_S	suspended load discharge [L^3T^{-1}]
$rate_d$	denudation rate [LT^{-1}]
rte	reservoir trap efficiency
Re_p	Reynold's number for sediment
R_H	channel hydraulic radius [L]
S	slope of channel bed
S_{ms}	settling rate of *ms* [$ML^{-2}\ T^{-1}$]
S_{ss}	settling rate of *ss* [$ML^{-2}\ T^{-1}$]
s	sand (bedload and suspended load) grain size fraction
sb	sand (bedload) grain size fraction
sg	ratio of sediment to water density, 2.65
ss	sand (suspended load) grain size fraction
t	model timestep (daily) [T]
$t_{L,j}$	time-lag in between mass wasting events for a given j [T]
$\bar{\boldsymbol{t}}_{\boldsymbol{L}}$	network-wide mean time-lag in between mass wasting events ($t_{L,j}$, for all j) [T]
$\boldsymbol{u}_*$	shear velocity [LT^{-1}]
U	streamflow velocity [LT^{-1}]

ν kinematic viscosity of water [L^2T^{-1}]

ν_{ms} falling velocity of mud (*ms*) [LT^{-1}]

ν_{ss} settling velocity of suspended sand (*ss*) [LT^{-1}]

$V_{b,i}$ sediment volumes on channel bed for *i=gb, s, ms* [L^3]

$V_{c,i}$ bedload transport volume capacity for *i=gb, sb* [L^3]

$V_{d,i}$ sediment volumes deposited by mass wasting for *i=gb, s, ms* [L^3]

$V_{o,i}$ sediment volumes transported out of *j* for *i=gb, sb, ss, ms* [L^3]

$V_{w,j}$ water volume for *j*

W channel width [L]

W^*_i dimensionless bedload transport parameter of *i*

z_b boundary layer thickness [L]

Z_R Rouse number

α_{gb} Proportion of gravel (*gb*) in mass wasting volume ($V_{d,j}$)

α_s Proportion of sand (*s*) in mass wasting volume ($V_{d,j}$)

α_{ms} Proportion of mud (*ms*) in mass wasting volume ($V_{d,j}$)

Δt span of each model iteration (*t*)

ξ geomorphic and fluvial state matrix

λ_{ms} fraction of erodible mud (*ms*) on the channel bed ($V_{b,ms}$)

λ_{mw} fraction of sand (*s*) and mud (*ms*) in mass wasting volume that are automatically added into suspension

λ_{ss} fraction of erodible sand of suspended load size (*ss*) on the channel bed ($V_{b,ss}$)

ρ density of water [ML^{-3}]

$\rho_{b,c}$ bulk density of coarse sediment [ML^{-3}]

$\rho_{b,f}$	bulk density of fine sediment [ML^{-3}]
τ	boundary shear stress [$ML^{-1}\ T^{-2}$]
$\boldsymbol{\tau}^*_{\boldsymbol{bf}}$	bankfull Shields stress [$ML^{-1}\ T^{-2}$]
$\boldsymbol{\tau}^*_{\boldsymbol{bf,x}}$	represents $\boldsymbol{\tau}^*_{\boldsymbol{bf,90}}$, $\boldsymbol{\tau}^*_{\boldsymbol{bf,sm}}$, or $\boldsymbol{\tau}^*_{\boldsymbol{bf,g}}$ in equation 2.33 [$ML^{-1}\ T^{-2}$]
$\tau_{c,ms}$	critical shear stress of *ms* [$ML^{-1}\ T^{-2}$]
τ_g	grain shear stress [$ML^{-1}\ T^{-2}$]
τ_{ri}	reference $\boldsymbol{\tau}$ of *i* [$ML^{-1}\ T^{-2}$]
$\boldsymbol{\tau}_{\boldsymbol{r_{mean}}}$	τ_{ri} for mean grain size on channel bed (D_{mean}) [$ML^{-1}\ T^{-2}$]
$\boldsymbol{\tau}^*_{\boldsymbol{r_{mean}}}$	dimensionless $\boldsymbol{\tau}_{\boldsymbol{r_{mean}}}$

Chapter 3. ESTIMATING IMPACTS OF DAM DEVELOPMENT AND LANDSCAPE CHANGES ON SUSPENDED SEDIMENT CONCENTRATIONS IN THE MEKONG RIVER BASIN'S '3S' TRIBUTARIES

Note: This chapter has been published mostly in its current form in the ASCE *Journal of Hydrologic Engineering* (Beveridge, Hossain, & Bonnema, 2020). Used with permission from ASCE.

Abstract: The Mekong River Basin (MRB) is undergoing rapid dam development which is altering the river suspended sediment concentration (SSC). In this study, we used satellite remote sensing records spanning 31 years to detect SSC changes (SSC prediction r^2=0.78, RMSE=21.2 mg/L) due to dam development. We focused on the '3S basin' of the MRB. We also used satellite data on nighttime lights, which reflects human settlement patterns, and land cover to explain SSC patterns. Our technique allowed for quantification of SSC changes due to dam construction (e.g., +120 mg/L near basin outlet), reservoir sediment trapping (e.g., -108 mg/L), deforestation, and human settlement (e.g., +117 mg/L near impacts). Our technique also demonstrated how the SSC of the 3S rivers have compared to that of the Mekong mainstem over time (e.g., from ~13% to 100% greater). Our comprehensive analyses of SSC records with dam development indicate that SSC changes will continue with ongoing dam and landscape development in the MRB. From a hydrologic perspective, SSC monitoring will be imperative for effective sediment and water management. Our satellite-based approach answers critical sediment needs of improved monitoring and adaptive management throughout the MRB and

other global locations for practitioners who are engaged in real-world management of their river basins.

3.1 INTRODUCTION

The Mekong River Basin (MRB; Figure 3.1) is a complex environmental and social system that spans six countries, hosts rich biodiversity, and has a population of approximately 70 million people. Suspended sediment is critical to the highly productive ecosystem, fisheries, and agriculture of the MRB. However, rapid dam development in the MRB is significantly altering suspended sediment transport. If all planned MRB dams are constructed and no reservoir sediment management measures are taken, it is estimated that dams will trap 96% of the basin's suspended sediment yield (Kondolf, Rubin, & Minear, 2014). Valuable nutrient loads of nitrogen and phosphate that are carried by suspended sediment are also estimated to reduce by 47-62% (Thanapon Piman & Shrestha, 2017). Thus, although dams provide numerous benefits such as hydropower and irrigation, they are a major threat to the MRB environment, food security, and vast number of natural resource-based livelihoods. Furthermore, the trapping of sediment in reservoirs decreases the lifespan of dams and compromises the intended benefits.

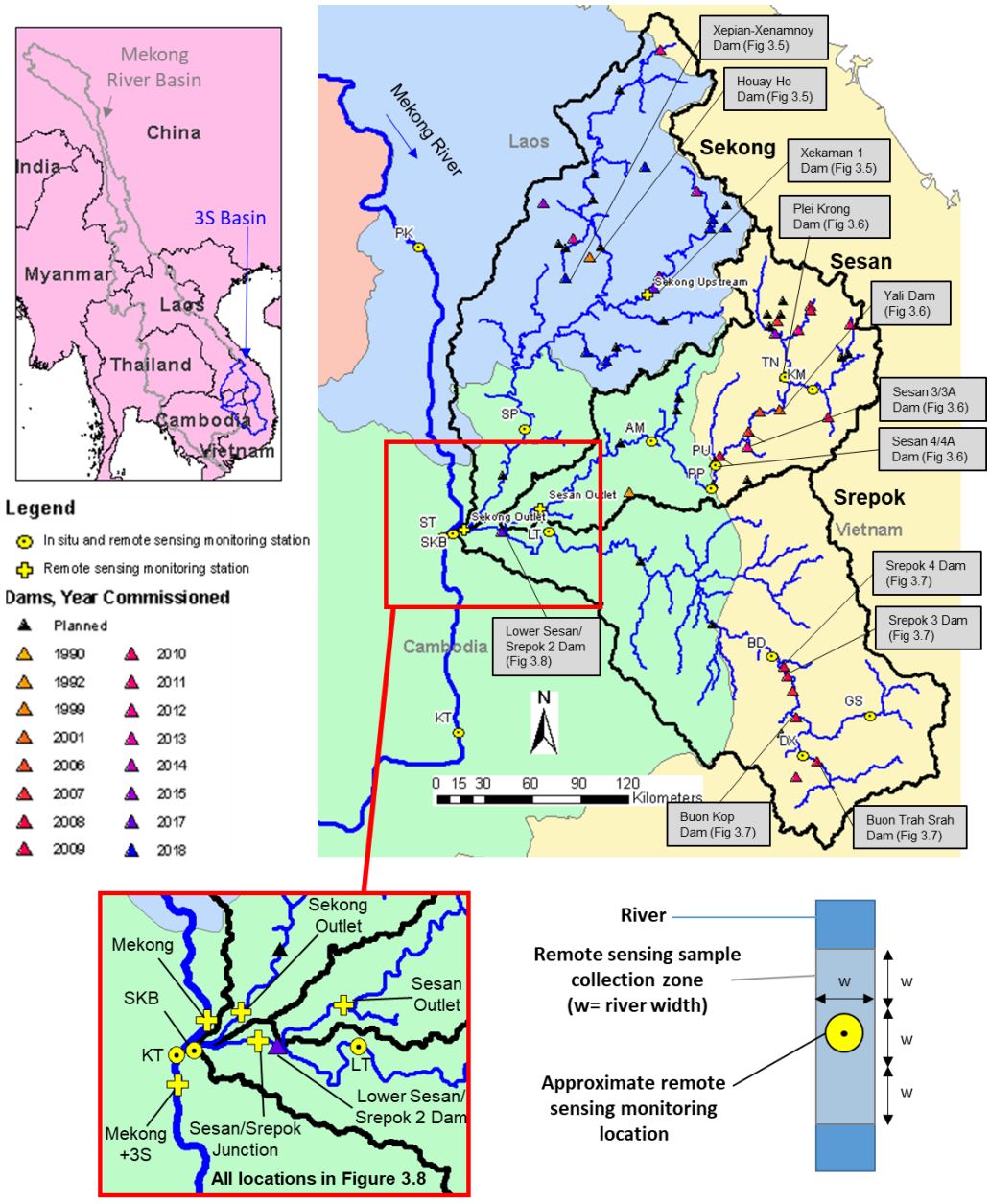

Figure 3.1. The Sekong, Sesan, and Srepok ('3S') tributaries of the Mekong River basin with dams and monitoring points.

Map developed using ArcGIS® software by Esri (2015). Watershed boundaries from Open Development Mekong (2015), country boundaries from World Resources Institute (2011), dam locations from WLE (2017), and monitoring point locations from Koehnken, L. (2014).

Most MRB dam projects do not have practices in place to address upstream and downstream impacts of dams on sediment throughout the various dam lifecycle stages (Thanapon Piman & Shrestha, 2017). At these different times and locations, dam impacts can be highly variable (e.g., channel aggradation or degradation) depending on river properties, sediment properties, dam construction and operation approaches, and compounding effects of dam sequences (Brandt, 2000; Kong et al., 2017; Lu, Oeurng, Le, & Thuy, 2015; J. Xu & Yan, 2010). Considering the complexity of dam impacts, there is an urgent need for strategies to sustainably monitor and manage suspended sediment throughout the MRB. The existing in situ suspended sediment monitoring system of the MRB is limited in its spatial and temporal coverage as well as its reliability (e.g., Walling DE, 2008). As a result, there is poor understanding of the baseline sediment conditions and the incremental impacts of dams and other landscape changes (Thanapon Piman & Shrestha, 2017). This limited understanding hinders the development of effective suspended sediment management and mitigation measures. The monitoring, evaluation, and management strategies that are needed must be relevant to the spatial and temporal scales at which water, land, and dam management practices are implemented, and be able to be sustained long-term (Kong et al., 2017). Strategies must also be conducive to broader coordination between agencies, from the local to international levels (MRC, 2017). Furthermore, as the environment, society, and technology continue to evolve, monitoring and management strategies must be adaptable.

Satellite remote sensing offers a practical response to the sustainable sediment monitoring and management needs in the MRB. Satellite remote sensing offers extensive spatial coverage, frequent and extensive temporal records, cost-effectiveness, and readily transferable data and methods. Satellite remote sensing has been broadly applied in literature for monitoring

suspended sediment concentrations (SSC) of water bodies due to the relationship between SSC and satellite remote sensing visible and near infrared (NIR) bands (e.g., Gholizadeh et al., 2016; Pavelsky & Smith, 2009; Ritchie et al., 1987; Yepez et al., 2018; Zhang et al., 2014). Within the MRB, satellite remote sensing has also been used to quantify SSC in river channels (Markert et al., 2018; Suif, Fleifle, Yoshimura, & Saavedra, 2016) and in the Mekong Delta (Dang, Cochrane, & Arias, 2018; Wackerman, Hayden, & Jonik, 2017). Collectively, these applications and advances in using satellite remote sensing for estimating SSC provide a platform for responding to practical engineering and management needs.

In this study, satellite remote sensing was used to detect SSC changes due to dam and landscape development in a sub-basin of the MRB. The focus was the Sekong, Sesan, and Srepok tributaries, collectively known as the '3S' basin (Figure 3.1). The 3S basin is a valuable case study area as it provides the largest tributary contribution of sediment and streamflow to the Lower MRB (Kondolf, Alford, & Rubin, 2011), and thus has a vital role in the broader MRB ecosystem. The 3S basin is also a microcosm for dam development in the MRB and other global developing regions, as rapid dam implementation is evolving on different timescales across the three tributaries.

The key guiding research question was: To what extent can satellite remote sensing monitor the hydrologic impacts of dam implementation on SSC in the 3S tributaries? The objectives were to:

- Develop an empirical model for predicting SSC in the 3S basin from satellite remote sensing visible and NIR band data and demonstrate the skill of the model in resolving seasonal river channel SSC patterns.

- Determine the mechanisms and scales of SSC changes due to dams in their different life-cycle phases, and how impacts on SSC may vary based on reservoir size and location.
- Determine the mechanisms and scales of SSC changes due to other landscape impacts, which are gathered from satellite remote sensing land cover and nighttime light data.
- Assess how SSC changes due to compounding dam and landscape development in the 3S basin have impacted SSC of the Mekong River mainstem.

This work provides practitioner and hydrologic engineering-oriented understanding of the strengths and limitations in using satellite remote sensing for the above objectives. The methods and results are relevant to the broader MRB as well as other global river basins undergoing rapid dam and landscape development with limited capacity for in situ monitoring.

Section 3.2 provides background on the 3S basin and the technique for estimating SSC using satellite remote sensing data. Section 3.3 provides an overview of the in situ and remote sensing data used as well as the methods for analyzing SSC patterns in the study area. Section 3.4 provides the results and discussion. Section 3.5 concludes with an overview, suggested improvements, and future research directions.

3.2 BACKGROUND

3.2.1 *3S basin*

The 3S basin is approximately 78,650 km^2 in area, which is ~10% of the total MRB area (795,000 km^2). Annual rainfall over the 3S basin varies from 1,100-3,800 mm (Thanapon Piman, Cochrane, Arias, Green, & Dat, 2013). The climate is monsoonal, and approximately 80% of annual runoff occurs during the monsoon season (June through November; Wild & Loucks, 2014). Mean annual streamflow discharge of the 3S is ~2,890 m^3/s, which is ~20% of the Mekong River's ~15,000 m^3/s mean annual discharge (Adamson et al., 2009; MRC, 2005). Mean

annual suspended sediment load of the 3S is estimated from limited in situ data to be in the range of ~10-25 million metric tons per year (Mt/yr). This range is ~6-16% of the Mekong River's suspended sediment load of ~160 Mt/yr (ICEM, 2010; Sarkkula et al., 2010).

3.2.2 *Estimating SSC from satellite remote sensing imagery*

Approaches for estimating SSC from satellite remote sensing are generally either empirical or physics-based (Wackerman et al., 2017). An empirical approach was used in this study since there is insufficient 3S basin sediment data available to properly parametrize physics-based models. The empirical approach was a regression between in situ SSC and remote sensing visible and NIR data collected for the same location and day. This technique was used because of its simplicity and widespread application. More advanced empirical techniques include non-linear multiple regression, principle components analysis, and neural networks (Gholizadeh et al., 2016).

Linear regression techniques for estimating SSC have commonly used the visible (red, green, blue) and NIR bands of the Landsat satellite series (TM, ETM+, OLI) to correlate to in situ SSC measurements (Gholizadeh et al., 2016). Regression was conducted between in situ measurements and a single band or band ratio, with the values in linear or exponential form. The red band (alone or in a ratio) was used most often. Using band ratios was more robust than using single bands, particularly when sediment color varies (Pavelsky & Smith, 2009). Regression relationships have typically been exponential, linear, or 2nd order polynomial (higher order polynomials often overfit). Exponential relationships have often been strongest, particularly for high SSC (>50 mg/L) (Pavelsky & Smith, 2009; Wackerman et al., 2017).

There are notable limitations and sources of uncertainty in developing and applying the linear regression technique for estimating SSC from satellite visible and NIR surface reflectance

data. River sediment properties (e.g., color, mineralogy, grain size distribution) can vary across a region and over time. This can limit the spatial and temporal applicability of empirical SSC-reflectance relationships (Pavelsky & Smith, 2009). Other reflective suspended or dissolved material (e.g., chlorophyll, carotenoids) may also alter river surface reflectance and therefore the validity of calibrated relationships (Wackerman et al., 2017). Another limitation comes from the penetration depth of satellite sensors for surface reflectance of water (top ~1-2 meters). When the river bottom is shallower than the sensor penetration depth, it will scatter the remote sensing reflectance (Volpe, Silvestri, & Marani, 2011). When the river bottom is deeper than the sensor penetration depth, the SSC measured in the surface layer may significantly differ from the depth-integrated SSC. This latter case is likely to occur at high discharges, when bedload and coarser sediment in the lower water column may be a higher proportion of the total load. Thus, SSC predicted from remote sensing cannot be directly used for depth-integrated SSC analyses and modeling. Furthermore, it is not possible to differentiate if increases in remotely-sensed SSC are resulting from suspended sediment increases in the entire water column or mixing between the lower and upper water columns (Markert et al., 2018).

The temporal extent and frequency of remote sensing imagery can also limit its capacity to monitor SSC (e.g., 8- or 16- day revist interval for Landsat; Sentinel-2 available since 2014). Imagery quality may be limited due to cloud cover. This issue is prevalent in the 3S basin due to its monsoonal hydroclimatology and moutainous landscape which lends to orographic lift and cloud development. Hence, it is generally appropriate to rely on remote sensing for monitoring background seasonal SSC rather than isolated events (Wackerman et al., 2017). In addition, seasonal SSC from dry, non-cloudy seasons is more reliable than that from wet, cloudy seasons. The spatial resolution of remote sensing imagery (e.g., 30 m for Landsat) can also limit the use

of satellite remote sensing for sediment. The stream locations where SSC can be monitored must have river channels wide enough that there are sufficient remote sensing pixels of water that do not mix with the river banks. Narrow channel widths are common for streams with low-orders and steep slopes. These conditions are often found in the uplands of mountainous regions which are typically large sources of sediment.

3.3 DATA AND METHODS

3.3.1 *Regression model for in situ SSC and remote sensing reflectance*

3.3.1.1 In situ SSC data

The in situ SSC data used in this study (Table 3.1, Figure 3.1) were from two Mekong River Commission (MRC) monitoring programs. The data are not publicly available and are the only datasets containing 3S basin SSC samples. The primary dataset was from the water quality monitoring program (WQMP) established by the MRC in 1985 (MRC, 2011). As part of the WQMP, MRC member countries monitor SSC throughout the lower MRB. Aside from PK, the WQMP stations have been monitored for only a subset of years since 1985. The WQMP monitoring is generally monthly, although SSC has been collected less frequently at some stations. The second dataset was from the MRC Discharge Sediment Monitoring Project (DSMP; Koehnken, 2014) which began in 2009. As part of the DSMP, 34 streamflow and SSC samples are collected at each site per year. Channel width and depth measurements at the station locations were obtained using the cross-section tool in Google Earth. Thus, the accuracy and precision of this data were limited and may not represent the channel conditions at satellite and in situ SSC sample collection times.

Table 3.1. Information on in situ monitoring stations and SSC samples of the 3S Basin and Mekong River mainstem used in this study.

Station Name	Station Abbrev-ation	Source	Tributary/ Location	SSC Sampling Start Date	SSC Sampling End Date	No. SSC samples	Channel Top Width (m)	Channel Depth (m)
Siempang	SP	WQMP	Sekong, lower	10/24/2004	8/25/2011	65	303	3.7
Kontum	KM	WQMP	Sesan, upper	10/15/1992	3/15/1995	34	104	1.0
Trung Nghia	TN	WQMP	Sesan, upper	6/15/1992	3/15/1995	35	61	4.8
Pleicu	PU	WQMP	Sesan, upper	7/15/2004	8/15/2011	81	203	11
Phum Pi	PP	WQMP	Sesan, upper	11/23/2004	2/26/2011	43	173	3.0
Andaung Meas	AM	WQMP	Sesan, lower	11/23/2004	6/27/2011	66	286	4.0
Giang Son	GS	WQMP	Srepok, upper	9/15/1993	2/15/1995	26	53	<1
Duc Xuyen	DX	WQMP	Srepok, upper	11/15/1992	2/15/1995	84	101	<1
Ban Don	BD	WQMP	Srepok, upper	10/15/2004	5/15/2011	84	120	2.0
Lumphat	LT	WQMP	Srepok, lower	11/23/2004	2/27/2011	66	350	8.5
Pakse	PK	DSMP	Mekong, upstream of 3S confluence	6/17/2011	3/25/2015	92	1615	3.9
		WQMP		12/18/1985	6/17/2011	267		
Stung Treng	ST	DSMP	Mekong, downstream of 3S confluence	6/8/2011	9/30/2014	83	1376	4.3
		WQMP		12/18/2004	2/26/2011	65		
Kratie	KT	DSMP	Mekong, downstream of 3S confluence	6/7/2011	9/29/2014	74	1108	8.0
		WQMP		12/19/1995	12/28/2011	160		
Sekong River at Bridge	SKB	WQMP	3S confluence	8/11/2012	9/30/2014	52	812	4.1

Sources

WQMP: Water Quality Monitoring Program (WQMP), Mekong River Commission (MRC, 2011)

DSMP: Discharge Sediment Monitoring Project, MRC (Koehnken, 2014)

Although the focus in calibrating the empirical SSC-reflectance relationship was on 3S basin SSC, data from the three Mekong (mainstem) stations within the vicinity of the 3S outlet

were incorporated because they provided a larger number of potential calibration samples. The Mekong SSC is generally higher than the 3S, which also extended the range of SSC in the calibration. However, incorporating these stations also introduced more uncertainty to the empirical SSC-reflectance relationship since the suspended sediment in the mainstem and 3S basin may have different properties. Uncertainty is also induced by different channel geometry conditions where stations are located, which can be broadly grouped between the mainstem and SKB stations, upper tributary stations, and lower tributary stations (Table 3.1, Column 4).

The WQMP samples were collected at shallow depths (0.3-0.5 m below water surface) in the middle of the active channel (MRC, 2013; Walling, 2008). The samples were also collected from a bottle, not specialized sampling equipment for depth-integrated SSC measurements. The sampling techniques used may have caused deficiencies in sample quality since the samples were not isokinetic (i.e., streamflow at sampler intake may be changing in velocity). Also, since SSC typically increases with depth, the shallow SSC samples likely underestimated the mean cross-section SSC (Desmond E. Walling, 2008). However, the shallow depths of the MRC observations were comparable with the shallow depth observed from remote sensing sensors (Markert et al., 2018). The DSMP samples were collected with a D-96 sampler for all samples except those collected at PK, where the bottle-sampling approach for the WQMP was used. The D-96 sampler collected depth-integrated and isokinetic samples (Federal Interagency Sedimentation Project, 1941) and thus mitigated the limitations of the WQMP samples. Although there were limitations in comparing the bottle and D-96 samples, none of the D-96 samples were used for calibrating the empirical SSC-reflectance relationship since they did not temporally coincide with satellite imagery.

3.3.1.2 Remote sensing as the Water Management tool

Satellite remote sensing data used in this study were from the Landsat satellite series; that is, Landsat TM (Landsat 4 and 5), ETM+ (Landsat 7), and OLI (Landsat 8). Collectively, these satellites have been operational from 1982 to present (Landsat 4: 1982-1994, Landsat 5: 1984-2012, Landsat 7:1999-present, Landsat 8: 2013-present). Each satellite had a sun-synchronous orbit and 16-day revisit orbital, with an 8-day offset between any two satellites that had overlapping operational periods. Landsat had a spatial resolution of 30m for the visible (red, blue, green) and NIR wavelengths. Landsat imagery was downloaded and processed using Google Earth Engine (GEE), a cloud-based remote sensing platform. Landsat collections of precomputed surface reflectance with the highest quality rating (Tier 1) were used. These scenes available in GEE have been atmospherically-corrected and have mapped pixels of cloud, cloud confidence, cloud shadow, and snow/ice (see Markert et al. (2018) for more information). Landsat 4 data of Tier 1 quality were sparsely available in the 3S Basin. Landsat 7 data are of limited availability since 2003, when a failure of the Scan Line Corrector occurred (Chander, Markham, & Helder, 2009).

Satellite visible and NIR reflectance data were collected at each in situ monitoring station location over a stream reach roughly three times as long as the stream width (Figure 3.1). Surface water pixels over the stream reach were mapped using the Dynamic Surface Water Extent algorithm (Jones, 2015). Pixels with clouds or cloud shadows were masked out using the Landsat quality assessment bands. Scenes were retained if they contained at least 90% of pixels classified as being free of clouds and cloud shadows over the sample reach. Scenes were excluded if the average NIR reflectance was greater than 0.5 because they were likely to have severe cloud contamination. The remaining image collections were manually inspected, and scenes were

excluded if a significant portion of pixels were impacted by clouds, cloud shadows, haze, and/or patches of sand.

Satellite data for 12 of the 14 in situ monitoring stations were used in this analysis. Data from GS (Srepok) and TN (Sesan) were excluded since the narrow river widths limited the number of surface water pixels at these locations. Satellite data were also used from six locations in the study area that are not in situ monitoring points (Figure 3.1). This resulted in a total of 4,556 images combined for the 18 monitoring points (12 in situ points, 6 non-in situ points). 1,355 (30%) of these images were from the wet season and 3,201 (70%) were from the dry season.

3.3.1.3 Empirical model development and application

A calibration dataset was developed to test for correlation between the in situ SSC and satellite reflectance data. The calibration dataset consisted of all quality-checked Landsat data collected on the same date and location as an in situ sample. This amounted to a total of 15 corresponding in situ and Landsat samples, coming from ten of the in situ monitoring points (Figure 3.2, bottom left). Of the corresponding samples, eight were collected during the dry season and seven during the wet season. In addition to the limitations for the in situ data previously discussed (Section 3.3.1.1), the calibration dataset was limited because of its small number (n=15), only two of the in situ observations are greater than 60 mg/L, and nine of the 15 calibration pairs come from four locations. These factors limited the precision of SSC values predicted from the empirical model, particularly for high SSC. However, the range of the calibration dataset was acceptable as the maximum observed SSC value in the calibration dataset (153 mg/L) is the 97th percentile of all in situ observations in the 3S basin. The empirical model was also biased towards locations/rivers where more calibration data were from. However, each of the three tributaries and the mainstem were represented in the calibration dataset.

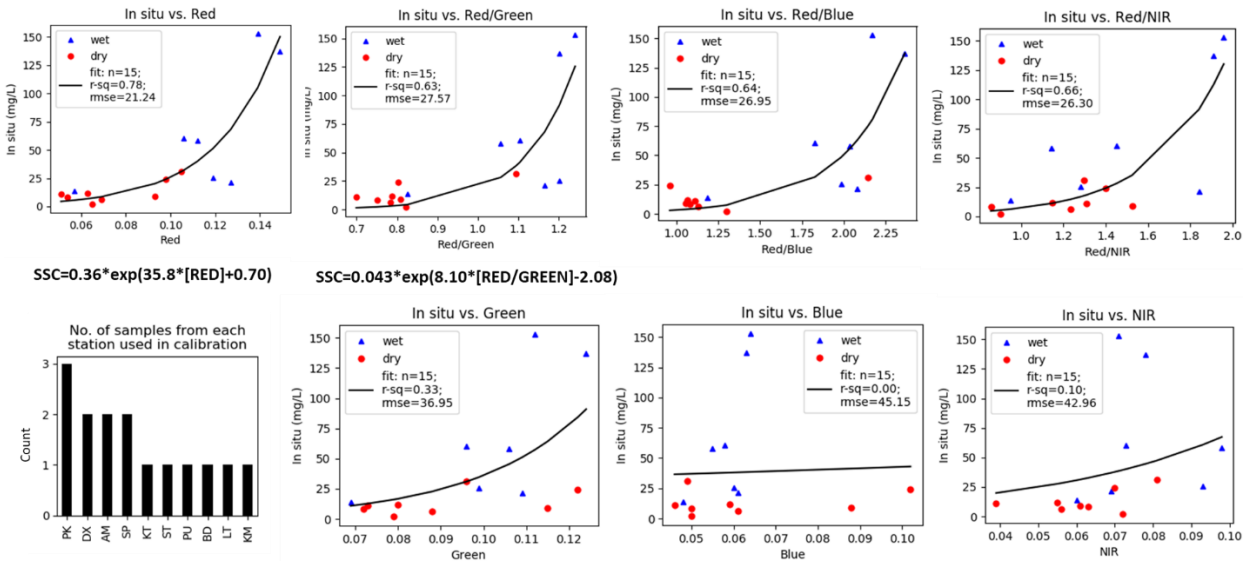

Figure 3.2. Regression results for in situ observations of SSC versus remote sensing reflectance for a single band or band ratio.

Using the calibration dataset, empirical regression models were tested between the in situ SSC and satellite reflectance data. Reflectance data were tested as individual visible (red, blue, green) and NIR band values as well as all permutations of band ratios (e.g., red/green, blue/NIR). The SSC and reflectance values were tested in linear and exponential forms with exponential, linear, and 2nd order models. Exponential models had the best coefficient of determination (r^2) and root mean square error (RMSE) metrics between the SSC observed in situ and SSC predicted from the empirical regression model with satellite data. Of the different band and band ratios correlated with in situ SSC, the best fit was the red band (r^2=0.78, RMSE=21.2 mg/L; Figure 3.2). The band ratios between red and the other three bands had relatively strong and similar performance (r^2=0.63-0.66, RMSE=26.3-27.6 mg/L; Figure 3.2).

When the calibrated red band-SSC equation was applied to time series of red reflectance at in situ monitoring stations, peak values of predicted SSC tended to be anomalously high. When the red/green, red/blue, and red/NIR calibration equations were applied to the respective

reflectance time series at stations, peak values predicted by the red/green bands-SSC equation did not have high anomalies and were closest to observations. Hence, the final empirical model conditionally used the red (R) and red/green (R/G) calibration equations: For R less than 0.14, the red band-SSC equation was applied; for R greater than or equal to 0.14, the R/G band ratio-SSC equation was applied. In equation form, this is:

$$SSC=0.36 \times \exp(35.8 \times R + 0.70) \qquad R>0.14 \qquad (3.1)$$

$$SSC=0.043 \times \exp(8.10 \times R/G-2.08) \qquad R\leq 0.14$$

The red reflectance threshold of 0.14 in the empirical model was determined through sensitivity testing. The monthly mean SSC from the empirical model was computed for a range of plausible thresholds (red=0.10- 0.17) and the results were compared to the monthly mean in situ SSC at each monitoring station. While the optimal red band threshold varied across stations, the threshold 0.14 performed best overall for SP (Sekong), AM (Sesan), and LT (Srepok). Optimizing model performance at these three stations was prioritized because they are closest to the outlet of each 3S watershed. The empirical model captured the general seasonal patterns and magnitudes of the in situ observations at the three stations, although there was still uncertainty for high SSC (Figure 3.3). The empirical model improved the monthly mean SSC prediction at AM (RMSE reduced from 393 mg/L to 65.5 mg/L) and LT (RMSE reduced from 50.7 mg/L to 23.6 mg/L) however had no change at SP (RMSE of 43.7 mg/L).

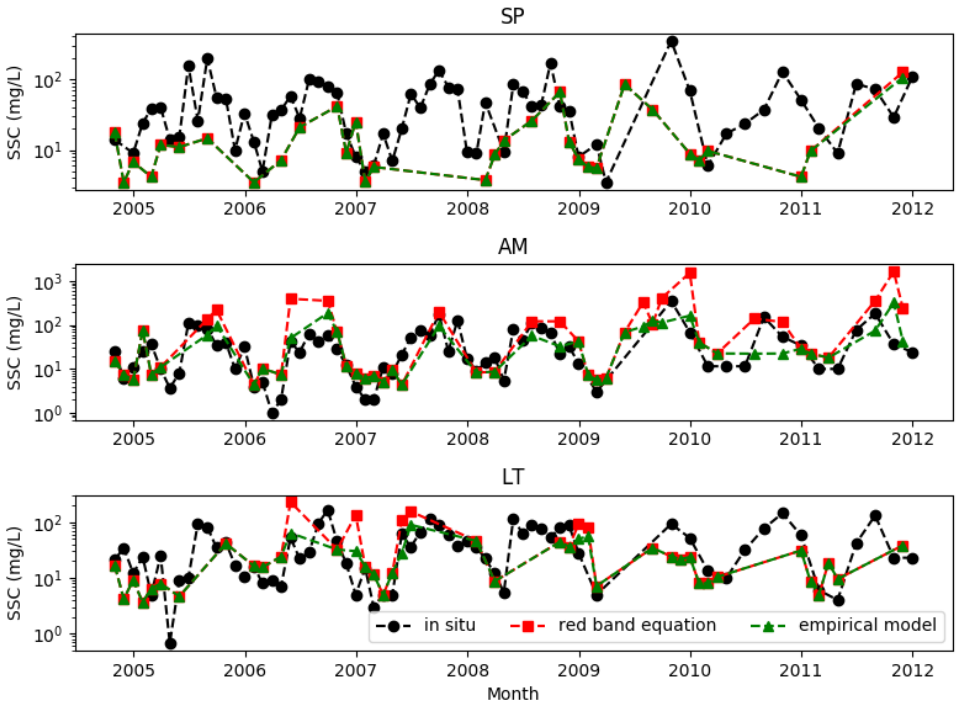

Figure 3.3. Time series of in situ and predicted monthly mean SSC at SP (Sekong), AM (Sesan), and LT (Srepok). Predictions are shown for both calibrated red band-SSC equation and empirical model, which uses the red band-SSC equation and red/green bands-SSC equation.

To develop long-term time series of predicted SSC for all monitoring stations, the empirical model was applied to all quality-checked Landsat surface reflectance data. The time series of instantaneous SSC predictions were smoothed using the locally weighted scatterplot smoothing technique (LOWESS; Cleveland, 1979). This robust, non-parametric technique was suitable for the non-equally spaced temporal frequency of the surface reflectance data. For each predicted value, a specified fraction of the dataset adjacent to the output was smoothed, with more weight given to points closest to the predicted value. The specified fraction was determined through sensitivity testing to be 0.07 since this preserved the seasonality of the data while limiting the noise.

3.3.2 *Data on dams, land cover, and nighttime lights*

3.3.2.1 Dams

The primary source of information on dams in the 3S basin was a dataset maintained by the CGIAR Research Program on Water, Land, and Ecosystems (WLE, 2017). The dataset was intended to contain every MRB hydropower or multi-use dam with an installed capacity of 15 megawatt (MW) or above, and/or every irrigation or water supply dam with a reservoir area of 0.5 km2 or above. Additional information on 3S basin dams was from the studies of Piman et al. (2016), Schmitt et al. (2018b), and Wild & Loucks (2014), which each focused explicitly on dam impacts in the 3S basin. These three studies included information from the MRC dam database, which is not publicly available. Each study also included calculations made in the respective analysis for relevant properties of the dams (e.g., drainage area).

Of the 65 dams existing, under construction, or planned in the 3S basin, 14 existing dams were focused on in this study (hereinafter referred to as 'focus dams'; Table 3.2). These focus dams were expected to have the greatest impact on the 3S sediment regime, largely based on their reservoir volume, surface area, and/or drainage area. Findings from other studies on the hydrologic impacts of 3S basin dams were also considered. Three sets of dams were grouped together in this analysis due to their spatial proximity and similar construction timelines: Sesan 3 and Sesan 3A; Sesan 4 and Sesan 4A; and Srepok 3 and Srepok 4. The Xepian-Xenamnoy dam construction was also considered in this analysis, however it collapsed in June 2018.

Table 3.2. Dams in 3S basin studied for sediment impact.

Sources were: WRE (2017) unless indicated with [1]Schmitt et al. (2018), [2]Piman et al. (2016), or [3]Wild and Loucks (2014).

Name	Basin	Commiss-ioning Date	Installed Capacity (MW)	Drainage Area (km^2)	Max Reservoir Surface Area (km^2)	Total Storage (million m^3)
Houayho	Sekong	1999	152	192 [2]	37	674 [1, 3]
Xekaman 1	Sekong	2015	290	3580 [2]	150	4804
Xepian-Xenamnoy	Sekong	2019	410	522 [2]	50	1092
Yali	Sesan	2001	720	7455 [2]	64.5	1073
Sesan 3	Sesan	2006	260	7788 [2]	6.4	92 [1,3]
Sesan 3A	Sesan	2007	96	8084 [2]	8.8 [1]	80.6 [1,3]
Plei Krong	Sesan	2008	100	3216 [2]	53.3	1049
Sesan 4A	Sesan	2008	63	9368 [2]	1.8	13.1
Sesan 4	Sesan	2009	360	9326 [2]	54	893.3
Buon Trah Srah	Srepok	2009	86	2930 [2]	37.1 [1]	787 [1,3]
Buon Kop	Srepok	2009	280	7980 [2]	5.6 [1]	73.8 [1,3]
Srepok 3	Srepok	2009	220	9410 [2]	17.7 [1]	219
Srepok 4	Srepok	2009	80 [2]	9568 [2]	3.8 [1]	29.3 [1,3]
Lower Sesan/ Srepok 2	Sesan, Srepok	2017	480	49200 [2]	335	1790

Detailed construction information about the MRB dams is typically not publicly available. Thus, to understand how different dam lifecycle phases impacted SSC, Landsat

imagery was manually reviewed to approximate when dam construction began and initial reservoir filling was complete for each of the 14 focus dams. The approximate dates obtained were the dates when relevant Landsat imagery was available and not necessarily the actual date that the milestone occurred. The accuracy of the dates was limited due to imagery availability, clouds covering the dam/reservoir in the imagery, and potential misinterpretation of the imagery. This, in turn, could have caused misinterpretation of dam construction and operation impacts on SSC in the results of this study. However, the dates are expected to be accurate within (+/-) one year, which is minor compared to the long time frame of this study (~31 years) and, typically, multi-year SSC trends.

The bulk of dam development has occurred differentially between the 3S basins (Table 3.2). In the Sesan basin, major development initiated primarily in 2006, although a large dam (Yali) was also constructed in 2001. Major development followed in the Srepok basin, initiating in 2009. Finally, major development initiated in the Sekong basin in 2015, although a large dam (Houayho) was constructed in 1999.

3.3.2.2 Land cover

Land cover data across the 3S basin came from the Moderate Resolution Imaging Spectroradiometer (MODIS) Aqua and Terra Land Cover Product (MCD12Q1 V6) and supervised land cover classification of this MODIS data from the International Geosphere-Biosphere Programme (IGBP; Belward et al., 1999; Loveland et al., 2000). The data were produced at 500m spatial resolution and annual time steps for years 2001 to 2017 (n=17). There were 12 land cover classifications found in the 3S. In this study, classifications were grouped into categories as follows: forest includes evergreen broadleaf forests, deciduous broadleaf forests, and mixed forests; savanna includes savannas and woody savannas; cropland includes

croplands and cropland/natural vegetation mosaics. The remaining land cover classifications were grassland, wetland, barren, water bodies, and urban.

3.3.2.3 Nighttime light

Nighttime light data were used in this analysis as a proxy for human settlement dynamics (Figure 3.4), as has been done in other studies (e.g., Mård et al., 2018; T. Xu et al., 2014). Human settlement dynamics reflect potential non-point sources of river sediment. Nighttime light data were a helpful complement to land cover data in the 3S basin since the region is largely rural and concentrated human settlement is not always apparent or quantifiable from land cover data. Nighttime light data across the 3S basin came from the Defense Meteorological Satellite Program Operational Linescan System (Version 4) (NOAA–Earth Observation Group, 2016). These data were produced at 30 arc second (~1 km) spatial resolution and annual time steps for years 1992 to 2013 (n=22). However, the start year of 2001 was used in Figure 4 for consistency with the land cover dataset temporal range. There was little increase in nighttime lights from 1992 to 2001 in the study area In this study, “stable” nighttime light data was used, which quantify light intensities from cities and towns, excluding background noise (e.g., sunlit data) as well as temporary light sources (e.g., fires) (Mård et al., 2018). Nighttime light units ranged from 0 (complete darkness) to 63 (bright areas).

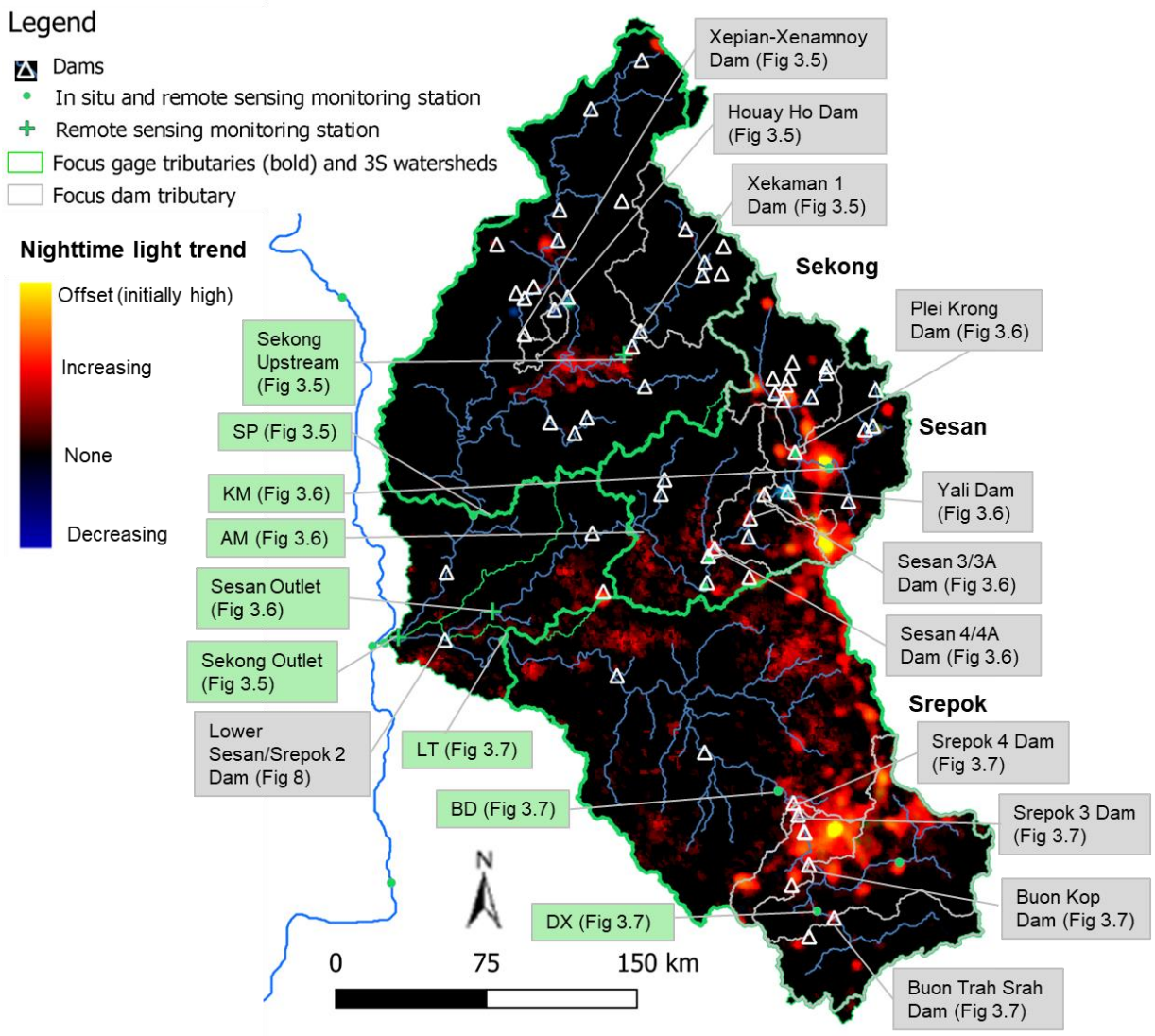

Figure 3.4. Stable nighttime light trends in 3S basin for years 2001 to 2013. Increasing red intensity indicates an increasing nighttime light trend; increasing blue intensity indicates a decreasing nighttime light trend; black indicates no trend; yellow indicates locations where brightness was initially high (i.e., trend offset) and has an increasing trend.

3.4 Results and Discussion

In the predicted SSC time series at each monitoring point (Figures 3.5a, 3.6a, 3.7a, 3.8a-c), there were frequent satellite data gaps beyond the 8- or 16-day Landsat revisit intervals (which would

be ~45 or ~22 points per year). Data gaps were prevalent in the wet season when clouds were a common issue. Thus, remote sensing reflectance data were mostly from the dry season (74% at SP, 69% at AM, 77% at LT) causing the dry season SSC to dominate the LOWESS-smoothed SSC patterns. SSC was generally lower and less variable in the dry season compared to the wet season. There were also exceptionally long periods where data were sparse in both the wet and dry seasons, such as 2010 to 2013 at SP (a). In these periods the LOWESS-smoothed SSC time series may have been biased, particularly by anomalously high or low SSC predictions.

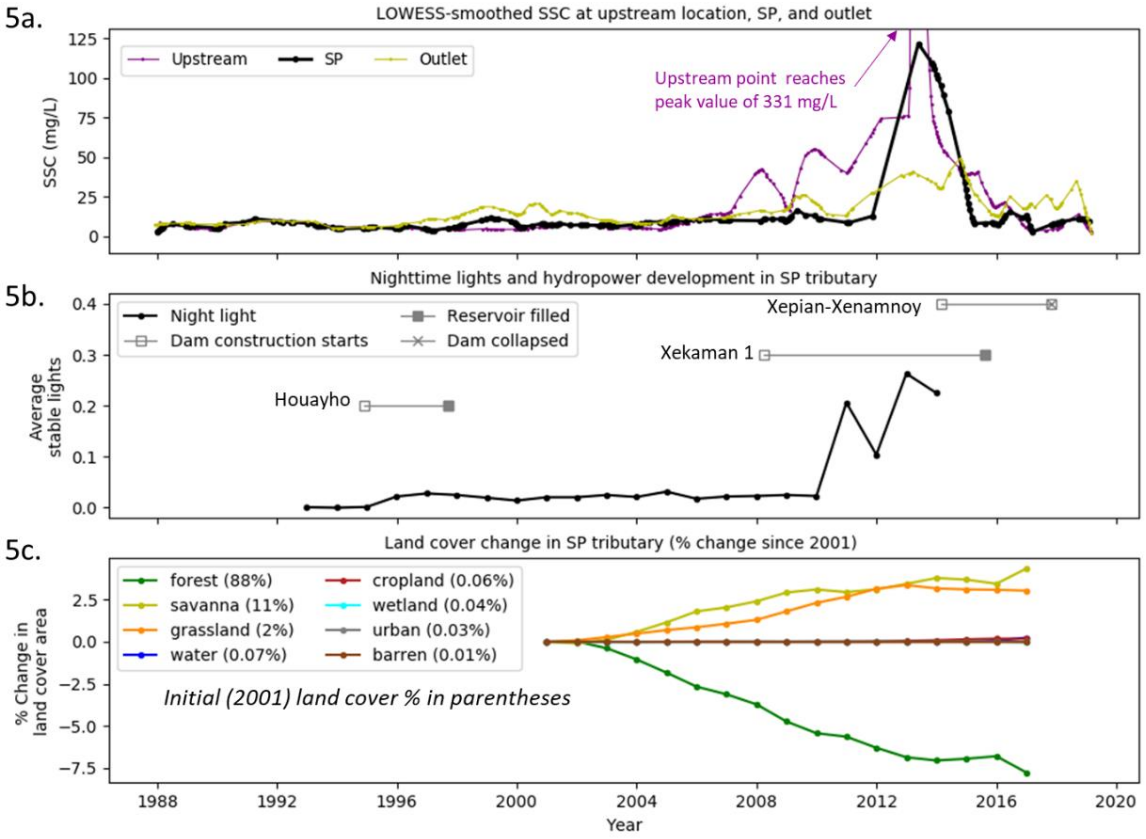

Figure 3.5. Time series of predicted LOWESS-smoothed SSC (a), dam implementation (b), nighttime light (b), and land cover change (c) in the Sekong watershed.

Although the LOWESS-smoothed SSC time series (Figures 3.5a, 3.6a, 3.7a, 3.8a-c) were impacted by biases, they show insightful changes in response to dam and landscape development (Figures 3.5b-c, 3.6b-c, 3.7b-c, 3.8) over the ~31 year period analyzed. In the initial ~17 years (up until ~2004/2005) of the SP, AM, and LT time series the SSC were generally at relatively low (<10 mg/L for SP and AM; <20 mg/L for LT) and stable baseline values. There were short periods where SSC slightly elevated due to early, isolated dam construction, such as the Yali dam from 1993 to 1998 (Figure 3.6b).

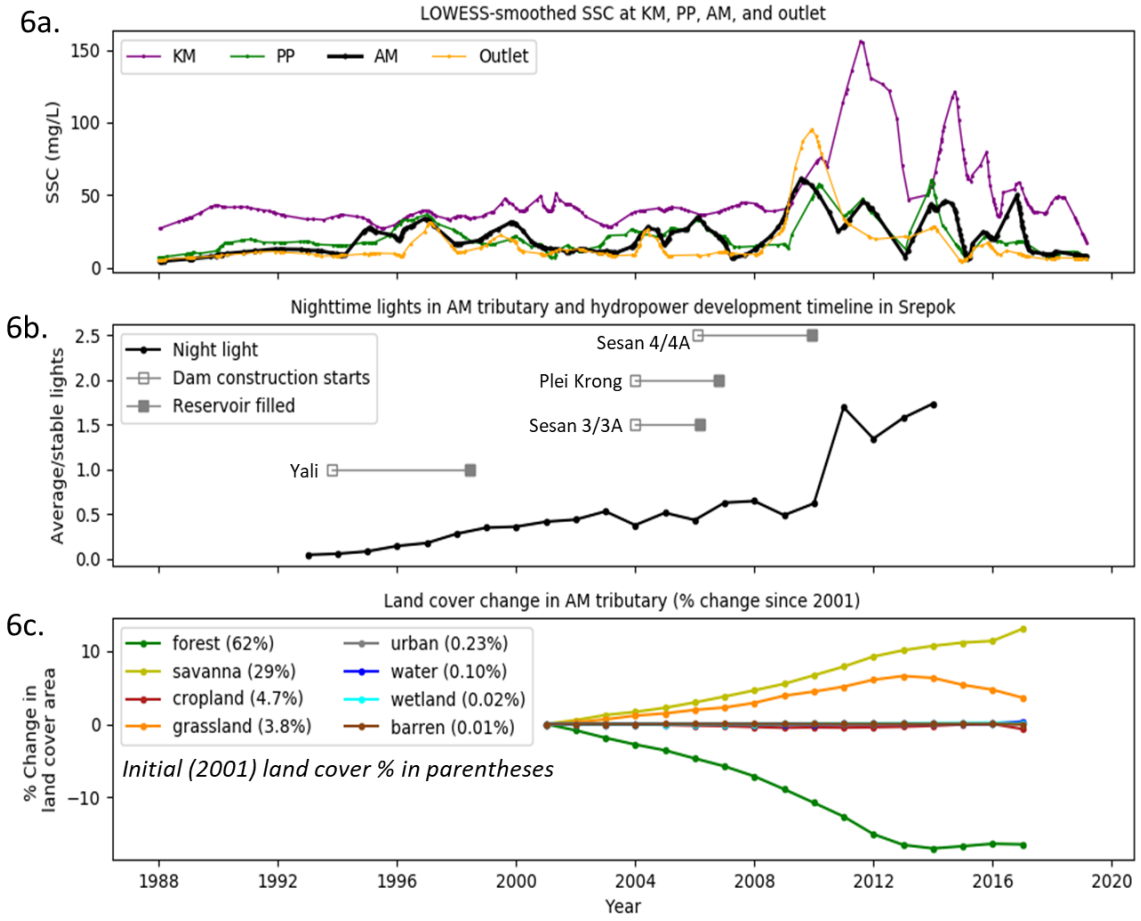

Figure 3.6. Time series of predicted LOWESS-smoothed SSC (a), dam implementation (b), nighttime light (b), and land cover change (c) in the Sesan watershed.

For the latter ~14 years (from ~2004/2005 to 2019) in each tributary, there were more dramatic changes in LOWESS-smoothed SSC caused by more extensive dam implementation and landscape development. Reservoirs with larger surface area, volume, and/or drainage area generally had a stronger influence on SSC trends. Dam impacts on SSC also depended on the lifecycle stage of the dam. Temporary increases in SSC occurred at the onset of dam construction (Figures 3.5b, 3.6b, 3.7b), as land surface disturbance from the construction of/related to dams eroded sediment. Because of localized construction impacts, SSC increases were typically higher at points closer to the dam(s) under construction compared to downstream points. For example, during Xekaman 1 dam construction (Figure 3.5a, b), SSC increased by >300 mg/L in the vicinity of the dam and 20-120 mg/L at monitoring points downstream. Overall SSC increases upon dam construction ranged from ~5-120 mg/L at SP, ~20-50 mg/L at AM, and ~3-40 mg/L at LT. The duration until reaching the peak SSC ranged from less than one year (Srepok 3 and Srepok 4, Figure 3.7a, b) to six years (Xekaman 1, Figure 3.5a, b).

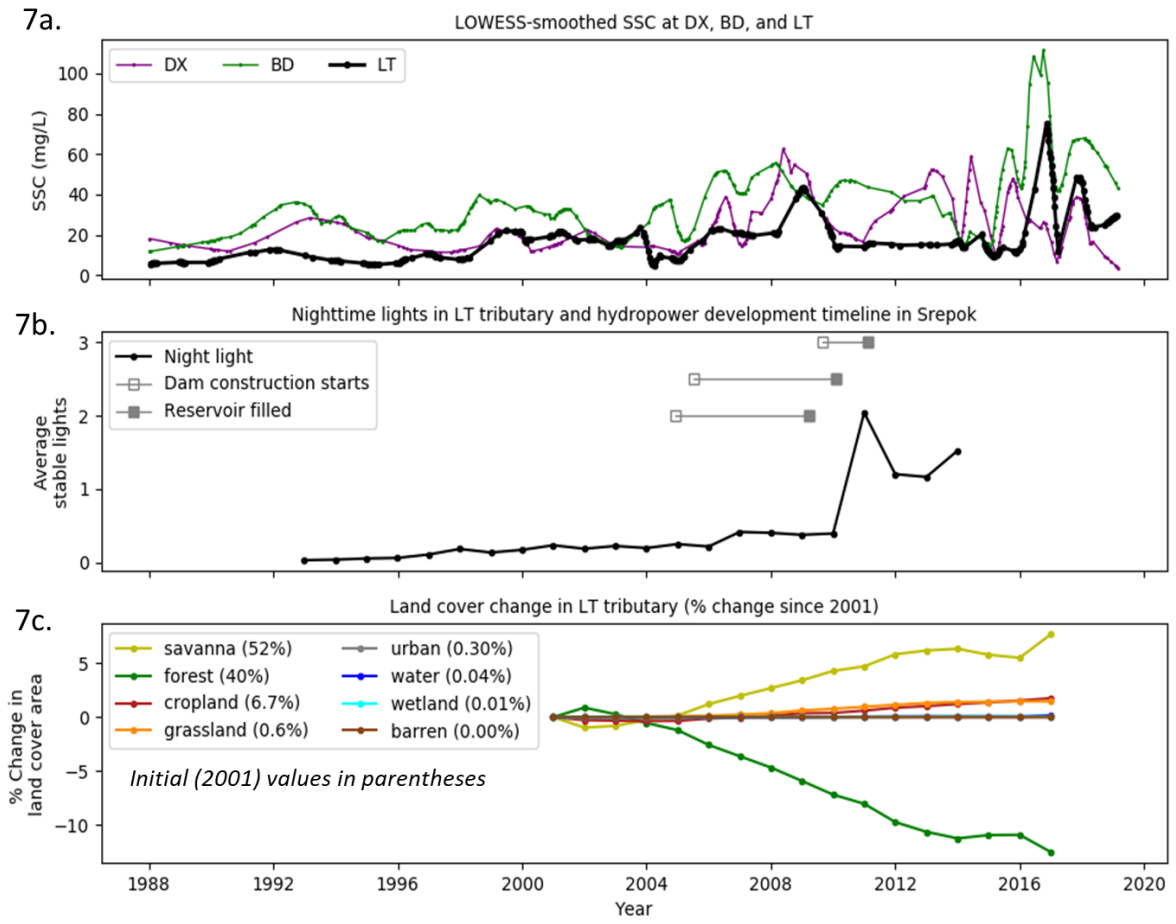

Figure 3.7. Time series of predicted LOWESS-smoothed SSC (a), dam implementation (b), nighttime light (b), and land cover change (c) in the Srepok watershed.

As the reservoirs filled, the LOWESS-smoothed SSC declined downstream of the reservoirs due to the lessening of construction impacts as well as the reservoir sediment trapping. For example, in the Sekong watershed (Figure 3.5a, b), SP declined to baseline SSC (122 to 8 mg/L) within two years of when Xekaman 1 reservoir filled. In the Srepok watershed (Figure 3.7a, b), LT decreased to near baseline conditions (47 to 14 mg/L) within the year that the Buon Trah Srah and Buon Kop reservoirs filled. Sediment trapping by the reservoirs was clearly demonstrated in the Sesan watershed (Figure 3.6a, b). When the SSC of KM, the point upstream of all major dams, most dramatically elevated from 2009 to 2012 (39 to 156 mg/L), the SSC at

AM simultaneously declined and remained below 50 mg/L. The difference in SSC between KM and AM was up to 108 mg/L, which is likely due to sediment trapping in reservoirs between the two points. The dams in between KM and AM—Yali, Sesan 3/3A, and Sesan 4/4A— had their reservoirs filled or were in the process of filling during this period.

Decreases in SSC typically occurred less rapidly at monitoring points located closer to dams compared to downstream points, which was likely due to persisting localized impacts of dam construction. Monitoring points near the dams may have also had relatively high SSC due to the scouring impact of the outflow near the dam spillway. This was seen, for example, in the Srepok watershed (Figure 3.7a, b) from 2008 to 2013 when BD (upstream) remained elevated at ~40 mg/L while LT (downstream) had declined to be steadily at ~13 mg/L.

At these two points in the Srepok watershed (BD, LT; Figure 3.7a, b), SSC also began to generally increase (with seasonal fluctuations) in 2015. In 2016, SSC peaked to unprecedented levels for LT at 76 mg/L and for BD at 112 mg/L. These increasing SSC patterns were not attributable to upstream dam construction, although the seasonal fluctuations could relate to dam operations. These increasing SSC patterns also diverged from the generally decreasing SSC patterns at DX, located upstream of Buon Kop, Srepok 3, and Srepok 4.

3.4.1 *Land cover and nighttime light impacts on SSC*

SSC time series patterns in conjunction with dam development were better understood using nighttime light and land cover satellite data. The prevalent landscape changes over time in all 3S watersheds were increases in human settlement patterns (as inferred from nighttime lights; Figures 3.4, 3.5b, 3.6b, 3.7b) and decreases in forest cover (Figures 3.5c, 3.6c, 3.7c). Each of these would have reasonably caused increases in SSC, although the increases may have been temporary. Forest clearing could have led to relatively large sediment loads to streams due to

impacts of heavy equipment and tree uprooting. After forest clearing, the lack of tree roots holding sediment in place allowed sediment to more readily erode. Subsequent construction, land cultivation, and human settlement on deforested land may have also eroded sediment. However, initial impacts of deforestation on SSC could have lessened over time. When deforested land was replaced with cropland, the impacts of land cultivation may have also contributed to elevating SSC. The installation of surfaces less conducive to erosion (e.g., concrete) may have allowed for increased surface water runoff but less sediment, which could have diluted SSC.

Deforestation and increasing nighttime lights (i.e., human settlement) generally occurred simultaneously with dam development (Figures 3.5, 3.6, 3.7), and thus had compounding impacts. For example, SSC increases that coincided with dam construction may have been exacerbated by landscape changes. These landscape changes were not just coincidental, but often interconnected with dam development. Areas with high economic development may have the demand and resources to implement dams. Then, following the dam construction, there was further capacity for development in surrounding areas. For example, the magnitude of stable nighttime lights was overall highest in the Sesan and Srepok watersheds (Figures 3.6c, 3.7c, 3.8c). Areas with initially high nighttime lights (yellow in Figure 3.4) as well as with increasing nighttime light trends (red in Figure 3.4) were most prominent in the Vietnam portions of these two watersheds (Figures 3.1, 3.4). Vietnam is the most economically developed of the countries spanning the 3S, and its regions of the Sesan and Srepok are also where historic dam development has been most prevalent.

In the Sesan watershed (Figure 3.6), KM was in an area of high human settlement that is upstream of dam development (Figure 3.4). Thus, the LOWESS-smoothed SSC patterns of KM reflected human settlement and deforestation impacts. The 117 mg/L increase in SSC at KM

from 2009 to 2012 coincided with the most dramatic increase (+283%) in nighttime lights after 2010 (Figure 3.6b) as well as decreasing forest cover (-16%) from 2001 to 2013 in the AM tributary (Figure 3.6c). The subsequent decline in SSC at KM corresponded to stabilization of deforestation after 2013 (Figure 3.6c) and nighttime lights after 2011 (Figure 3.6b). As discussed above, the dams downstream of KM (Yali, Sesan 3/3A, Sesan 4/4A; cumulative volume of ~2,152 million m^3) likely trapped suspended sediment which modulated SSC increases downstream.

In Srepok watershed LT tributary (Figure 3.7), there was similarly a dramatic increase (+512%) in nighttime lights after 2010 (Figure 3.7b) as well as decreasing forest cover (-12%) from 2002 to 2013 (Figure 3.7c). Human settlement patterns (Figure 3.4) were concentrated just upstream of the Srepok 3 and Srepok 4 reservoirs and BD. Like at KM in the Sesan tributary, the dramatic increase in SSC at BD and LT after 2016 was likely related to the upstream landscape development activities. The downstream Srepok 3 and Srepok 4 dams may have modulated SSC increases prior to 2016. However, the cumulative volume of these dams (248 million m3) was much lower that of the dams downstream of KM (in Sesan). This may help to explain why the Srepok 3 and Srepok 4 reservoirs were less effective at trapping sediment over time.

3.4.2 *Impacts of 3S basin on Mekong River mainstem SSC*

The impact that the each of the 3S rivers had on the SSC of their junction, SKB, as well as on the Mekong River mainstem varied between the 3S rivers and over time (Figure 3.8). SKB increased most dramatically (peak of 70 mg/L) from early 2007 to early 2009, which coincided with elevated SSC from the Sesan and Srepok outlets (peak of 118 mg/L; Figures 3.8a,b). When the Sekong outlet SSC elevated up to 50 mg/L from 2011 to 2017 (Figure 3.8b), the SKB SSC continued to decline from its 2009 peak, although less rapidly. The SKB SSC temporarily

elevated by ~20 mg/L from 2016 to 2018 during construction of the Lower Sesan 2 dam and when SSC was elevated (to ~50 mg/L) at the Sesan/Srepok outlet. However, it then decreased to <8 mg/L after the Lower Sesan/Srepok 2 dam reservoir filled, likely due to sediment trapping.

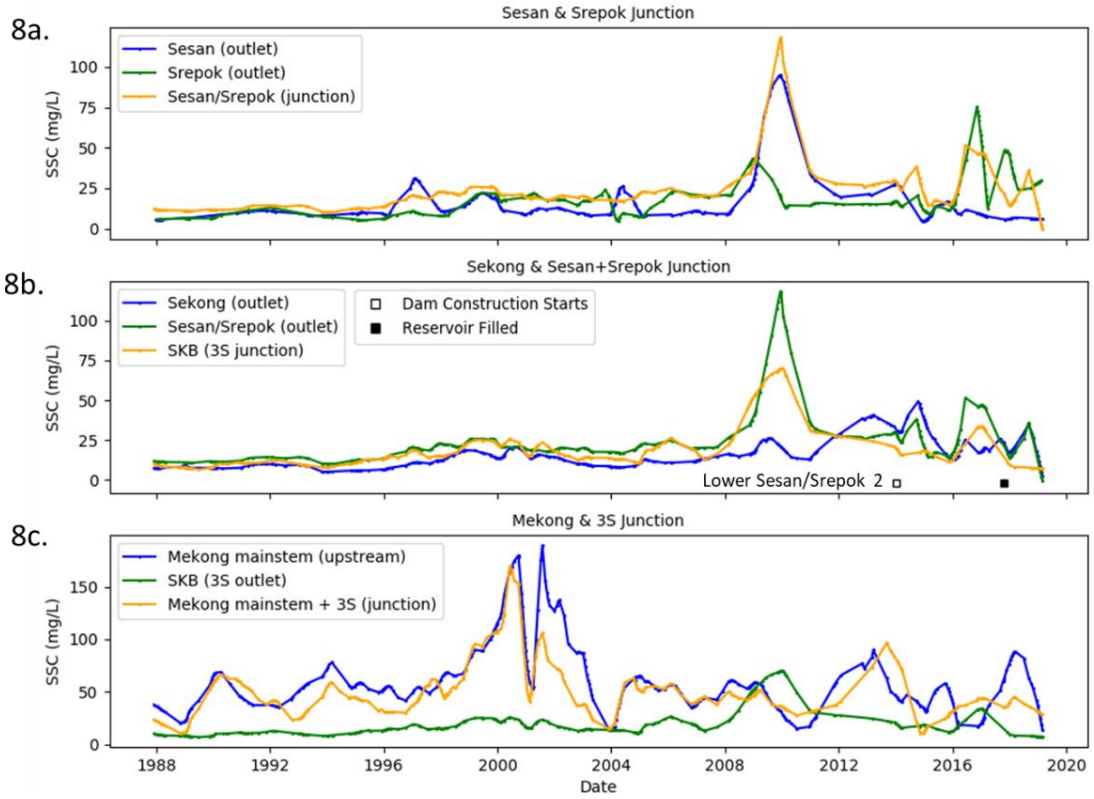

Figure 3.8. Time series of predicted LOWESS-smoothed SSC at the outlets and junctions of the 3S watersheds (a, b) along with the 3S basin and the Mekong mainstem (c).

Compared to the Mekong SSC, the SKB SSC was relatively low prior to 2007 (Figure 3.8c). When the Mekong SSC dramatically peaked in 2000 and 2001, there was up to 125 mg/L difference between SKB and the combined Mekong and 3S SSC (or SKB SSC being ~13% of Mekong SSC). As the Mekong SSC subsequently declined and SKB SSC dramatically elevated starting in 2007, the SKB SSC was up to 35 mg/L greater (+100%) than the combined Mekong and SKB SSC in 2010. However, the SKB SSC then continued to generally decline and had

diminishing influence on the Mekong SSC. An exception to this was from 2016 to 2018 when the spike in SKB SSC temporarily elevated the combined Mekong and 3S SSC from 10 to 44 mg/L.

These patterns demonstrate that the Mekong mainstem, like the 3S basin, has had temporary increases in SSC due to dam and landscape development impacts upstream. However, over the past two decades, the SSC of the Mekong has repeatedly reached exceptionally low levels of SSC. This has been due to upstream reservoir trapping as well as other natural and anthropogenic (e.g., aggregate mines) influences on sediment (Kondolf et al., 2018). The temporary increases in SSC of the 3S due to dam development and landscape change have modulated the decline in SSC of the Mekong. However, as dam building and operations in the 3S basin continue, its contribution of sediment to the Mekong will continue to decline, likely to unprecedented levels.

3.5 CONCLUSION

This study demonstrated that satellite remote sensing is a practical management tool to use for detecting the hydrologic impacts of dam development on SSC at the sub-basin scale (3S basin) of the MRB. The capacity of satellite remote sensing for broad temporal and spatial comparison of SSC patterns in sub-basins allowed for refined understanding of where and when dams and landscape changes influenced SSC patterns. This understanding is a critical step towards improved sediment monitoring and adaptive management throughout the MRB. This study showed the capacity of satellite remote sensing to monitor dam and landscape change impacts on SSC as follows:

- Satellite remote sensing was primarily suitable for monitoring background seasonal sediment loads. Dry season SSC patterns tended to dominate long term time series since more remote sensing data were available in the dry season due to lack of cloud cover.
- The performance of empirical models in predicting SSC from visible/NIR band data was improved by using separate equations for low (red band) and high (red/green band ratio) SSC. For monthly mean SSC predictions, the RMSE decreased (improved) up to 328 mg/L.
- The remote sensing technique detected changes in SSC due to dam construction (e.g., +120 mg/L at SP) and reservoir sediment trapping (e.g., -108 mg/L between KM and AM).
- Satellite data on nighttime lights, which reflects human settlement patterns, and land cover helped to better explain SSC patterns. Deforestation and increasing human settlement caused SSC increases (e.g., +117 mg/L at KM). The extent to which reservoir sediment trapping downstream of landscape impacts modulated SSC increases depended on reservoir size.
- The technique demonstrated how the SSC of the 3S rivers have compared to that of the Mekong mainstem over time (e.g., from ~13% to 100% greater).. SSC changes will continue with ongoing dam and landscape development in the MRB, and thus SSC monitoring will be imperative for effective sediment management.

A primary limitation of this work was the precision of the SSC predicted by the empirical model. The calibration of the empirical model introduced large uncertainty due to the small number of data (n=15), a low number of high SSC (<60 mg/L) data values (n=2), unequal distribution of the monitoring stations where the data were from, and different sediment

properties and channel conditions for the different monitoring stations. The wet season SSC predictions are also sparse due to high cloud cover and may be biased, particularly by anomalously high or low SSC predictions. Hence, future work should involve collecting and integrating additional in situ and satellite data, including data from other satellites (e.g., Sentinel-2). Further research on the river basin geomorphology and sediment properties (e.g., mineralogy) may also aid in improving the empirical model, and more complex techniques (e.g., neural networks) can be explored. Additional factors that influence sediment dynamics such as climate and other human interventions can also be integrated to improve this work and similar applications. The workflow for the approach used would be expedited and more reliable with improvements to Landsat could masking techniques.

While there are limitations in the data, techniques, and scope of this work, it should not hinder practitioners from leveraging the information that satellites can provide in better informing river, dam, and sediment management. The information that satellites provided in this study and in similar applications provide first-order system understanding which can inform where additional localized investigations should be conducted. The approach used can be implemented for ongoing monitoring and analysis of SSC in the MRB and other global river basins undergoing dam development and landscape changes. Findings from this work and future applications can also inform hydrologic engineers or water managers where and how suspended sediment impacts can be managed and mitigated. Furthermore, methods and results of this work can be used synergistically with computational modeling (e.g., Wei et al., 2019) and additional remote sensing data (e.g., precipitation) to address related scientific, engineering, and management questions. Overall, satellite remote sensing is shown in this study to be an effective tool for understanding dam impacts to suspended sediment on broad spatial and temporal scales.

It can help to address critical needs for improved sediment monitoring, adaptive sediment management, and effective land and water management policies throughout the MRB and other global basins.

Acknowledgements

This work was primarily funded by The National Science Foundation Graduate Research Fellowship Program under Grant No. DGE-1762114 to the first author. This work also benefitted from NASA Earth System and Science Fellowship grant 80NSSC17K0379 to second author (Matthew Bonnema) and the NASA Water Applied Science Program (grant NNX15AC63G) to third author (Faisal Hossain). The authors would like to thank MRC, Kel Markert of the NASA/USAID SERVIR program, and ADCP for providing in situ sediment data; Kensey Daly for assistance in retrieving land cover data; and Nishan Kumar Biswas for GIS assistance.

Chapter 4. STAKEHOLDER-DRIVEN DEVELOPMENT OF A CLOUD-BASED, SATELLITE REMOTE SENSING TOOL TO MONITOR SUSPENDED SEDIMENT CONCENTRATIONS IN MAJOR BANGLADESH RIVERS

Note: This chapter has been adapted from an article submitted to *Environmental Modelling and Software*. At the time of writing, this article has been accepted and is in press.

Abstract: Environmental decision-support tools often fail to be effectively applied in society because tools are "use-inspired" rather than "user-ready." Stakeholder engagement by researchers is frequently the missing, critical component. Here, university researchers collaborated with the Bangladesh Water Development Board (BWDB) in developing a cloud-based, satellite remote sensing tool for monitoring suspended sediment concentrations (SSC) in major Bangladesh rivers. Bangladesh faces complex river erosion and sediment management challenges. The tool helps to overcome BWDB's constraints of limited resources and ground-based monitoring capacity. The tool maps estimated SSC over satellite images and provides long-term estimated SSC time series at user-designated points. The key elements of success in the engagement process were the partnership and trust between the researchers and stakeholder; stakeholder leadership and ownership; diversity of stakeholder roles engaged; researcher's understanding of the stakeholder, problem, and context; and open-source, easy-to-use tool. Weaknesses in the engagement process can be improved on in future work.

4.1 INTRODUCTION

Environmental researchers frequently develop “use-inspired” tools to improve monitoring, modeling, and understanding of Earth systems. However, these research tools are not always “user-ready,” or directly integrated into societal application and decision-making (Hossain, 2015; Hossain, Siddique-E-Akbor, Yigzaw, et al., 2014; Irwin et al., 2018; McIntosh et al., 2011; Prados et al., 2019). This situation is analogous to two standalone mountains, one symbolizing research and the other symbolizing society. In between the mountains is a desolate “valley of death” (National Research Council, 2000), as tools from research often perish before making it to society for uptake. The crux is that research tools cannot cross the valley and go from use-inspired to user-ready on their own. Researchers must take their tools, descend from their mountain, and journey across the valley with stakeholders.

Although stakeholder engagement is critical for environmental decision-support tools to become operational in society, it is rarely made a priority. For researchers, stakeholder engagement is typically seen as being time-consuming, expensive, complicated, risky, and unworthy of high-impact scientific journal publication (Glicken, 2000). Environmental researchers that do aim to conduct stakeholder engagement may struggle with developing a sound approach and tangible goals. Stakeholder engagement entails the integration of technical and social processes (Korfmacher, 2001), which environmental researchers are rarely trained to do. While stakeholder engagement is not new (e.g., Baroudi et al., 1986; King and Rodriguez, 1981), there is no consensus in environmental literature about best practices (Sandink, Simonovic, Schardong, & Srivastav, 2016). Examples in literature have varying project contexts and constraints, and therefore standards for success are highly variable.

Despite these challenges, there are valuable recommendations and criteria for stakeholder engagement in literature. For example, best practice recommendations for successful use of environmental decision-support systems were given by McIntosh et al. (2011). Practices were grouped into five categories: designing for ease of use; designing for usefulness; establishing trust and credibility; promoting the decision support system for acceptance; and starting small and simple. Eleven criteria for success in stakeholder engagement were developed by Sandink et al. (2016) based on those commonly found in literature. These included: clear problem has been defined with the assistance of stakeholders; know the stakeholder group; stakeholders involved early and in as many development phases as possible; gain trust, establish neutrality; and iterative processes applied. Seven recommendations for "crossing the valley of death" were provided by Hossain et al. (2014). These included: aim for full ownership of a system by stakeholders; seek two-way feedback and listen more than talk; train stakeholder agency from the ground up through hands-on tasks in a thorough and patient way. Insights on user requirements and stakeholder interaction have also been well explored in the context of participatory modeling (e.g., Voinov & Bousquet, 2010; Voinov & Brown, 2008).

Along with the recommendations in literature, increasing environmental data availability and technological capacity provide immense opportunities to expand stakeholder engagement in developing environmental decision-support tools. Two specific examples of advancements are satellite remote sensing and cloud computing. Earth-observing satellites are rapidly increasing the volume and types of environmental data. Over 500 earth-observing satellites have been launched over the past 50 years, and over 150 more are planned to launch over the next 12 years (CEOS, 2020; Guo, 2017; Yao et al., 2020). Earth-observing satellites provide a global vantage and repeatable objective measurements (United Nations Office for Outer Space Affairs, 2018).

Most satellite data are freely and publicly available, but there are barriers to effectively using these data such as their massive storage size, high variability, and high complexity. However, expansion of cloud storage and computing capabilities are lowering these barriers. For example, Google Earth Engine (GEE) is a fully cloud-based, high performance computing platform that stores multi-petabytes of pre-processed satellite imagery (Gorelick et al., 2017). GEE has web-based JavaScript API and integrated development environment in which developers can rapidly implement algorithms and visualize outputs on an interactive map. Developers can also create apps with graphical user interfaces that allow non-programmers to interact with maps and algorithm outputs. GEE and its datasets are freely available for non-commercial use.

The advances of satellite remote sensing and cloud computing have immense potential to support environmental management in economically developing regions. These regions typically have limitations in their in situ environmental data (quality and quantity), local computing bandwidth, power supply, and internet reliability. Satellite remote sensing supplements in situ data, and cloud-computing lessens dependence on local computer resources. However, for effective technology transfer and local capacity building in developing regions, there must also be proper education, training, and co-development of decision-support tools. While there are researchers and institutions forging these paths (e.g., Biswas and Hossain, 2018; Hossain et al., 2014c; Prados et al., 2019), significant needs remain. Considering that economically developing regions are generally most vulnerable to the increasing pressures of environmental change, it is urgent that technologies are effectively implemented to support their adaptation, resilience, and capacity (Independent Group of Scientists appointed by the Secretary-General, 2019).

Globally, the “new normal” continues to evolve with interconnected environmental, health, economic, and social challenges. At the same time, environmental data and technological

capabilities are rapidly expanding and providing immense opportunities for innovative and scalable decision-support tools. For the tools to directly serve society, the scientific research community must intentionally evolve, rethink priorities, and enter into new territories of stakeholder engagement. In doing so, it is imperative that institutions and funding agencies support these efforts and equipped the next generation of environmental researchers for this paradigm shift (Brown et al., 2015; Irwin et al., 2018; Lettenmaier, 2008; National Research Council, 2014). Examples of environmental researchers conducting convergence and "user-ready" research in partnership with stakeholders can help to guide these efforts.

This paper describes the stakeholder engagement process in developing a cloud-based, satellite remote sensing tool for monitoring suspended sediment concentrations (SSC) in major rivers of Bangladesh. This tool, called BROSS, (Bangladesh Remote Sensing of Suspended Sediments) was co-developed by researchers from the University of Washington in USA and staff from a stakeholder agency, the Bangladesh Water Development Board (BWDB). The tool development and stakeholder engagement process were conducted over one year.

The guiding research question of this paper is: *What were the critical elements to a successful stakeholder engagement process in co-developing BROSS?* The objectives of this paper are to: (1) demonstrate a generalizable path by which researchers can conduct productive stakeholder engagement in a relatively short time-frame (~one year); (2) highlight the key strengths and weaknesses of the stakeholder engagement process; and (3) provide socially-relevant research directions for satellite remote sensing of river sediment and related software. While various publications highlight strengths and lessons learned in stakeholder engagement processes, this results in an extensive list for researchers which may distract their focus from the most important elements. This study is unique in that it distills critical steps, strengths, and

lessons learned and can help researchers and stakeholders in prioritizing the elements of their engagement approach. Also, while stakeholder engagement has largely been explored in the context of participatory hydrologic modeling, this study focuses on a far less studied topic of satellite-based monitoring of sediment. Thus, socially-relevant research directions for the scientific community are unique and have the potential to lead to more widespread use of a technology that is underutilized in societal decision-making.

In the text that follows, section 4.2 provides the background on the study area, stakeholder, and problem. Section 4.3 contains the BROSS tool purpose and description. Section 4.4 describes the methods used in the stakeholder engagement process. Section 4.5 provides the results, discussion, and lessons learned on the key strengths and weaknesses of the process. Section 4.6 concludes the paper.

4.2 BACKGROUND ON STUDY AREA, STAKEHOLDER AGENCY, AND PROBLEM

4.2.1 *Bangladesh hydrology, geomorphology, and sediment dynamics*

The country of Bangladesh (Figure 4.1) lies in the active delta of three of the world's largest rivers: the Ganges, Brahmaputra, and Meghna. In Bangladesh, the Brahmaputra is known as the Jamuna River. Downstream of the Jamuna and Ganges rivers confluence is the Padma River. The Meghna River is divided between the Upper Meghna River, upstream of its confluence with the Padma River, and the Lower Meghna river, downstream of its confluence with the Padma River. Bangladesh also has hundreds of smaller rivers throughout the landscape. Bangladesh's major rivers originate in the Himalayan and east Indian mountains, flowing through various countries before reaching Bangladesh and discharging into the Bay of Bengal. Average annual streamflow discharge from the three major rivers is 1.35×10^{12} (trillion) m^3/year (Small et al., 2009). Average annual sediment discharge estimates range from 500 to 2,400 MT per year, and are

dominated (>98%) by sediment loads from the Padma and Jamuna rivers (M. Rahman et al., 2018). The majority (>80%) of streamflow occurs during the summer (June to September), due to the combined impacts of seasonal monsoons and snowmelt from upstream mountains (Small et al., 2009; Subramanian & Ramanathan, 1996).

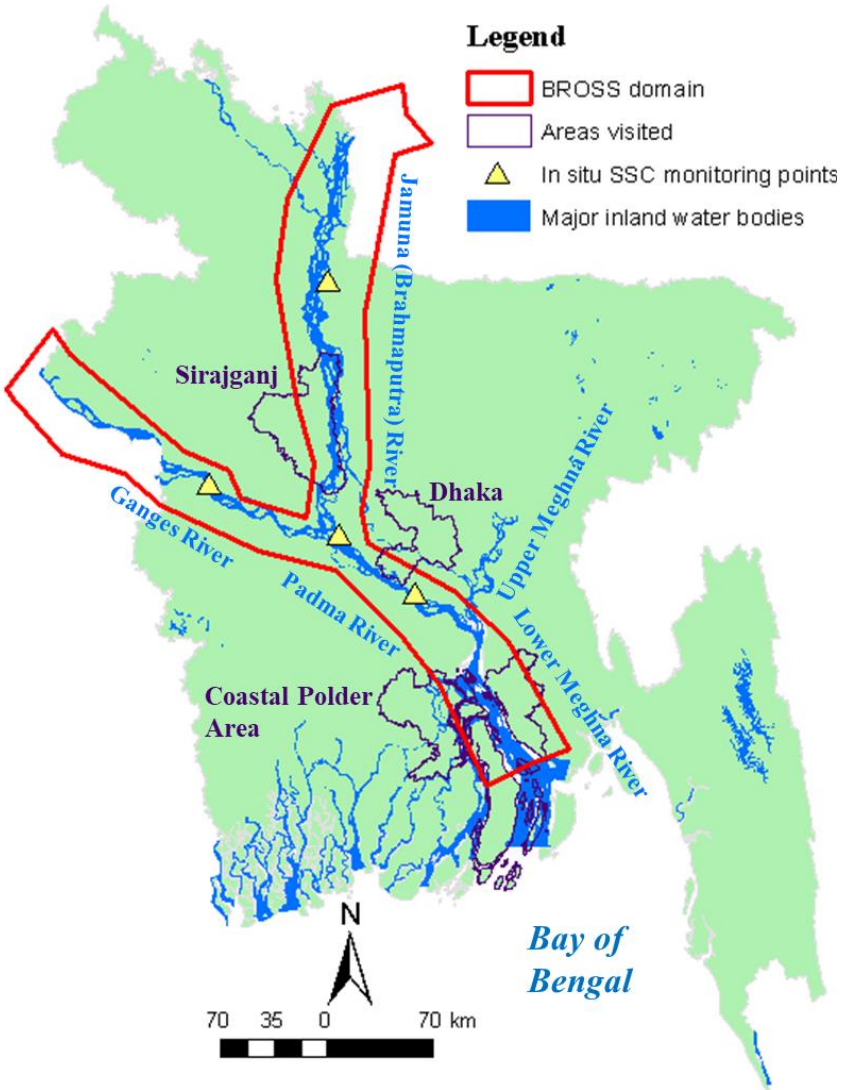

Figure 4.1. Map of Bangladesh with major rivers, BROSS domain, and sites visited during stakeholder agency engagement trip. In situ SSC monitoring locations are maintained by the stakeholder agency, BWDB. Map developed with ArcGIS software (Esri, Redlands, California). Geographical boundaries from OCHA ROAP (2019).

Bangladesh's major rivers are highly prone to erosion/deposition, channel shifting, and char (riverine islands and bars) development. This is largely due to the extremely high rate and fluctuation of streamflow and sediment transport, particularly in the summer monsoon season (Sarker, Akter, & Ruknul, 2011). The riverbanks and channel beds, primarily consisting of fine sand and silty sediments with occasional clay, have little resistance against erosive forces (Billah, 2018; McLean, Vasquez, Oberhagemann, & Sarker, 2012; Sarker et al., 2011; Sarker, Huque, Alam, & Koudstaal, 2003). The rivers are mostly flat (2-7.5 cm/km) (Sarker et al., 2003), making erosion/accretion and shifting patterns widespread and difficult to predict.

The Jamuna River is an intensely braided river that erodes thousands of hectares of mainland floodplain each year. In recent years, its braiding intensity and width have increased (Sarker, Thorne, Aktar, & Ferdous, 2014). The Ganges River is predominantly a meandering planform with some braided reaches. The Padma and Lower Meghna rivers vary spatially and temporally between single- thread meandering and multi-channel braiding patterns (Sarker et al., 2003; Shajahan & Reja, 2012). Length-average bank erosion rates are higher in the Jamuna, Padma, and Lower Meghna rivers compared to the Ganges and Upper Meghna rivers (Sarker et al., 2003). However, compared to the Jamuna and Meghna rivers, SSC is highest in the Ganges. Storm surges and cyclones also cause severe erosion, deposition, and channel shifting, primarily amongst the Lower Meghna River.

4.2.2 *Societal impacts of river sediment dynamics*

Bangladesh is a developing/emerging country (International Monetary Fund, 2019). Its population is ~160 million people, and its population density of 1,240 people per square km of land is one of the highest in the world (Food and Agriculture Organization & World Bank, 2018). Millions of people in Bangladesh live alongside rivers or on chars throughout the river

system, and many livelihoods are directly tied to natural resources (e.g., agriculture, fisheries) (Sarker et al., 2003; Shajahan & Reja, 2012). Riverbank erosion frequently degrades and destroys housing, farmland, property, and public infrastructure. Each year, erosion leaves thousands of people landless and homeless, and millions negatively impacted in other ways (Islam & Rashid, 2011). Accretion along the banks and channel beds also inhibits ship navigation. Hence, river erosion/accretion is directly and heavily integrated into the society and economy of Bangladesh.

4.2.3 *Stakeholder agency mission and needs*

The stakeholder agency, BWDB, is a federal government entity focused on water resources engineering and management, environmental sustainability, and improvement of livelihoods throughout the country. The agency has major, long-standing efforts to monitor, manage, and mitigate the impacts of riverbank erosion and accretion. However, the vastness and complexity of the river system as well as limited resources available to the agency are major constraints.

The stakeholder agency's existing in situ suspended sediment monitoring capacity is not adequate for the needed understanding and prediction of river system sediment dynamics. The agency has 25 in situ sediment monitoring points (M. Rahman et al., 2018), but only four are located along the major rivers (Figure 4.1). The agency has conducted in situ suspended sediment monitoring throughout the river system since the 1960s. However, sediment data have not been collected continuously and data from some time periods and locations is less reliable (M. Rahman et al., 2018). A large reason for these issues is that in situ sediment monitoring is time-consuming, complicated, and expensive, and the agency has not had the resources to bolster their sediment monitoring approach. In situ sediment monitoring can also be difficult and

dangerous during the monsoon season, when erosion/accretion is prominent and sediment loads are highest.

Riverbank protection has been implemented along the major rivers since the early 1970's (Sarker et al., 2011). However, there are substantial lengths of non- or poorly-protected, vulnerable riverbanks where people live and farm. The stakeholder agency continuously installs permanent riverbank protection, which is mostly revetments layered with concrete blocks and geotextile bags filled with sand. However, along with limited resources, there is also the constraint of time between monsoon seasons to implement permanent protection measures. During the monsoon season, the agency also rapidly responds to emergency erosion events by implementing temporary protection, which is typically geotextile bags filled with sand. Since erosion points are difficult to predict, it is challenging for the agency to prioritize and prepare for both permanent and temporary protection needs. In addition, the agency conducts river dredging to manage erosion and accretion, however the submerged locations of sediment deposition are difficult to determine. The costs for these various measures are extremely high.

The stakeholder agency is interested in improving their prediction of erosion and accretion hotspots so that they may more effectively allocate limited resources to engineering and mitigation measures, and ultimately protect human livelihoods. Areas of erosion/accretion frequently migrate throughout the vast, complex rivers and are difficult to strategically monitor with the agency's sparse in situ sediment monitoring capacity. The ability to monitor sediment dynamics throughout the entire river system, particularly using satellite remote sensing, can help to inform the agency where potential erosion/accretion points may be, and where further on-the-ground investigation is warranted.

4.3 BROSS TOOL PURPOSE AND DESCRIPTION

4.3.1 *BROSS tool purpose*

BROSS estimates SSC throughout major Bangladesh rivers using satellite remote sensing surface reflectance data. The agency primarily plans to use BROSS to improve understanding of where migrating points of significant erosion/accretion are occurring. In addition, BROSS is intended to help improve mandated forecasting of sediment loads during monsoon seasons and to help improve the understanding of the horizontal and vertical profiles of river sediment. The purpose and plans for BROSS were directly defined by the stakeholder agency, BWDB, in the early stages of the tool development.

4.3.2 *BROSS tool description*

The BROSS domain is within Bangladesh, along the mainstems of the Jamuna, Ganges, Padma, and Lower Meghna rivers (Figure 4.1). SSC predictions are of two forms: time series of SSC averaged over a region of interest (ROI) within the BROSS domain; and SSC mapped throughout the domain for a single satellite image. BROSS uses visible (red, green, blue) and near-infrared (NIR) band data from the Landsat, Sentinel-2, and MODIS satellite series (Table 4.1). The different spatial resolutions, temporal resolutions, and durations of these satellites have trade-offs in decision-making. Landsat and Sentinel-2 data have relatively high spatial resolution and can distinguish SSC patterns along river cross-sections and banks. However, the temporal resolutions are relatively low and can miss critical hydrologic events. MODIS data have high temporal resolution, however the spatial resolution is relatively poor and only appropriate for reach-scale SSC averages of wide (>500m) rivers. While Sentinel-2 data have relatively high spatial and temporal resolution, the short historical records inhibit strong calibration for predicting SSC. Models for predicting SSC from satellite data were calibrated using in situ

suspended sediment data collected by the stakeholder agency, BWDB, from 1968 to 2019 at the four monitoring points along the Jamuna, Ganges, and Padma rivers (Figure 4.1).

Table 4.1. Satellites used in BROSS

Satellite	Spatial Resolution	Temporal Resolution	Data duration
Landsat 5 (TM)	30 m	16 days*	1/1/1984-5/5/2012
Landsat 7 (ETM+)	30 m	16 days*	4/15/1999- 5/31/2003**
Landsat 8 (OLI)	30 m	16 days*	2/11/2013- Present
Sentinel-2	10 m	5 days	3/28/2017- Present***
MODIS (MOD09GA)	500 m	1 day	2/24/2000- Present

Notes:
** There is an 8-day offset between Landsat satellites with overlapping operational durations.*
*** Landsat 7 is operational at the time of publication, however due to equipment failure on 5/31/2003, subsequent images are not reliable for this application.*
**** Sentinel-2 was launched in October 2014, however surface reflectance data are not available in GEE until 3/28/2017.*

BROSS integrates two modeling approaches to predict SSC from satellite data: regression and artificial neural networks (ANN). Regression is a simple, widespread approach that is relatively simple to implement (e.g., Beveridge et al., 2020; Markert et al., 2018). For BROSS, an exponential model is used to relate SSC to a ratio of satellite band data (e.g., SSC=a*exp(b*(red/green)+c) where values for a, b, and c are determined by regression). ANN uses pattern recognition to capture both linear and non-linear relationships (Peterson, Sagan, Sidike, Cox, & Martinez, 2018; Sudheer, Chaubey, & Garg, 2006). ANN is relatively complex and challenging to implement, therefore is less commonly used for remote sensing of river sediment. However, in this study and others (e.g., Peterson et al., 2018), ANN overall has superior performance to regression (Table 4.2). BROSS uses ANN model inputs of single bands, band combinations, month of the sample collection, and satellite identification. Together,

regression and ANN give a plausible range of SSC which is valuable for decision-making under uncertainty.

Table 4.2. Performance of regression and ANN models used in BROSS. Combined satellites (Landsat 8 +Sentinel-2, Landsat 5+Landsat 7) were calibrated in models together. Stronger result between ANN and regression for each line is in bold.

	ANN	**Regression**
Root mean square error (RMSE)		
Landsat 8 + Sentinel-2	139 mg/L	**134 mg/L**
Landsat 5 + Landsat 7	**123 mg/L**	165 mg/L
MODIS	228 mg/L	**202 mg/L**
Coefficient of determination (r^2)		
Landsat 8 + Sentinel-2	**0.74**	0.71
Landsat 5 + Landsat 7	**0.35**	0.22
MODIS	0.31	**0.40**
Anomaly correlation coefficient		
Landsat 8 + Sentinel-2	**0.86**	0.83
Landsat 5 + Landsat 7	**0.93**	0.89
MODIS	0.52	**0.61**
Anomalies		
Landsat 8 + Sentinel-2	**-102 mg/L**	-130 mg/L
Landsat 5 + Landsat 7	**-236 mg/L**	-386 mg/L
MODIS	**-70.2 mg/L**	-278 mg/L
Spearman r		
Landsat 8 + Sentinel-2	**0.88**	0.81
Landsat 5 + Landsat 7	**0.60**	0.46
MODIS	**0.64**	**0.64**

BROSS has two operational platforms, which are both are easily accessible for users via a web browser. One platform is GEE (https://earthengine.google.com/; section 4.1; Gorelick et al., 2017) where BROSS is implemented using the GEE JavaScript and user interface APIs. The second platform operates via a local desktop server and Google cloud, and is hereinafter called the 'local server' platform. The local server platform back-end uses scripts written in the Linux Operating System using Python scripting language. The front-end development uses all open-

source tools and software, following Ahmad and Hossain (2019a) and Biswas and Hossain (2018). Briefly, this entails:

- local web server environment setup using XAMPP (Cross-Platform (X), Apache (A), MariaDB (M), PHP (P), and Perl (P); https://www.apachefriends.org/index.html)
- map visualization using the JavaScript library called Leaflet (https://leafletjs.com)
- chart production using the JavaScript library called HighCharts (http://www.highcharts.com)
- SSC outputs processed to the GeoTIFF format for rendering on the webpage and exporting using Geospatial Data Abstraction Library (https://www.gdal.org)
- dynamic and interactive user interface development using the styling and event-handling libraries of Materialize (https://materializecss.com) and jQuery (https://jquery.com)

Both platforms produce long-term time series of estimated SSC for user-designated regions based on satellite data (Figures 4.2 to 4.5). The time series can be downloaded. Both platforms also produce colored maps of the estimated SSC distribution in the BROSS domain (Figure 1) for individual satellite images (Figures 4.2 and 4.4). Users can click on individual pixels of mapped SSC to obtain the value. When generating SSC time series and maps, both platforms mask out pixels of the land surface, clouds, and cloud shadows so that only water surface pixels are included. While these are the commonalities of the platforms, there are notable differences in the key features (Table 4.3), interfaces (Figures 4.2 and 4.4), and workflows (Figures 4.3 and 4.5) of the two platforms. For example, the local server platform includes both the ANN and regression models, whereas GEE only includes the regression model. Also, GEE allows users to sketch the region-of-interest for the SSC time series, whereas the local server

only generates time series at predefined locations (the stakeholder can add predefined locations as desired).

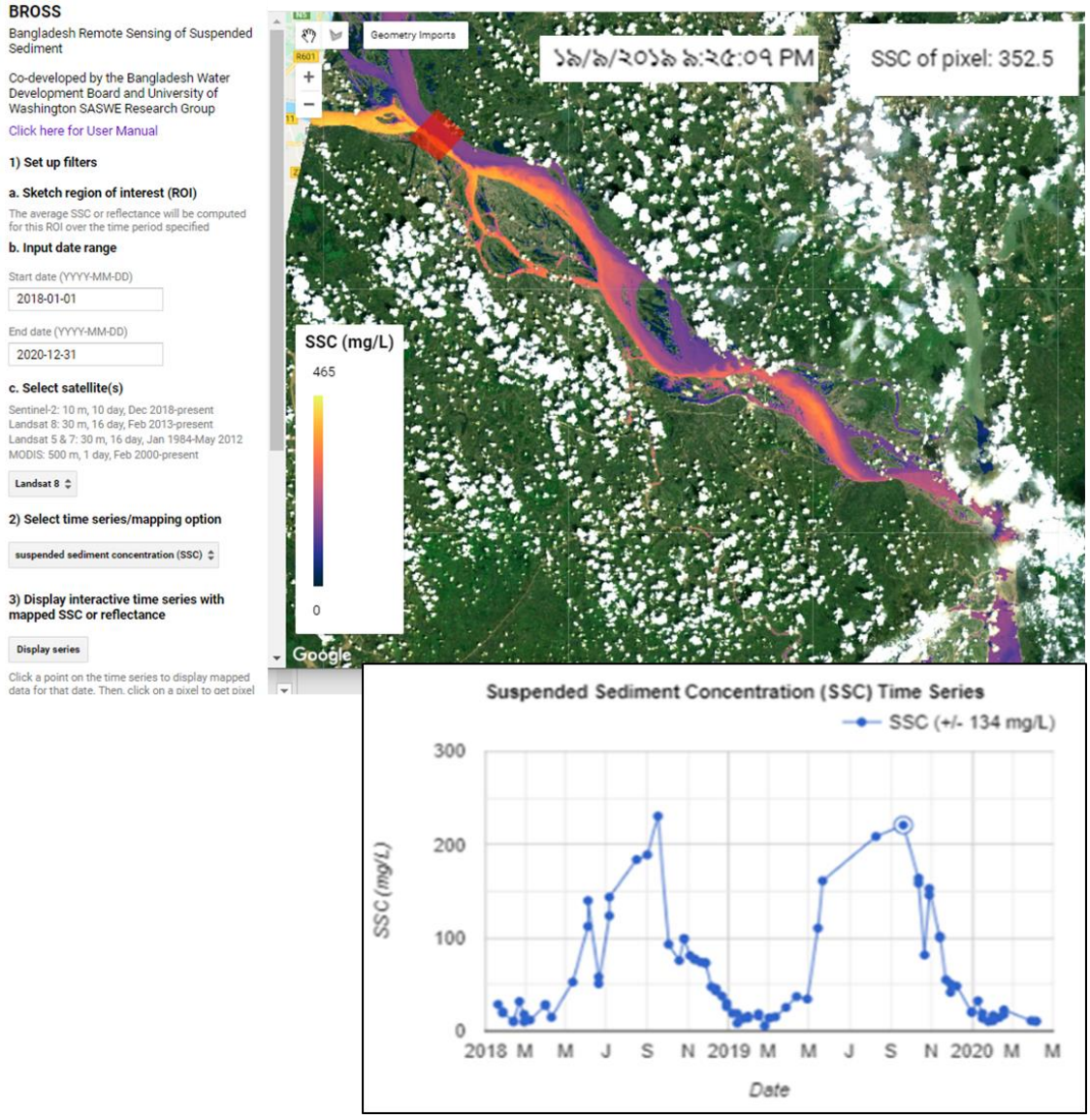

Figure 4.2. Interface and outputs for BROSS on GEE.

A map of SSC and a time series chart (moved and enlarged for readability) of the SSC averaged for the user-specified region of interest (red box, upper left of satellite image). Predictions are from regression model. Web address for tool is https://bross.users.earthengine.app/view/gee

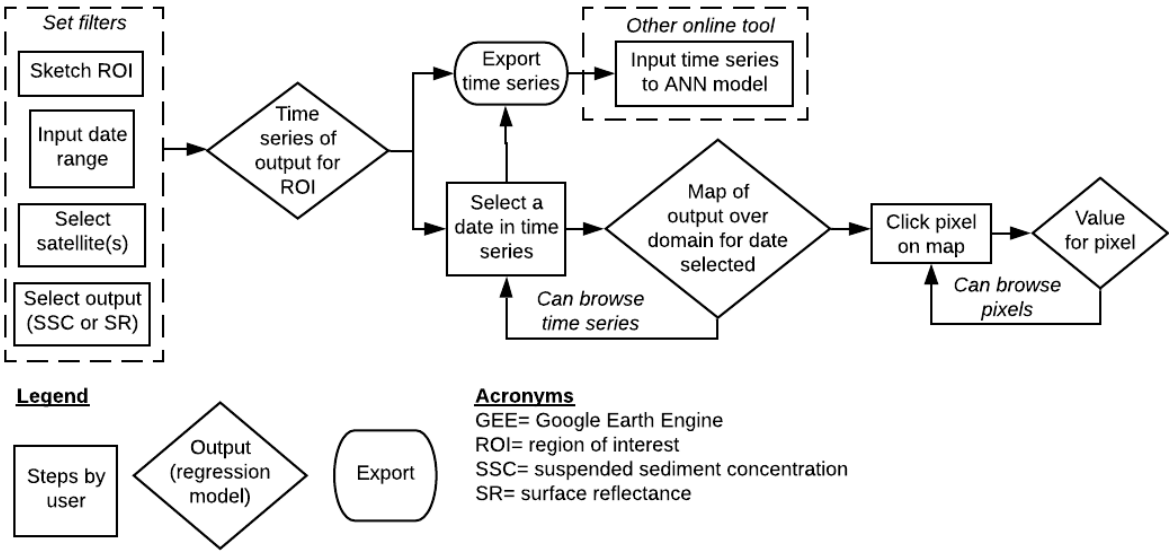

Figure 4.3. Workflow for BROSS on GEE

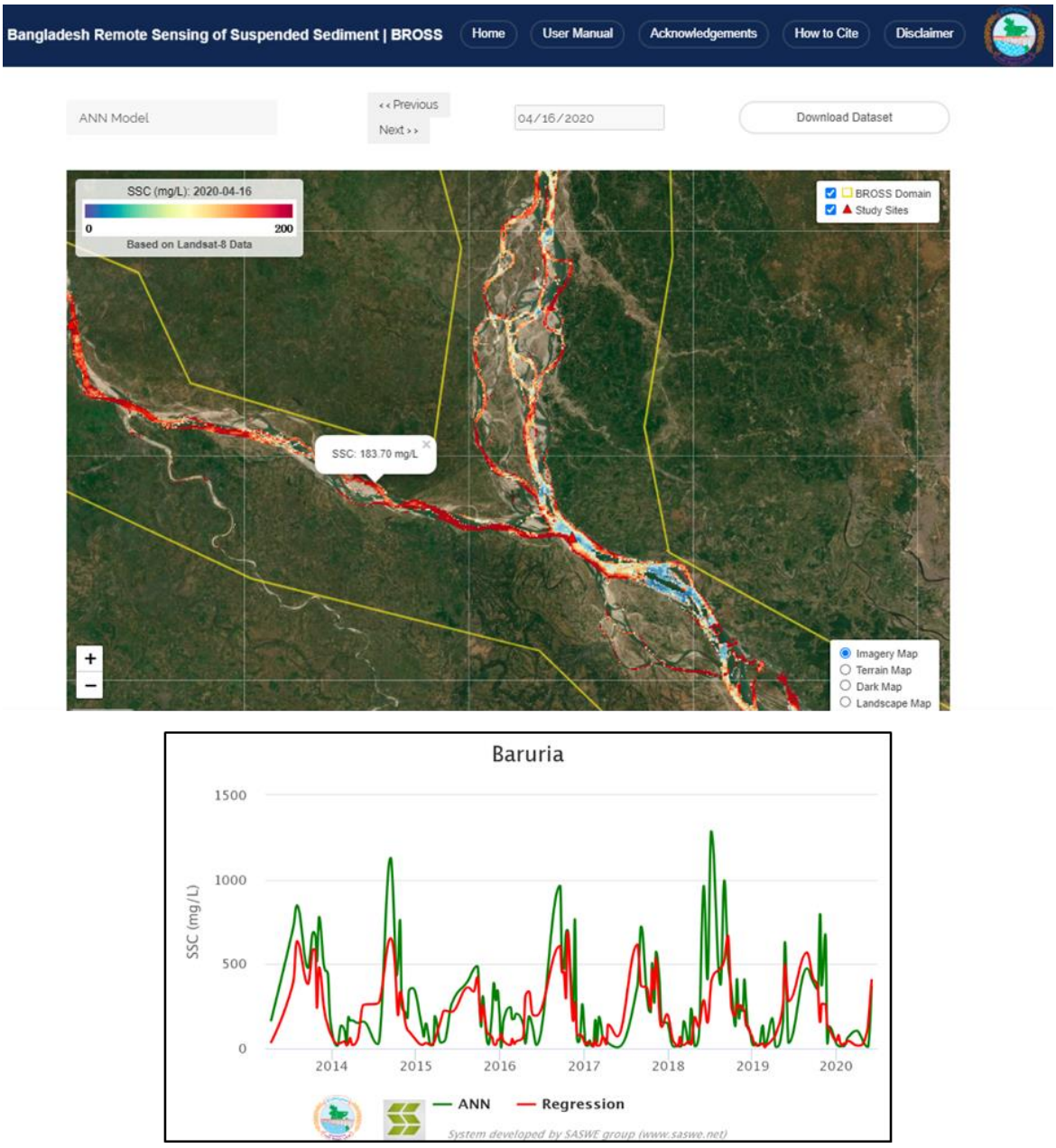

Figure 4.4. Interface and outputs for BROSS on local server.

A map of SSC predicted from ANN and a long-term time series of SSC (moved and enlarged for readability) predicted from satellite data using ANN and regression models at the in situ monitoring point called "Baruria." Web address for tool is *http://depts.washington.edu/saswe/bross.*

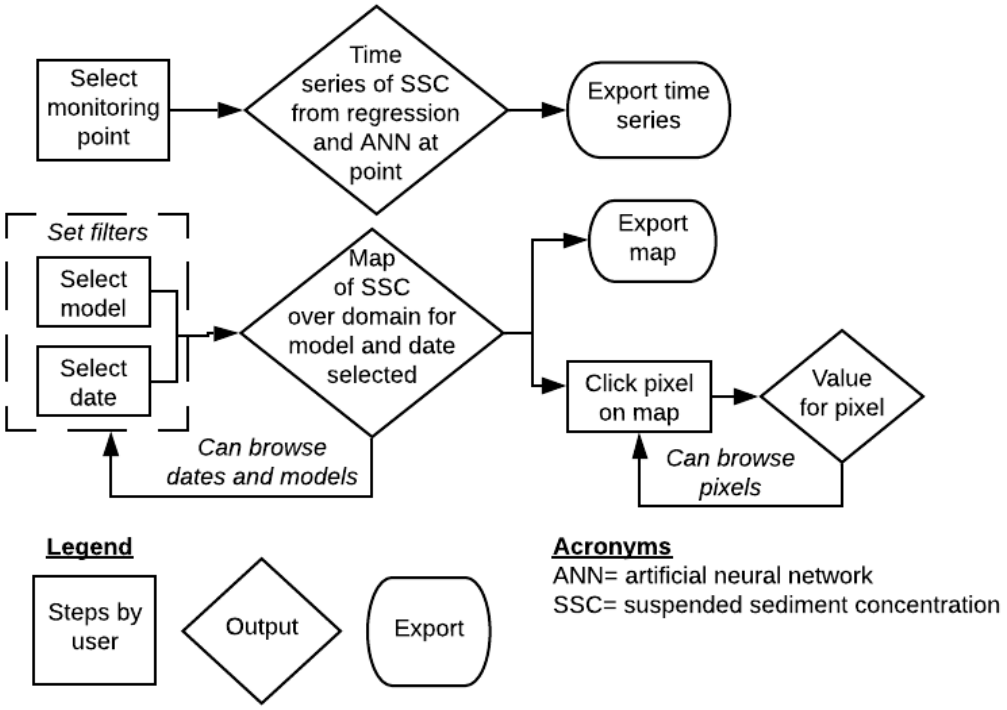

Figure 4.5. Workflow for BROSS on local server

Table 4.3. Comparison of key features for BROSS platforms

Feature	Google Earth Engine	Local server
Mapped SSC from regression	X	X
Mapped SSC from ANN		X
SSC time series from regression	X	X
SSC time series from ANN	Use separate computational notebook	X
SSC time series for user-defined region of interest	X	
SSC time series auto-generated at in situ monitoring stations		X
Satellite data availability	Landsat 5, 7, 8; Sentinel-2; MODIS	Landsat 8
Spatial resolution of maps	Landsat: 30 m, Sentinel-2: 10 m, MODIS: 500 m	Regression: 100m, ANN: 200 m
Temporal availability	Full extent of satellite data	Time Series: Full extent of Landsat 8 data Map: Past 6 months
Able to export time series	X	X
Able to export map		X
Able to view values of individual pixels	X	X
Able to view and download satellite reflectance data	X	
Data storage source	Google Cloud	Local server
Computing source	Google Cloud	Google Cloud
Computing language	JavaScript	Python (back-end); JavaScript & HTML (front-end)

The BROSS GEE tool is at https://bross.users.earthengine.app/view/gee. The BROSS local server tool is at http://depts.washington.edu/saswe/bross. Further technical details about BROSS are in the technical manual, and further details about the user interfaces and functionality are in the two user manuals. All manuals and codes for both BROSS tools are found on GitHub at https://github.com/cbev/bross.

4.4 STAKEHOLDER AGENCY ENGAGEMENT METHODS

The approach to co-developing BROSS followed strategies commonly applied and recommended in conducting convergence research and stakeholder engagement (National Research Council, 2014; Sandink et al., 2016; Voinov & Bousquet, 2010). The generalized steps and timeline are adaptable to other researcher-stakeholder partnerships, locations, and environmental challenges (Figure 4.6). For example, the steps can also be applied for researchers and stakeholders in the same country/region and social/cultural context. Throughout sections 4.4.1 to 4.4.6, figures depict generalized sub-steps while the text describes the BROSS co-development process as a case study of how these steps may be carried out by early-career researchers. Hereinafter, the following terminology is used to describe the primary roles in the co-development process:

- 'developer' is the primary university researcher engaging in the co-development process
- 'researchers' or 'research group' is the university research group that the developer is part of
- 'stakeholder agency,' or 'agency' for short, is BWDB
- 'leading agency staff' is three staff from BWDB that have executive decision-making powers in the agency and play a leading role in the co-development process
- 'agency sediment expert' is one of the leading agency staff who is an expert on numerical modeling of sediment transport and riverbank erosion

Figure 4.6. General approach and timeline to BROSS co-development process for researchers

4.4.1 *Step 1: Establish partnership and become familiar with stakeholder agency*

The research group focuses on conducting user-ready research, promoting access to water resources information, and improving livelihoods in challenging environments with sustainable satellite remote sensing and hydrologic modeling applications. As part of this mission, the research group has been collaborating with the stakeholder agency and other Bangladesh water management institutions on satellite remote sensing applications since 2011. The research group has provided education and training on satellite remote sensing (Figure 4.7, part a), co-developed

multiple tools to support agency operations, and provided ongoing technical support (Hossain, Maswood, et al., 2014; Hossain, Siddique-E-Akbor, Yigzaw, et al., 2014; Hossain, Siddique-E-Akbor, Mazumder, et al., 2014).

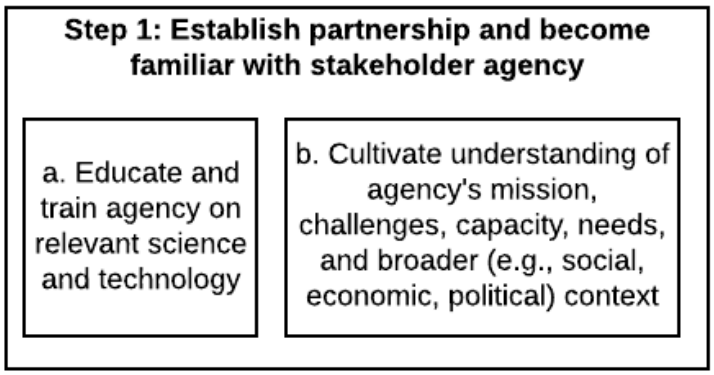

Figure 4.7. Sub-steps to foundational relationship with stakeholder agency

Through this long-standing partnership, the research group has institutional understanding of the stakeholder agency's context, challenges, capacity, and priorities (Figure 4.7, part b). From a technical standpoint, this includes understanding of Bangladesh's hydrologic system, where and what forms of hydrologic data the agency collects, and how the agency operates between office and field operations. From a social standpoint, the research group is also familiar with the culture of the agency and broader geographical region, the agency's management structure, and the agency's resource constraints. Having this broad technical and social understanding is important before narrowing to a specific project topic.

The partnership was initially established by the research group leader contacting stakeholder agencies, expressing interest in collaborating, and focusing on building relationships with multiple members of the agencies. Through these relationships, there was mutual learning about how the researchers and agencies could work together and where initial education and training was needed. Researchers that do not have the privilege of a preexisting relationship with a stakeholder agency may need to initiate a partnership building process. They can do this by

similarly networking with stakeholders and first focusing on robust relationship building (Voinov & Bousquet, 2010). The time and effort to establish partnerships is situational and depends on multiple, diverse factors such as the familiarity of the agency with research approaches. The establishment of the partnership can be integrated with the remaining steps.

4.4.2 *Step 2: Meet with stakeholder agency to match agency priorities to researcher expertise*

The co-development of BROSS was initiated by the agency during an in-person meeting between the researchers and stakeholder agency to discuss general collaboration opportunities for decision-support tools. The steps for matching agency priorities to researcher expertise were carried out in this meeting. The researchers organized this meeting and hosted the three leading agency staff at the researchers' university for two days. The researchers presented their focus areas and related decision-support tools as examples of what could be implemented for the agency (Figure 4.8, part a). The developer discussed their work on satellite remote sensing for SSC estimation in another region (Beveridge et al., 2020). The developer also demonstrated a web-based tool for satellite monitoring of SSC that was implemented by another group of researchers and stakeholders (Markert et al., 2018). The agency expressed interest in co-developing a similar satellite-based application for SSC to support their engineering and management priorities for river sediment, erosion, and accretion. The primary interest of the leading agency staff was for the SSC distribution of major rivers to be qualitatively mapped on individual satellite images in order to improve understanding of where migrating points of significant erosion/accretion are occurring. The agency invited the developer to conduct a follow-up trip to Bangladesh to facilitate the agency engagement process. Upon the agency's invitation, the developer committed to the co-developing BROSS and conducting the trip.

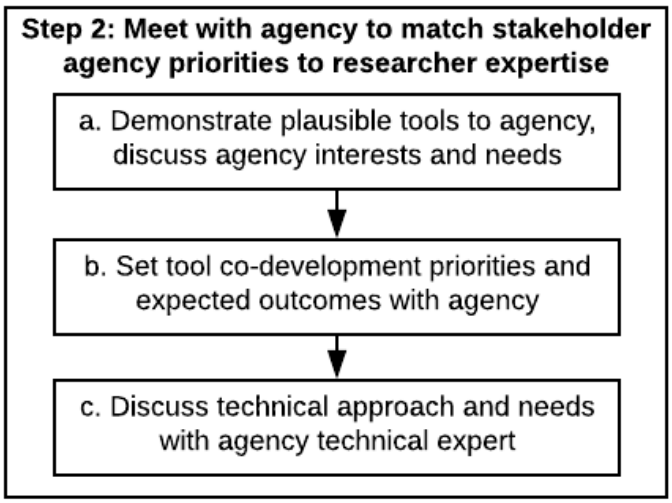

Figure 4.8. Sub-steps to initial meeting with agency

Next, the researchers and leading agency staff established the short-, mid-, and long-term priorities and action items for the BROSS co-development and agency uptake (Figure 4.8, part b). These were:

- Apply local in situ suspended sediment data to calibrate and validate a SSC regression model from satellite data (short to mid-term priority).
- Develop a cloud computing-based automated system for visualizing remotely-sensed SSC of Bangladesh major rivers using GEE (mid-term priority).
- Assign a dedicated agency staff to master the remote sensing technique and carry out research to monitor riverbank erosion and accretion hot spots (short to mid-term priority).

In addition, the developer met with the agency sediment expert, who shared about the agency's in situ sediment monitoring approach and data availability (Figure 4.8, part c). Based on this information, they planned the regression model calibration and BROSS prototype development. The agency sediment expert agreed to obtain the relevant in situ sediment and streamflow data from the agency and provide them to the developer. The developer and agency sediment expert also discussed the prototype design (workflow, etc.) based on the earlier

meetings. The workflow for BROSS on GEE (Figure 4.3) was devised (without consideration of ANN), with the understanding that it may change based on feedback from the agency during the follow-up engagement trip. During this meeting, the agency sediment expert also expressed interest in using BROSS in conjunction with models to better understand the horizontal and vertical profile of SSC.

It is possible that there would not be as readily of a match between the stakeholder agency priorities and plausible tools presented by the researcher. In that case, it is still valuable for the researchers and agency to discuss the agency's general management priorities and expected outcomes for the short-term and long-term. While there may not be an immediate need that the researcher can respond to, it may be discovered that there is potential for tool co-development in the future (e.g., after a certain milestone is met). Similarly, it will help for the agency to understand plausible tools that the researchers can develop, as an unexpected need for a similar tool may arise in the future. It is important that co-developed tools are not forced or implemented prematurely. This will likely detract from the effectiveness and long-term sustainability of the tool, and generally be a poor use of time and resources. With a partnership in place (Step 1), there is more flexibility to be patient with opportunities and let them develop in appropriate time.

4.4.3 *Step 3: Develop prototype tool and prepare for follow-up stakeholder agency engagement meeting/event*

Prior to the follow-up agency engagement trip, the developer prioritized calibrating models for predicting SSC from satellite reflectance data, producing a prototype system for the agency's trial use, and preparing for the trip. The model calibration and prototype system production were primarily conducted by the developer (Figure 4.9, parts a & b). However, the agency sediment

expert was involved in reviewing intermittent results, discussing issues, and determining next steps throughout the process (Figure 4.9, part c). The leading agency staff provided the developer with the in situ data and the developer downloaded relevant satellite data from GEE. Initially, models to predict SSC from satellite data were calibrated and tested using regression. Strong regression model results were difficult to obtain due to the high complexity of the river system and limitations of the satellite data and in situ data (Rahman et al., 2018; see technical manual). Because of the regression model limitations, the researchers proposed using ANN models to predict SSC from satellite data. To initially test the feasibility of ANN model in the BROSS domain, the researchers used the MATLAB Neural Network Toolbox (The MathWorks Inc., Natick, Massachusetts) and training approach from Ahmad and Hossain (2019b). After the ANN results proved to be stronger than the regression results, ANN models were developed using the Keras library in Python. The MATLAB toolbox is simpler to use, however the ANN models had to be programmed in Python to be implemented in BROSS.

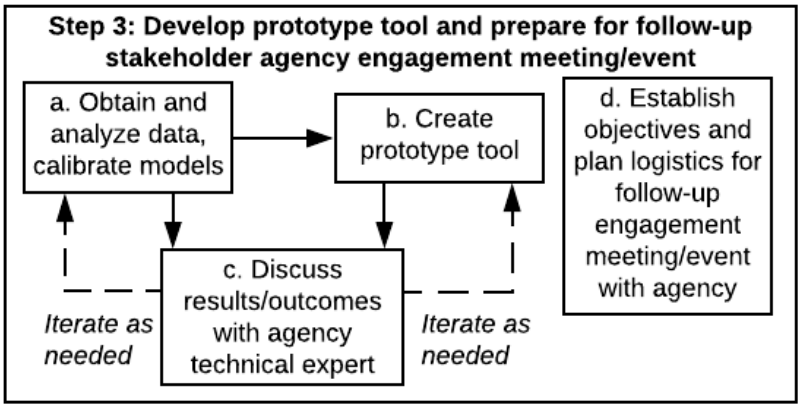

Figure 4.9. Sub-steps to prototype development and follow-up agency engagement meeting/event preparations

The BROSS prototype was developed in GEE based on the design discussed by the researchers and leading agency staff (Step 2). The prototype had limited user-interface

capabilities compared to the proposed final version so that excessive time was not spent on functionalities that may not be used. However, the prototype design allowed users to envision the proposed BROSS workflow and outputs. The prototype only used Landsat 8 satellite data and the regression model to predict SSC. The prototype design allowed users to select an in situ monitoring location, review the regression-predicted SSC time series for the full Landsat 8 record, and click on points of the time series to view the predicted SSC map for the specified date.

The researchers and leading agency staff scheduled the developer's follow-up engagement trip to Bangladesh for two weeks of January 2020 (Figure 4.9, part d). They collaboratively established the trip objectives, developed the itinerary, and determined coverage of costs. There was mutual understanding that the trip objectives were focused on agency engagement and would entail both office meetings and field site visits. The leading agency staff directed the trip preparations by inviting meeting attendees and planning the field site travel logistics. The agency planned to cover the expenses for room and board during the field site visits and the researchers planned to cover the airfare and remaining room and board costs. During this preparation period, the developer also prepared for the trip by studying the regional language, culture, and social customs. Part of this was by leveraging the research group's institutional knowledge about the region and the agency culture and operations.

4.4.4 *Step 4: Conduct follow-up agency engagement meeting/event to collect feedback on tool and validate societal impact*

The follow-up stakeholder agency engagement trip primarily composed of meetings with agency staff and collaborators; and visits to field sites where sediment challenges are prominent (Figure

4.10). The leading agency staff organized all activities and involved a diversity of participants (Table 4.4).

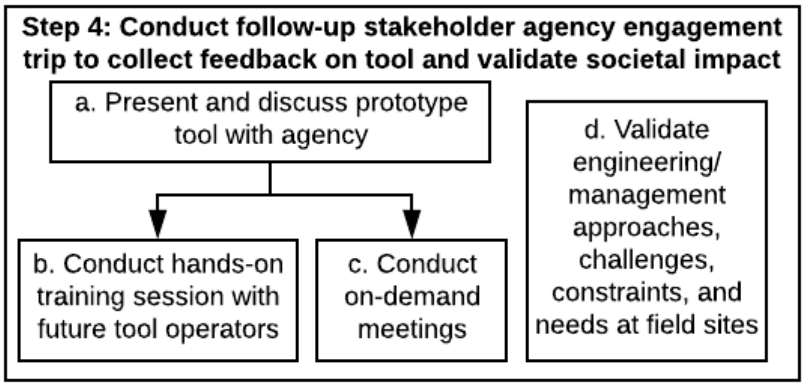

Figure 4.10. Sub-steps to follow-up agency engagement meeting/event

Table 4.4. Summary of event/meeting participants

Event/Meeting Type	No. of partic-ipants	Description of event/meeting participants (in addition to developer)
Formal presentation and discussion with agency (Dhaka)	31	All were agency staff except three, who were collaborators from external institutions. Agency participants mostly had engineering backgrounds. They came from various departments of planning, design, flood forecasting, and field operations; and their staff level ranged from junior to department chiefs. A fisheries department chief also participated. Of the three participants from external institutions, one was an engineering professor from a local university, one was a senior advisor in geomorphology from a local nonprofit environmental research institution, and one was a director from a commerce and industry government institution
Hands-on training session with agency (Dhaka)	8	Junior engineers and mid-level engineering supervisors from agency. These staff would likely operate or directly supervise those that would operate BROSS.
On-demand meetings with agency flood forecasting unit (Dhaka)	2	Executive engineers that conduct flood forecasting and warning operations
On-demand meeting with university researchers (Dhaka)	10	Three faculty, one senior research advisor, and six graduate student researchers of university research group focusing on water and flood management
On-demand meeting with nonprofit environmental research institution (Dhaka)	8	One senior advisor and seven junior and mid-level staff of river, delta, and coastal morphology division
Field site visit (Sirajganj)	3	Two field construction managers for bank protection and one engineering design staff
Field site visit (Coastal Polder Area)	6	One program manager, two field construction managers, three field engineers

The formal presentation at the agency headquarters in Dhaka (Figure 4.1) was the first major activity of the trip (Figure 4.10, part a). During the formal meeting, the developer first gave a presentation that encompassed the following: objectives of the agency engagement process; objectives of the BROSS tool; brief technical background on satellite remote sensing of SSC, including what the primary limitations are; preliminary regression and ANN model calibration

results; demonstration of the BROSS prototype operation; and description of additional features proposed for the final BROSS design. Then, the meeting participants asked questions and provided feedback (section 4.5.1). Following the agency's typical standard protocol, meeting participants were provided with a printed memo at the beginning of the meeting which summarized the presentation. The memo also contained questions from developer to the participants that could be responded to during the meeting and/or after the meeting in an optional online survey. The questions were about the value of BROSS in addressing agency needs, points of confusion about BROSS, and how BROSS could be improved. The memo and survey questions helped to focus the meeting objectives and discussion. It also allowed meeting participants multiple opportunities to provide questions and feedback.

Following the formal presentation, the developer led an informal, hands-on session on operating BROSS (Figure 4.10, part b). There was a brief, step-by-step demonstration of how to operate BROSS and the potential additional functionalities that could be integrated. The participants were asked to suggest changes in the BROSS workflow and design, and share whether the potential additional functionalities would be confusing or complicated for operators.

While the formal meeting and hands-on training session were planned before the trip, multiple unplanned, 'on-demand' meetings arose after the formal meeting with attendees interested in further discussion (Figure 4.10, part c). Two additional meetings were held with executive engineers of the flood forecasting department. The engineers posed an additional BROSS objective of supporting mandated forecasting of flood suspended sediment loads. One meeting was held with a local university research group which was conducting synergistic ground-based and remote monitoring of river erosion (M. M. Rahman et al., 2019). One meeting was held with the staff from a local nonprofit research institution which was conducting satellite-

based monitoring of river geomorphology. As a result of these meetings there were potential additional uses of BROSS, additional feedback on the BROSS design, and additional technical information shared with the developer to support the BROSS performance.

The developer also spent five days visiting two large project field sites where there are major engineering and management challenges that motivate the agency's interest in BROSS (Figure 4.10, part d). One site was Sirajganj (two days) and the other was the Coastal Polder Area (three days) (Figure 4.1). Sirajganj is along the Jamuna River and is one of the most vulnerable riverbank erosion areas in Bangladesh. The Coastal Polder area is along the Lower Meghna River and the coast of the Bay of Bengal. The area is subject to severe riverbank erosion, storm surge, and cyclones. Both areas are considered high risk because of the density of human communities living near water bodies that frequently suffer loss and damage of land and property. At the field sites that were visited, the agency conducts ongoing engineering measures such as riverbank protection and dyke/levee installation.

The field site visits were guided by agency staff with extensive site knowledge and experience. The agency staff demonstrated the on-the-ground approaches, constraints, challenges, and needs related to sediment, erosion, and accretion. The agency staff validated that the broad spatial and temporal perspective of BROSS would help to direct, monitor, and evaluate their field efforts. The developer and agency staff also visited the local communities surrounding the field sites. The community members and agency staff validated the potential societal impact of BROSS by sharing about how the communities are impacted by sediment-related disasters, how current engineering measures are improving livelihoods, and what issues remain.

4.4.5 *Step 5: Update and deliver tool, iterating as needed*

After completing the follow-up stakeholder agency engagement trip, the developer updated BROSS based on agency feedback. The calibration of regression and ANN models were enhanced by incorporating the technical information and agency feedback gathered during the follow-up engagement trip (Figure 4.11, part a). The BROSS tool back-end and front-end updates (Figure 4.11, part b) and writing of the user and technical manuals (Figure 4.11, part c) were done with careful consideration of the agency needs and concerns as well as the technical expertise of the agency's BROSS operators.

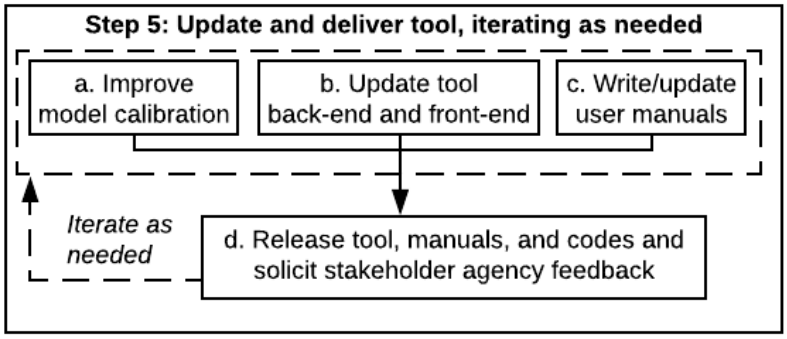

Figure 4.11. Sub-steps to updating and delivering tool

In April 2020, the BROSS tool, manuals, and codes were released to the leading agency staff (Figure 4.11, part d). In the email delivery, the developer provided a summary of the tool updates and deliverables along with links to the BROSS platforms and manuals, which were publicly available online. The developer encouraged BROSS to be tested and disseminated in the agency as appropriate, and for agency staff to contact the developer with questions, concerns, and needs. One week after the release, the agency sediment expert organized a call with the developer and research group leader to share feedback, ask questions, and discuss next steps (section 4.5.1). The expert's questions were largely technical, and follow-up action items were strategically delegated between the researchers and agency. The developer and expert carried out

follow-up action items as appropriate. Additional time (beyond one week) may be needed for stakeholders to fully assess issues, and multiple iterations of meetings and subsequent tool improvements may be needed over extended periods of time.

4.4.6 *Step 6: Provide ongoing complimentary technical support*

Moving forward, the stakeholder agency is the primary owner of BROSS and responsible for leading its ongoing use and improvement. Since the deployment of BROSS, the agency has been working to integrate BROSS into their sediment monitoring, engineering, and management approaches. Recommended future improvements for BROSS were included in the technical manual and were largely based on agency concerns and feedback collected throughout the engagement process. Users that have questions or find issues with BROSS can fill out an online form which is linked to in the tools and user manuals. The researchers maintain the responses to the form and will transition this responsibility to the agency when appropriate. The researchers are available for ongoing technical support and intend to fix issues and answer questions as they arise. Major updates to BROSS may be conducted by the researchers in the future at the request of the agency. The agency also has potential to engage with other institutions that may use and/or expand on BROSS.

4.5 RESULTS, DISCUSSION, AND LESSONS LEARNED

4.5.1 *Stakeholder agency feedback*

The stakeholder agency feedback on BROSS can be used by the broader research community to help guide future research directions in satellite remote sensing, river sediment dynamics, and stakeholder engagement. Overall, the agency staff had constructive feedback and clearly grasped BROSS's purpose, functionality, underlying theory, and limitations. The agency also strongly

took initiative in having full ownership of BROSS's future application and development. This demonstrated effective and sustainable capacity building.

The majority of stakeholder feedback was provided during the formal meeting on the follow-up agency engagement trip (section 4.4.4). Of the thirty-one meeting participants, eight provided verbal feedback at the meeting and one provided written responses, however none responded to the optional online survey. The verbal feedback at the meeting was generally from upper-level/management agency staff and experts from external institutions. The questions, concerns, and comments about BROSS were broadly on the science and technology, application to engineering and management, and ongoing research and development (Table 4.5). The concerns about the science and technology were largely inherent issues of satellite remote sensing in general (N. K. Biswas & Hossain, 2018) and in particular for sediment (Beveridge, Hossain, & Bonnema, 2020). Concerns about application to engineering and management were largely unknown in the present state of sediment research and management (Fu, Merritt, Croke, Weber, & Jakeman, 2019). However, the concerns could be addressed with ongoing research and application from the broader researcher community and from the agency. For example, BROSS outputs can be integrated with erosion prediction models developed for Bangladesh rivers (e.g., Biswas et al., 2016). Through discussions with the developer, the agency staff came to understand which questions and issues they posed were largely active research topics and beyond the present scope of BROSS. The agency was interested in pursuing the unknowns in partnership with the researchers and local institutions. The agency staff agreed with the proposed design and features (e.g., including ANN and multiple satellite options). However, if they had disagreed, this formal meeting would have been the opportunity to revise the final BROSS workflow and design.

Table 4.5. Questions and comment on BROSS prototype during formal meeting of follow-up agency meeting/event

Comment category	Comment type	Comment summary
Scientific and technological	Satellite data capacity and limitations	There are limitations due to the satellite penetration depth (~2m). The river channel depths are highly variable and sometimes <2m. SSC appears higher where depth is shallow, particularly in dry seasons.
		There is sparse satellite data during monsoon season due to clouds. How can there be better understanding of sediment during monsoon season, when SSC is highest and erosion/accretion are prevalent?
		Recognize the shortcomings and trade-offs of Landsat and MODIS for spatial and temporal resolution
	Sediment properties	Is it possible to differentiate between silt, sand, and bedload fractions?
		Is it possible to differentiate between organic and inorganic substances?
Application to engineering and management	Erosion prediction	There is stronger concern about the erosion/accretion along Brahmaputra-Jamuna and Padma (relative to Ganges-Padma)
		How strong is the relation of SSC to erosion/accretion?
		Can char (island) formation be predicted?
	Sediment volume	It would be valuable to incorporate sediment volume error calculation
Ongoing research and development	--	Recognize research is ongoing and that this is a work in progress
		There is potential for collaboration between agency, researchers, and local (Bangladesh) research institutions on large-scale monitoring system that integrates remote sensing and ground-based observations.

During the hands-on training session with eight junior and mid-level agency staff that would be directly involved in BROSS operations (section 4.4), the proposed final BROSS design was accepted. The staff found the graphical user interface to be easy-to-use. The staff felt comfortable with the user customization options for the models, satellites, monitoring points, and outputs. However, it was not ideal to have customization beyond this (e.g., different options for

regression equations). Most of the staff were not confident with updating the BROSS programming codes, so staff familiar with computer programming would need to be dedicated to BROSS updates. The staff concerns were similar to those discussed in the formal meeting (Table 4.5), but primarily focused on cloud cover impacts and satellite penetration depth. They recognized that they needed to be aware of these limitations in using BROSS.

After BROSS was released for testing, feedback from the agency sediment expert (section 4.5) revealed opportunities to further improve the tool's uptake and sustainability (Table 4.6). Notably, the expert explained that quantification of the predicted annual sediment load volume would help decision-makers to better understand the reliability of BROSS. This task was delegated to the agency to facilitate technology transfer and stakeholder ownership. Similarly, other follow-up action items were appropriately delegated between the researchers and agency. The agency sediment expert planned to involve junior staff that had computer programming expertise in the agency's follow-up tasks and ongoing BROSS development and application.

Table 4.6. Agency sediment expert feedback on BROSS release

Feedback	Action item
Interested in computing sediment load volume	Agency will take next steps to compute this and will follow-up with researchers on outcome and any support needed
ANN model has complex architecture	Developer shared ANN model calibration scripts with agency, agency can simplify model design in future. Developer will be available for support as needed.
Interested in adding feature to plot SSC distribution along cross-sections in BROSS	Developer will investigate feasibility of this feature and then future action will collaboratively be determined
Suggested improvements to manual and application text	Developer implemented suggested improvements

4.5.2 *BROSS skill assessment*

The sustainability and stakeholder agency uptake of BROSS critically depend on the tool's skill. Overall, the stakeholder agency found the performance of BROSS to meet expectations and show promise for supporting operations. The skill of BROSS was largely enhanced by iterating the data analysis and model calibration with the agency sediment expert as well as by obtaining supporting technical information during the follow-up engagement trip. The familiarity of the agency staff and external institutions with the river system, in situ data, and pre-existing agency satellite remote sensing applications helped to integrate local understanding and overcome technical challenges. For example, the agency staff shared which in situ data monitoring points had more reliable data and could be focused on in the model calibration. The agency staff and experts also explained how and why sediment reflectance properties varied spatially and temporally throughout the river system. Various insights from the agency staff and external institutions could not have been obtained by the developer in isolation from the agency and external organizations.

The performance of BROSS varies for each satellite and model (Table 4.2). The annual sediment load predictions for the river system derived from BROSS (Table 4.7) are the same order of magnitude as most recently published estimate based on observations, 470 MT/year (year 2015; it was also found that the load is decreasing ~10 MT/year) (M. Rahman et al., 2018). Annual suspended load estimates were computed using monthly SSC predictions from BROSS and monthly streamflow discharge observations collected by the agency. The agency understands BROSS is not currently reliable for precise estimates of SSC and sediment fluxes. However, BROSS does provide realistic outputs which meet the agency's interest in qualitative SSC

distribution maps. The results are also adequately skillful to supplement existing sediment monitoring and forecasting approaches.

Table 4.7. Annual sediment load predictions derived from BROSS. Predictions were made using data at the confluence of the Padma and Lower Meghna river. For comparison, the most recently published estimate of total sediment load for the river system based on observations is 470 MT/year from year 2015 (Rahman et al., 2018).

Model	Satellite	Year(s)	Predicted Annual Sediment Load (MT/year)	
			Average	Range
ANN	Landsat 5/7	1999-2012	232	46-420
	Landsat 8	2014-2019	491	154-823
	Sentinel-2	2019	181	--
Regression	Landsat 5/7	2000-2012	254	145-416
	Landsat 8	2014-2019	397	213-536
	Sentinel-2	2019	202	--

4.5.3 *Lessons learned, strengths and weaknesses of stakeholder engagement process*

The constructive stakeholder agency feedback (section 4.5.1) and the skill of BROSS (section 4.5.2) are two standards by which the stakeholder engagement process and user-ready outcome of BROSS are considered successful. However, there are also five overarching strengths of the BROSS stakeholder engagement process that are highlighted as the key elements of success. These strengths relate to stakeholder engagement and convergence research approaches, practices, and principles commonly recommended in literature (Hossain, Siddique-E-Akbor, Yigzaw, et al., 2014; McIntosh et al., 2011; National Research Council, 2014; Sandink et al., 2016; Voinov & Bousquet, 2010; Voinov & Brown, 2008). The five key strengths of this study are interconnected and can be meaningfully understood hierarchically (Figure 4.12). It was critical that more time and resources were dedicated to underlying strengths in order to support

the overlying strengths and, essentially, the user-ready outcome of BROSS. Along with these strengths were key weaknesses of the study. These strengths and weaknesses translate to lessons learned, as presented below. Like the engagement approach (Section 4.4), the strengths and lessons learned are generalizable to other convergence research and stakeholder engagement efforts in various contexts.

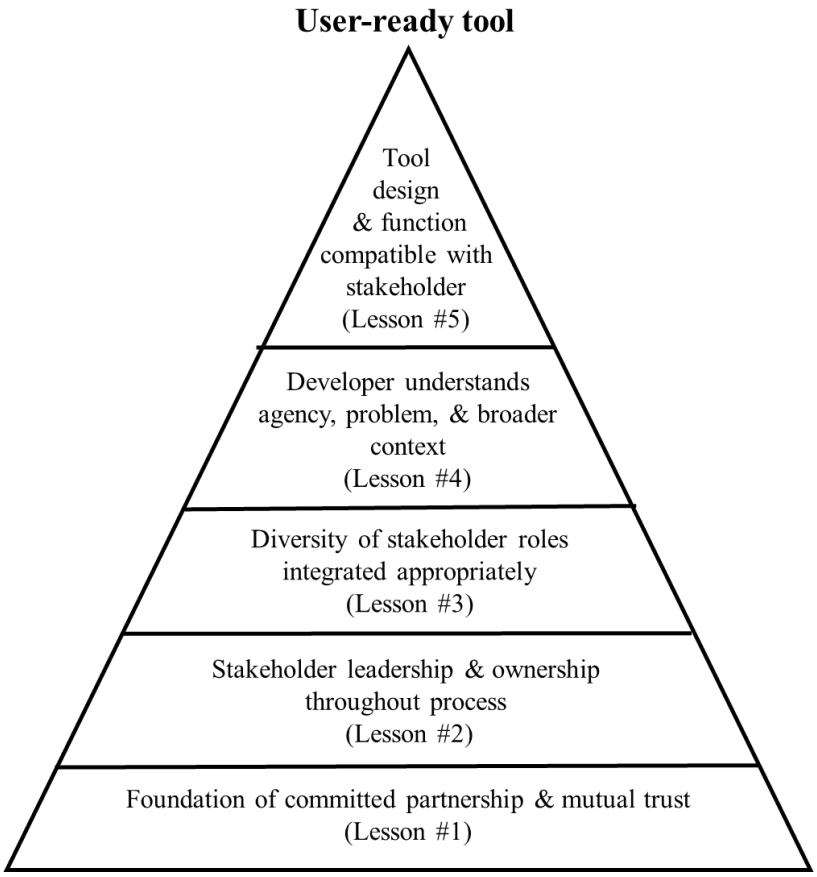

Figure 4.12. Hierarchy of strengths in BROSS co-development process for a user-ready tool. Underlying elements of the hierarchy enabled overlying elements and, essentially, a user-ready tool outcome. Strengths directly translate to the key lessons learned.

Lesson #1: Build a foundation of committed partnership and mutual trust

The foundational strength of the stakeholder engagement process was that BROSS was initiated from a long-standing partnership and mutual trust between the stakeholder agency and research group. While the developer was not involved in collaborations with the agency prior to co-developing BROSS, the developer was able to leverage this foundation for a timely and effective engagement process. The research group's ultimate aim in the partnership has been to support the agency in building long-term capacity and autonomy in overcoming water management challenges with accessible science and technology. The research group has demonstrated that they are not using the agency for their own benefit of achieving publications; neither is the research group developing such complex technologies that the agency is indefinitely depending on the researcher group's guidance. Rather, the research group has invested time and energy into an authentic partnership by training and properly transferring technology to the agency. This has facilitated multiple ongoing co-development projects between the researchers and agency. The agency is empowered to confidently initiate and take ownership of satellite remote sensing tools, including BROSS, over time.

Lesson #2: Support agency leadership and ownership throughout the co-development process

The second key strength was that the agency led and owned the BROSS initiation, development, and plans for moving forward. This ensures authentic capacity building and long-term sustainability of BROSS. The agency initiated the BROSS collaboration based on operational challenges and priorities that they perceived on their own, rather than having been imposed by researchers. This had two main implications. One was that BROSS was directly answering the agency's perceived needs and there were immediate benefits that the agency

realized. The second implication was that the agency was invested in BROSS throughout the co-development process and will deliberately take ownership of BROSS moving forward, as the involvement of the developer lessens.

After the initiation, agency leadership and ownership was supported in multiple ways. For example, the BROSS co-development process involved multiple iterations of results and outcomes with agency staff, which ultimately enabled the agency to guide the process and final product. Also, the follow-up engagement trip occurred early in the co-development process. Hence, early on, a broad range of agency staff could understand the underlying theory, outputs, strengths, weaknesses, and limitations of BROSS and meaningfully shape the tool design and functions. Moving forward, the agency is in the position to independently manage and improve BROSS with local resources. The researchers will continue to provide complimentary BROSS support as a "technical backstop" so that the agency is more confident with long-term ownership (Hossain, Siddique-E-Akbor, Yigzaw, et al., 2014).

The primary weakness relating to agency leadership and ownership was that, other than the agency sediment expert, the agency staff did not have the opportunity to review the prototype BROSS tool prior to the follow-up engagement trip. To improve this, the prototype tool, a short memo, and an online survey could have been provided to relevant agency staff and other meeting attendees prior to the engagement trip. This would have given the agency more time to test the prototype tool, reflect, provide preliminary feedback, and prepare for the in-person meeting discussions. The developer could have also reviewed preliminary feedback prior to the engagement trip and addressed it during the formal presentation. Although the follow-up engagement trip was fruitful, these steps could have likely enhanced the outcomes.

Lesson #3: Integrate and solicit feedback from diverse stakeholder roles in appropriate contexts

A diversity of stakeholder agency staff and external institution personnel were involved throughout the engagement process, and notably during the follow-up engagement trip (Table 4.4). The different roles were engaged in the appropriate ways. This strength is directly attributable to the leading agency staff guiding the trip plans, as they (more than the researchers) understood who should be involved and how to properly involve them. For example, junior staff were important to involve since they would be the primary tool operators. Junior staff were more comfortable sharing feedback during the informal, hands-on meeting rather than the large, formal meeting. Hence, involving them in both meetings was important. In addition, field staff demonstrated the agency's sediment engineering and management approaches and challenges, and validated how BROSS could support field operations. It was valuable to engage with field staff onsite where they could directly show these elements. Field staff also facilitated conversations with the local communities that they have developed relationships with as a result of their ongoing presence in the communities. While planning the involvement with diverse stakeholder roles was critical, it was also valuable that the developer's schedule intentionally had open time for on-demand meetings with any interested staff and collaborators. Along with benefitting the skill of BROSS, these spontaneous meetings strengthened the diversity of perspectives that the developer received.

A weakness of the integrating diverse feedback in the engagement process was that some of the agency staff did not share verbal or written feedback on BROSS since they were uncomfortable with their ability to communicate in English. Thus, it would have been beneficial to provide opportunities for the agency to share feedback in Bengali (the national language of

Bangladesh). For example, surveys could have been more extensively integrated throughout the co-development process (e.g., immediately following the trip, immediately after the release), and staff could have been encouraged to respond in their native language, if preferred. Along these lines, it would have also been valuable to provide deliverables (e.g., user manuals) in both English and Bengali.

Lesson #4: Strive to understand the stakeholder agency, problem, and broader context with humility and respect

As a direct result of the underlying strengths of the engagement process (long-term partnership, stakeholder agency leadership, and diversity of stakeholder roles involved), the developer gained a rich understanding of the technical problem, the agency's capacity and operations, and the broader (e.g., political, economic, social, cultural) context. This strength of having a holistic understanding enabled the developer to effectively support sustainable capacity building of the agency. However, the developer also aimed to maintain humility, respect, and flexibility throughout the co-development process. With this disposition, the developer was aware of their own role as an outsider amidst the broader context, their own limits and gaps in understanding, and the limits of their scientific and technological contributions in solving the agency's complex challenges. The developer's overall efforts to inform their own perspective strengthened the relationship with agency staff, external institutions, and general public, and fostered support and knowledge sharing. The perspective also enabled the developer and agency to share realistic expectations for the co-development process and tool outcomes.

To cultivate understanding of the agency, problem, and broader context, the developer took extensive measures that would often be considered unnecessary in co-developing a decision-support system. For example, the developer took a Bengali language and scripting

course in the months prior to the follow-up engagement trip. Although English is widely spoken in Bangladesh, the developer aimed to have basic Bengali communication skills to show respect and foster a stronger connection with the Bangladeshi people. The developer also studied social and cultural norms and prepared to follow them to the extent feasible, such as by dressing in a culturally-appropriate clothing style. While the developer was working across a dramatically different culture, this concept also applies to researchers working with stakeholders in their same region or country. Researchers and stakeholders may speak the same official language and be immersed in the same socio-political context. However, there are likely differences in their institutional vernacular and culture that it is important for researchers to understand and adapt to.

Lesson #5: Aim for a tool function and design that is compatible with the stakeholder's operations

Dedicating time to the underlying strengths (long-term partnership, stakeholder agency leadership, diversity of stakeholder roles involved, and understanding stakeholder context) naturally yielded tool functionality and design that was compatible with the stakeholder agency's operations. This strength of a compatible tool design and functionality entails multiple facets, such as:

- ease-of-use, which was supported by the BROSS graphical user interface design and simple accessibility via web browser.
- supplementation of existing practices (e.g., in situ suspended sediment monitoring).
- not needing to replace or significantly change existing protocols (McIntosh et al., 2011; Sandink et al., 2016).
- open-source and adaptable design of BROSS, allowing it to be maintained by the agency long-term without major outsourcing or overhead costs.

- similarity to other satellite remote sensing-based applications that the agency uses.

4.6 CONCLUSION

This paper described the stakeholder engagement process for the co-development of an environmental decision-support tool, BROSS, and highlighted key strengths, weaknesses, and lessons learned. Overall, the agency and researchers determined the co-development process and end-product to be successful. The primary researcher (developer) involved in the stakeholder engagement process was a university researcher. The stakeholder agency was BWDB, a Bangladesh federal government agency focused on water resources engineering and management. The agency faces complex river sediment management challenges of widespread erosion and accretion. The agency has been constrained in addressing them due to limited resources and sediment monitoring capacity. BROSS was primarily co-developed to improve understanding of where migrating points of significant erosion/accretion are occurring using SSC predictions. BROSS integrates the technologies of satellite remote sensing and cloud computing, which help to overcome the agency's main operational challenges.

BROSS estimates SSC throughout major Bangladesh rivers using satellite remote sensing surface reflectance data. BROSS provides broad spatial and temporal coverage of SSC patterns via maps and time series for user-specified areas. BROSS has two platforms which are both easy-to-use, interactive, and freely accessible via web browser. BROSS has acceptable skill for the agency's operations, predicting annual sediment loads within the observed ranges. These scientific and technological elements and outcomes of BROSS are critical to it being directly integrated onto the agency's operations and decision-making, i.e., user-ready. However, the success of BROSS being user-ready is also attributable to the key strengths in stakeholder engagement process.

The foundation of the BROSS stakeholder engagement process was a strong partnership between the stakeholder agency and research group that the developer was part of (strength #1). Out of this partnership, the agency initiated and led the co-development process (strength #2). The developer calibrated models and prepared the tool in close, iterative communication with the agency. A major milestone of the engagement process was the follow-up stakeholder engagement trip to Bangladesh that the developer conducted to solicit feedback on the BROSS prototype and validate its societal impact. During this trip, the developer engaged with a diversity of stakeholder roles (strength #3) and sought to understand the stakeholder agency, problem, and broader context with humility and respect (strength #4). Following the trip, the developer updated the tool according to the stakeholder feedback and other insights gained on the trip. The tool was released to the stakeholder agency along with user manuals and code to support long-term agency ownership. The developer iterated the final release with the agency and will continue to provide complimentary technical support. Moving forward, the stakeholder agency is the primary BROSS owner. The agency position to independently manage and improve BROSS with local resources due to the tool's design and functionality being compatible with agency operations (strength #5). The long-term success of BROSS will be determined by its ability to support the agency's erosion/accretion engineering and management decisions, forecasting of suspended sediment loads, and understanding of river sediment profiles. These long-term outcomes are likely to be achieved due to the skill of BROSS, the strong measures taken for sustainability and adaptability of BROSS, and the agency's increasing capacity.

Unfortunately, it is rare for stakeholder engagement to be integrated in the training of researchers that are developing environmental monitoring and modeling tools. This paper is intended to demonstrate a generalizable approach and lessons learned in crossing the valley of

death as a road map for researchers. However, research institutions and stakeholders can also use this study to support user-ready research. For example, all can invest time and resources in researcher-stakeholder partnerships and promote opportunities for scientists/engineers to develop stakeholder engagement skills. Furthermore, all can support the shift of environmental research agendas to be authentically driven by societal needs (Brown et al., 2015). This journey across the valley of death may seem risky to some, but it is a greater risk to the future society and environment not to make it.

Software & Data Availability

Name	**BROSS- Google Earth Engine (GEE)**
Developer name, email	Claire Beveridge, cbev@uw.edu
Developer address	Dept. of Civil and Environmental Engineering, University of Washington, USA
Date first available	April 2020
Software required	Web browser
Availability/cost	Free
Program language	JavaScript
Program code	https://code.earthengine.google.com/b5e957d40b1f1f41d7df05c754df68f2 & https://github.com/cbev/bross

Name	**BROSS- Local server**
Developer name, email	Claire Beveridge, cbev@uw.edu Shahryar Khalique Ahmad, skahmad@uw.edu
Developer address	Dept. of Civil and Environmental Engineering, University of Washington, USA
Date first available	April 2020
Software required	Web browser, Google Cloud, Keras (https://keras.io/), XAMPP (https://www.apachefriends.org/index.html), Geospatial Data Abstraction Library (https://www.gdal.org), Leaflet (https://leafletjs.com), HighCharts (http://www.highcharts.com), Materialize (https://materializecss.com), and jQuery (https://jquery.com)
Availability/cost	Free
Program language	Python (back-end); JavaScript & HTML (front-end)
Program code	https://github.com/cbev/bross/tree/master/local_server_scripts

Acknowledgements

This work was primarily funded by The National Science Foundation Graduate Research Fellowship Program under Grant No. DGE-1762114 to the first author. This work also benefitted from NASA Water Applied Science Program (grant NNX15AC63G) and NSF INFEWS Program (EAR 1740042) to the second author and travel support from the University of Washington Department of Civil & Environmental Engineering to the first author.

The first author thanks BWDB for generously supporting this work by providing data and thoughtful feedback on BROSS, as well as hosting the first author for two weeks in Bangladesh. The authors thank those who attended meetings and supported field visits on the developer's trip to Bangladesh. Special thanks to Dr. Maminul Haque Sarker; the Center for Environmental and Geographic Information Services (CEGIS) River, Delta and Coastal Morphology group; Professor Md. Munsur Rahman; and Bangladesh University of Engineering and Technology (BUET) Institute of Water and Flood Management (IWFM) for their valuable insights on Bangladesh rivers and feedback on BROSS. The authors also thank Hisham Eldardiry and Dr. Matthew Bonnema for support on BROSS development; Indira Bose for support with stakeholder engagement; and Shrabanti Paul, Md. Shariful Alam, Shofekul Islam, Udoy Raihan, and Md. Delwer Hossain for their support during the follow-up engagement trip. The authors thank Dr. Alexander Horner-Devine, Dr. David Butman, Dr. Alison Duvall, and two anonymous reviewers for their feedback on the manuscript which greatly improved it.

Chapter 5. CONCLUSIONS

This dissertation explored how research approaches to understanding watershed sediment dynamics—particularly computational modeling and satellite remote sensing—can be more effectively oriented towards watershed planning, management, engineering, and decision-making. This objective was explored from two interconnected perspectives: One is a scientific and computational perspective of integrating research approaches and developing tools. The other is a stakeholder engagement perspective of transferring tools and technologies to end-users. The sediment dynamics research pipeline must properly integrate both perspectives for outcomes to authentically support societal needs. This dissertation contained a relatively broad scope with regards to these two perspectives (Table 5.1). The chapters, taken together, give a holistic understanding of transitioning sediment modeling and satellite remote sensing research from use-inspired to user-ready. This is especially important considering: the overwhelming impact that humans are having on sediment dynamics; the importance of sediment in the interconnected environmental and social systems; the inherent complexity of sediment dynamics; the limitations of in situ sediment monitoring; the current disconnect between sediment research and application; and the need for improved tools to support sediment management. While these challenges are global, they are heightened in resource-limited regions where dam and landscape development are rapidly occurring.

Table 5.1. Dissertation summary

	Chapter 2	**Chapter 3**	**Chapter 4**
Research Tool/Approach	Computational modeling	Satellite remote sensing	Satellite remote sensing; Stakeholder engagement
Sediment Realm	Bedload & Suspended Load; Gravel-bedded river	Suspended Sediment Concentration (SSC); Sand/Gravel-bedded rivers	SSC; Sand-bedded rivers
Management Focus	Spatially and temporally distributed sediment yields and dynamics	Dam and landscape change impacts on SSC	SSC mapping; Erosion and accretion
Study Region	Glines Canyon Dam tributary (Elwha); 513 km^2; Maritime climate	3S tributary (Mekong); 82,400 km^2; Monsoonal climate	Ganges-Brahmaputra-Meghna basin (Bangladesh); 147,570 km^2; Tropical monsoonal climate

In **Chapter 2,** a unique, interdisciplinary modeling approach was developed, combining state-of-the-art hydrologic and sediment transport research modeling methods. The model was tested in the Elwha River basin upstream of the former Glines Canyon dam, producing accurate lifetime reservoir sedimentation volume estimates. Additionally, it provided spatially- and temporally-distributed outputs that are meaningful for watershed management (e.g., annual outputs at all Strahler-ordered segments). Hence, Chapter 2 showed that integrating existing interdisciplinary research on watershed network geomorphology, hydrology, and sediment dynamics has strong potential to address management-oriented questions when it is intentionally oriented to do so. However, there are still theoretical and computational research advancements needed, which Chapter 2 revealed. The improvements will support the reliability and robustness of application-oriented network sediment models, as well as their scalability to different

watersheds. Chapter 2 is considered use-inspired research is that it did not directly involve stakeholders but was an important predecessor to doing so. The feasibility and performance the model was tested before making it user-ready, which is particularly important for complex interdisciplinary aspects of modeling source-to-sink network sediment dynamics.

In **Chapter 3,** satellite remote sensing was used to assess the impacts of dam development and other landscape changes on SSC in the 3S tributaries of the Mekong River Basin. The technique quantified significant changes in SSC due to dam construction, reservoir sediment trapping, deforestation, and human settlement. Chapter 3 supported watershed management by demonstrating the following: the capacity and limitations of using satellite remote sensing reflectance data to quantify SSC patterns; a technique to improve regression models for predicting SSC from satellite data; and the ability of using land cover and nighttime light maps derived from satellite data to help interpret SSC patterns. Chapter 3 answered a critical river management need in the Mekong River Basin and other global river basins that are rapidly evolving with dam implementation and landscape changes yet have limited resources for modeling and ground-based monitoring. Like Chapter 2, Chapter 3 was use-inspired work in that it was not conducted with stakeholders, as it was vital to test the feasibility and performance of the application-oriented technique before it could reliably become user-ready. However, compared to most network models such as that of Chapter 2, the satellite remote sensing technique used in Chapter 3 has advantages to becoming user-ready. The application of the Chapter 3 satellite-based approach requires limited ground-based input data compared to network models. Also, satellite data used in Chapter 3 is global, making the approach readily transferrable to other regions. The work was largely conducted with the Google Earth Engine

platform, which is free, global, entirely web- and cloud-based, and allows developers to build publicly-available graphical user interface applications.

In **Chapter 4,** stakeholder engagement was conducted to co-develop a user-ready tool called BROSS for satellite-based monitoring of SSC along the Ganges, Brahmaputra, and Meghna rivers of Bangladesh. The primary interest of the stakeholder, BWDB, was to use qualitative SSC mapping from satellite data to support river erosion and accretion management. Although this management objective differed from that of Chapter 3, the capacity and limitations of satellite-based SSC monitoring assessed in Chapter 3 were transferrable to Chapter 4. There was clear understanding of how reliable and robust the satellite-based monitoring technique was, which was properly communicated with BWDB and enabled realistic expectations for BROSS. Chapter 4 demonstrated lessons learned for both the BROSS's technological development and stakeholder engagement. The strengths in this process led to a successful user-ready outcome that supported capacity building and resilience of BWDB. BWDB has tool ownership along with confidence in applying and adapting it to their management priorities. While there are biases, uncertainties, and limitations of BROSS, they are understood by BWDB. Despite the shortcomings, BWDB gains information from BROSS and can use it to better direct their limited resources on the ground. The long-term outcomes of BROSS will not just support BWDB, but also the research community. The stakeholder's ongoing application of the tool will continue to inform research topics such as the relation between SSC and erosion/accretion patterns, techniques for satellite-based monitoring of SSC, and the capacity of satellite-based technologies to support engineering and management under real-world constraints (e.g., time, budget, legal barriers).

Watershed sediment dynamics research can be improved by using the chapters of this dissertation as a guide for taking it from use-inspired to user-ready. Use-inspired and user-ready research can have an ultimate goal of supporting stakeholder capacity building and resilience. Use-inspired research can focus on integrating interdisciplinary methods and complex physical watershed processes that occur over a range of space- and time- scales in ways that are relevant to managers and decision-makers. Use-inspired research can focus on assessing feasibility, performance, and scalability of research tools and approaches in answering management-oriented questions as well as informing basic research directions. User-ready tools can appropriately deliver use-inspired research to stakeholders, but strong engagement processes are critical for communicating biases, uncertainties, and limitations and making tools locally-relevant. User-ready tools can be primarily stakeholder-owned so that stakeholders can adapt tools to their changing priorities over time, while have a foundational partnership with researchers as a backstop for technical support.

As human impacts continue to vastly impact natural sediment regimes, computational modeling and satellite remote sensing tools can be especially useful in distinguishing the extent of these impacts. With this understanding, adverse impacts on the environment and society can be mitigated and managed. A topic that was not explored in this dissertation but would be a valuable advancement of it would be combining modeling and satellite-based monitoring to support management. For example, satellite remote sensing measurements of sediment and evolving landscape patterns can be integrated into computational network models to improve understanding of watershed sediment dynamics and improve short- and long- watershed sediment yield predictions.

Application-oriented approaches to understanding watershed sediment dynamics that are explored in this dissertation are highly dependent on the local context and available resources. For example, there are significant differences in the data and computational resources in developed versus developing nations. The Elwha River basin (Chapter 2) had relatively abundant hydrologic data compared to the 3S tributaries (Chapter 3) and major Bangladesh rivers (Chapter 4). In addition, the Elwha basin has had relatively little landscape changes compared to the other two rapidly developing regions. Hence, while the network sediment modeling approach conducted in the Elwha watershed was lucrative in that setting and context, the same network model would have had significantly more limitations in the 3S tributaries or major Bangladesh rivers. This is largely because the extent of input data is not available in these basins. Furthermore, even with the appropriate data inputs and computing power, the channel network model outputs would not have been as relevant to the research questions on SSC in the other two study areas. Conversely, satellite-based estimates of SSC alone are not adequate for the watershed sediment yield predictions developed in Chapter 2.

Thus, as researchers advance sediment modeling and monitoring approaches and transfer them to stakeholders, it is imperative for researchers to properly understand the relevant science and technology as well as the end-user context and priorities. Furthermore, researchers must understand how research transitions across the spectrum from fundamental research, to use-inspired, to user-ready. Researchers must also be able to communicate with those that specialize in all different parts of the spectrum. Particularly, feedback from stakeholders, such as that of Chapter 4, must be more effectively communicated to scientists working in other parts of the spectrum where more fundamental scientific and technological research is conducted. Unfortunately, having this spectrum of scientific understanding and communication is rarely

emphasized in the training environmental and engineering researchers (i.e., doctoral programs). Particularly, the step of transferring science and technology to stakeholders is seldom made a priority. Yet, this step is essential for basic and use-inspired research to reach its full realization, and for environmental research to have a meaningful impact on society. A valuable way for researchers to be trained with these skills is for institutions to support opportunities for individuals to work across the spectrum, as done in this dissertation. This could bring about a paradigm shift to an engineering research agenda that is authentically oriented to societal application, which is desperately needed in the face of growing global environmental challenges. It is the responsibility of researchers to society to promptly embrace this research agenda and bring life to the valley of death.

BIBLIOGRAPHY

Abad, J. D., Buscaglia, G. C., & Garcia, M. H. (2007). 2D stream hydrodynamic, sediment transport and bed morphology model for engineering applications. *Hydrological P*, *22*(November 2008), 1443–1459. https://doi.org/10.1002/hyp.6697

Abad, J. D., & Garcia, M. H. (2006). Discussion of "Efficient Algorithm for Computing Einstein Integrals" by Junke Guo and Pierre Y. Julien. *J. Hydraul. Eng*, *130*(12), 1198–1201.

Adamson, P. T., Rutherford, I. D., Peel, M. C., & Conlan, I. A. (2009). The hydrology of the Mekong River. In I. C. Campbell (Ed.), *The Mekong: Biophysical environment of an international river basin* (pp. 53–76). Amsterdam, Netherlands: Elsevier.

Ahmad, S. K., & Hossain, F. (2019a). A generic data-driven technique for forecasting of reservoir inflow: Application for hydropower maximization. *Environmental Modelling and Software*, *119*(March), 147–165. https://doi.org/10.1016/j.envsoft.2019.06.008

Ahmad, S. K., & Hossain, F. (2019b). A web-based decision support system for smart dam operations using weather forecasts. *Journal of Hydroinformatics*, *21*(5), 687–707. https://doi.org/10.2166/hydro.2019.116

Baroudi, J. J., Olson, M. H., & Ives, B. (1986). An Empirical Study of the Impact of User Involvement on System Usage and Information Satisfaction. *Management of Computing*, *29*(3), 232–238. https://doi.org/10.1145/5666.5669

Barry, J. J., Buffington, J. M., & King, J. G. (2004). A general power equation for predicting bed load transport rates in gravel bed rivers. *Water Resources Research*, *40*(10), 1–22. https://doi.org/10.1029/2004WR003190

Batt, G. E., Brandon, M. T., Farley, K. A., & Roden-Tice, M. (2001). Tectonic synthesis of the Olympic Mountains segment of the Cascadia wedge, using two-dimensional thermal and kinematic modeling of thermochronological ages. *Journal of Geophysical Research: Solid Earth*, *106*(B11), 26731–26746. https://doi.org/10.1029/2001JB000288

Belward, A. S., Estes, J. E., & Kline, K. D. (1999). The IGBP-DIS Global 1-Km Land-Gover Data Set DlsGover: A Proiect Overview. *Photogrammetric Engineering & Remote Sensing*, *65*(9), 1013–1020. Retrieved from http://edcwww.cr.usgs.gov/landdaac/rKIWrkmhome-

Benda, Lee; Dunne, T. (1997a). Stochastic forcing of sediment routing and storage in channel networks. *Water Resources*, *33*(12), 2865–2880. https://doi.org/10.1016/j.rmed.2004.03.018

Benda, Lee; Dunne, T. (1997b). Stochastic forcing of sediment supply to channel networks from

landsliding and debris flow, *33*(12), 2849–2863. https://doi.org/https://doi.org/10.1029/97WR02388

Beveridge, C., Hossain, F., Biswas, R. K., Haque, A. A., Ahmad, S. K., Biswas, N. K., … Bhuyan, M. A. (2020). *Stakeholder-driven development of a cloud-based, satellite remote sensing tool to monitor suspended sediment concentrations in major Bangladesh rivers*. *Environmental Modelling and Software*.

Beveridge, C., Hossain, F., & Bonnema, M. (2020). Estimating Impacts of Dam Development and Landscape Changes on Suspended Sediment Concentrations in the Mekong River Basin's 3S Tributaries. *Journal of Hydrologic Engineering*, *25*(7), 1–14. https://doi.org/10.1061/(ASCE)HE.1943-5584.0001949

Beveridge, C., Istanbulluoglu, E., Bandaragoda, C., & Pfeiffer, A. M. (2020). A Channel Network Model for Sediment Dynamics Over Watershed Management Time Scales. *Journal of Advances in Modeling Earth Systems*, *12*(6), 1–29. https://doi.org/10.1029/2019ms001852

Billah, M. M. (2018). Mapping and monitoring erosion-accretion in an alluvial river using satellite imagery - The river bank changes of the Padma river in Bangladesh. *Quaestiones Geographicae*, *37*(3), 87–95. https://doi.org/10.2478/quageo-2018-0027

Biswas, N. K., & Hossain, F. (2018). A scalable open-source web-analytic framework to improve satellite-based operational water management in developing countries. *Journal of Hydroinformatics*, *20*(1), 88–99. https://doi.org/10.2166/hydro.2017.073

Biswas, R. K., Yorozuya, A., & Egashira, S. (2016). Numerical model for bank erosion in the brahmaputra river. *Journal of Disaster Research*, *11*(6), 1073–1081. https://doi.org/10.20965/jdr.2016.p1073

Bohn, T. J., Livneh, B., Oyler, J. W., Running, S. W., Nijssen, B., & Lettenmaier, D. P. (2013). Global evaluation of MTCLIM and related algorithms for forcing of ecological and hydrological models. *Agricultural and Forest Meteorology*, *176*, 38–49. https://doi.org/10.1016/j.agrformet.2013.03.003

Brandon, K. A., Roden-Tice, T. M., & Garver, J. I. (1998). Late Caneozoic exhumation of the cascadia accretionnary wedge in the Olympic montains, northwest Washington State. *Geological Society of America Bulletin*, *110*(8), 985–1009. https://doi.org/10.1130/0016-7606(1998)110<0985:LCEOTC>2.3.CO;2

Brandt, S. A. (2000). Classification of geomorphological effects downstream of dams. *Catena*, *40*(4), 375–401. https://doi.org/10.1016/S0341-8162(00)00093-X

Bray, D. I. (1979). Estimating average velocity in gravel-bed rivers. *Journal of Hydraulics Division, American Society of Civil Engineers*, *105*, 1103–1122.

Brown, C. M., Lund, J. R., Cai, X., Reed, P. M., Zagona, E. A., Ostfeld, A., … Brekke, L. (2015). Scientific Framework for Sustainable Water Management. *Water Resources Research*, 6110–6124. https://doi.org/10.1002/2015WR017114.Received

Buffington, J., & Woodsmith, R. (2003). Fluvial processes in Puget Sound rivers and the Pacific Northwest. *Book: Restoration of Puget Sound Rivers*.

Camenen, B. (2007). Simple and General Formula for the Settling Velocity of Particles. *Journal of Hydraulic Engineering*, *133*(2), 229–233. https://doi.org/10.1061/(ASCE)0733-9429(2007)133:2(229)

CEOS. (2020). The Committee on Earth Observation Satellites (Ceos) Database. Retrieved June 2, 2020, from http://database.eohandbook.com/

Chander, G., Markham, B. L., & Helder, D. L. (2009). Summary of current radiometric calibration coefficients for Landsat MSS, TM, ETM+, and EO-1 ALI sensors. *Remote Sensing of Environment*, *113*(5), 893–903. https://doi.org/10.1016/j.rse.2009.01.007

Childers, D., Kresech, D. L., Gustafson, S. A., Randle, T. J., Melena, J. T., & Cluer, B. (2000). Hydrologic Data Collected During the 1994 Lake Mills Drawdown Experiment, Elwha River, Washington.

Cleveland, W. S. (1979). Robust locally weighted regression and smoothing scatterplots. *Journal of the American Statistical Association*, *74*(368), 829–836. https://doi.org/10.1080/01621459.1979.10481038

Cui, Y. (2007). The unified gravel-sand (TUGS) model: Simulating sediment transport and gravel/sand grain size distributions in gravel-bedded rivers. *Water Resources Research*, *43*(10), 1–16. https://doi.org/10.1029/2006WR005330

Cui, Y., Parker, G., Braudrick, C., Dietrich, W. E., & Cluer, B. (2006). Dam Removal Express Assessment Models (DREAM). Part 1: Model development and validation. *Journal of Hydraulic Research*, *44*(3), 291–307. https://doi.org/10.1080/00221686.2006.9521683

Cuo, L., Beyene, T. K., Voisin, N., Su, F., Lettenmaier, D. P., Alberti, M., & Richey, J. E. (2011). Effects of mid-twenty-first century climate and land cover change on the hydrology

of the Puget Sound basin, Washington. *Hydrological Processes*, *25*(11), 1729–1753. https://doi.org/10.1002/hyp.7932

Curran, C. A., Konrad, C. P., Higgins, J. L., & Bryant, M. K. (2009). Estimates of Sediment Load Prior to Dam Removal in the Elwha River, Clallam County, Washington. *Scientific Investigations Report 2009-5221*.

Czuba, J. A. (2018). A Lagrangian framework for exploring complexities of mixed-size sediment transport in gravel-bedded river networks. *Geomorphology*, *321*, 146–152. https://doi.org/10.1016/j.geomorph.2018.08.031

Czuba, J. A., Foufoula-Georgiou, E., Gran, K. B., Belmont, P., & Wilcock, P. R. (2017). Interplay between spatially explicit sediment sourcing, hierarchical river-network structure, and in-channel bed material sediment transport and storage dynamics. *Journal of Geophysical Research: Earth Surface*, *122*(5), 1090–1120. https://doi.org/10.1002/2016JF003965

Daly, C., Neilson, R. P., & Phillips, D. L. (1994). A Statistical-Topographic Model for Mapping Climatological Precipitation over Mountainous Terrain. *Journal of Applied Meteorology*, *33*, 140–158. https://doi.org/10.1175

Dang, T. D., Cochrane, T. A., & Arias, M. E. (2018). Quantifying suspended sediment dynamics in mega deltas using remote sensing data: A case study of the Mekong floodplains. *International Journal of Applied Earth Observation and Geoinformation*, *68*(February), 105–115. https://doi.org/10.1016/j.jag.2018.02.008

Downs, P. W., Cui, Y., Wooster, J. K., Dusterhoff, S. R., Booth, D. B., Dietrich, W. E., & Sklar, L. S. (2009). Managing reservoir sediment release in dam removal projects: An approach informed by physical and numerical modelling of non-cohesive sediment. *International Journal of River Basin Management*, *7*(4), 433–452. https://doi.org/10.1080/15715124.2009.9635401

Duda, J., Warrick, J., & Magirl, C. (2011). Coastal and lower Elwha River, Washington, prior to dam removal—history, status, and defining characteristics. *Scientific Investigations Report*, 26 p.

Dunn, F. E., Darby, S. E., Nicholls, R. J., Cohen, S., Zarfl, C., & Fekete, B. M. (2019). Projections of declining fluvial sediment delivery to major deltas worldwide in response to climate change and anthropogenic stress. *Environmental Research Letters*, *14*(8).

https://doi.org/10.1088/1748-9326/ab304e

East, A. E., Pess, G. R., Bountry, J. A., Magirl, C. S., Ritchie, A. C., Logan, J. B., … Shafroth, P. B. (2015). Large-scale dam removal on the Elwha River, Washington, USA: River channel and floodplain geomorphic change. *Geomorphology*, *228*, 765–786. https://doi.org/10.1016/j.geomorph.2014.08.028

Entrix, I. (2009). *LiDAR survey of lower Elwha River, Clallam County, Washington*. Seattle, Washington.

Federal Interagency Sedimentation Project. (1941). *Laboratory investigation of suspended-sediment samplers. Interagency Rep. No. 5.* Iowa City, IA.

Finlayson, D. P., Haugerud, R. A., Greenberg, H., & Logsdon, M. G. (2000). Puget Sound digital elevation model. Seattle, Washington: University of Washington. Retrieved from https://www.ocean.washington.edu/data/pugetsound/psdem2000.html

Flanagan, D. C., & Nearing, M. A. (1995). *USDA-Water Erosion Prediction Project: Hillslope profile and watershed model documentation. NSERL Report No. 10.* West Lafayette, Indiana.

Food and Agriculture Organization, & World Bank. (2018). Population density (people per sq. km of land area) - Bangladesh. Retrieved June 1, 2020, from https://data.worldbank.org/indicator/EN.POP.DNST?locations=BD&most_recent_value_desc=true

Frans, C. (2015). Implications of Glacier Recession for Water Resources. *Doctoral Dissertation*. https://doi.org/10.1017/CBO9781107415324.004

Fu, B., Merritt, W. S., Croke, B. F. W., Weber, T. R., & Jakeman, A. J. (2019). A review of catchment-scale water quality and erosion models and a synthesis of future prospects. *Environmental Modelling and Software*, *114*(December 2018), 75–97. https://doi.org/10.1016/j.envsoft.2018.12.008

Garcia, M., & Parker, G. (1991). Entrainment of bed sediment into suspension. *Journal of Hydraulic Engineering, 117*(4), 414–435.

Gasparini, N. M., Tucker, G. E., & Bras, R. L. (2004). Network-scale dynamics of grain-size sorting: Implications for downstream fining, stream-profile concavity, and drainage basin morphology. *Earth Surface Processes and Landforms*, *29*(4), 401–421. https://doi.org/10.1002/esp.1031

Gholizadeh, M. H., Melesse, A. M., & Reddi, L. (2016). A comprehensive review on water quality parameters estimation using remote sensing techniques. *Sensors (Switzerland)*, *16*(8). https://doi.org/10.3390/s16081298

Glicken, J. (2000). Getting stakeholder participation "right": A discussion of participatory processes and possible pitfalls. *Environmental Science and Policy*, *3*(6), 305–310. https://doi.org/10.1016/S1462-9011(00)00105-2

Gorelick, N., Hancher, M., Dixon, M., Ilyushchenko, S., Thau, D., & Moore, R. (2017). Google Earth Engine: Planetary-scale geospatial analysis for everyone. *Remote Sensing of Environment*, *202*, 18–27. https://doi.org/10.1016/j.rse.2017.06.031

Guo, H. (2017). Big Earth data: A new frontier in Earth and information sciences. *Big Earth Data*, *1*(1–2), 4–20. https://doi.org/10.1080/20964471.2017.1403062

Gwynne, P. (2020, July 3). Bipartisan bill aims to revamp National Science Foundation – Physics World. Retrieved July 4, 2020, from https://physicsworld.com/a/bipartisan-bill-to-revamp-us-agency/

Hossain, F. (2015). Data for All: Using Satellite Observations for Social Good. *Eos*, *96*(October 2015), 1–7. https://doi.org/10.1029/2015eo037319

Hossain, F., Maswood, M., Siddique-E-Akbor, A. H., Yigzaw, W., Mazumdar, L. C., Ahmed, T., … Turk, F. J. (2014). A promising radar altimetry satellite system for operational flood forecasting in flood-prone bangladesh. *IEEE Geoscience and Remote Sensing Magazine*, *2*(3), 27–36. https://doi.org/10.1109/MGRS.2014.2345414

Hossain, F., Siddique-E-Akbor, A. H. M., Yigzaw, W., Shah-Newaz, S., Hossain, M., Mazumder, L. C., … Limaye, A. (2014). Crossing the "Valley of Death": Lessons learned from implementing an operational satellite-based flood forecasting system. *Bulletin of the American Meteorological Society*, *95*(8), 1201–1207. https://doi.org/10.1175/BAMS-D-13-00176.1

Hossain, F., Siddique-E-Akbor, A. H., Mazumder, L. C., Shahnewaz, S. M., Biancamaria, S., Lee, H., & Shum, C. K. (2014). Proof of concept of an altimeter-based river forecasting system for transboundary flow inside Bangladesh. *IEEE Journal of Selected Topics in Applied Earth Observations and Remote Sensing*, *7*(2), 587–601. https://doi.org/10.1109/JSTARS.2013.2283402

Hydrologic Engineering Center. (1993). *HEC-6, scour and deposition in rivers and reservoirs:*

User's manual. Davis, CA.

Independent Group of Scientists appointed by the Secretary-General. (2019). *Global Sustainable Development Report 2019: The Future is Now – Science for Achieving Sustainable Development*. New York.

International Centre, & for Environmental Management (ICEM). (2010). "Hydrology and sediment baseline assessment working paper." In Baseline assessment report, strategic environmental assessment of hydropower on the Mekong mainstream for the MRC, *85*.

International Monetary Fund. (2019). *World Economic Outlook Database*. Washington DC. Retrieved from https://www.imf.org/external/pubs/ft/weo/2019/02/weodata/index.aspx

Irwin, E. G., Culligan, P. J., Fischer-Kowalski, M., Law, K. L., Murtugudde, R., & Pfirman, S. (2018). Bridging barriers to advance global sustainability. *Nature Sustainability*, *1*(7), 324–326. https://doi.org/10.1038/s41893-018-0085-1

Islam, M. F., & Rashid, A. B. (2011). Riverbank erosion displacees in Bangladesh: need for institutional response and policy intervention. *Bangladesh Journal of Bioethics*, *2*(2), 4–19. https://doi.org/10.3329/bioethics.v2i2.9540

Jerolmack, D. J., & Brzinski, T. A. (2010). Equivalence of abrupt grain-size transitions in alluvial rivers and eolian sand seas: A hypothesis. *Geology*, *38*(8), 719–722. https://doi.org/10.1130/G30922.1

Jones, J. W. (2015). Efficient wetland surface water detection and monitoring via landsat: Comparison with in situ data from the everglades depth estimation network. *Remote Sensing*, *7*(9), 12503–12538. https://doi.org/10.3390/rs70912503

Julien, P. Y. (1995). *Erosion and sedimentation*. Cambridge: Cambridge University Press.

Kalnay, E., Kanamitsu, M., Kistler, R., Collins, W., Deaven, D., Gandin, L., … Joseph, D. (1996). The NCEP/NCAR 40-year reanalysis project. *Bulletin of the American Meteorological Society*. https://doi.org/10.1175/1520-0477(1996)077<0437:TNYRP>2.0.CO;2

Kelleher, C., Wagener, T., McGlynn, B. (2015). Model-based analysis of the influence of catchment properties on hydrologic partitioning across five mountain headwater subcatchments. *Water Resources Research, 51*, 4109–4136. https://doi.org/10.1002/2014WR016147.Received

King, W. R., & Rodriguez, J. I. (1981). Note—Participative Design of Strategic Decision

Support Systems: An Empirical Assessment. *Management Science*, *27*(6), 717–726. https://doi.org/10.1287/mnsc.27.6.717

Koehnken, L. (2014). *Discharge sediment monitoring project (DSMP) 2009 – 2013 summary & analysis of results, Final Report*. *Mekong River Commission Secretariat*.

Kondolf, G. M., Alford, C., & Rubin, Z. (2011). *Cumulative effects of tributary dams on the sediment loads and channel form in the lower Mekong River: Progress report through 30 September 2011*. Berkeley, CA.

Kondolf, G. M., & Piégay, H. (Eds.). (2003). *Tools in fluvial geomorphology*. Chichester, England ; Hoboken, NJ : Wiley, [2003] ©2003. Retrieved from https://search.library.wisc.edu/catalog/999948277402121

Kondolf, G. M., Rubin, Z. K., & Minear, J. T. (2014). Dams on the Mekong: Cumulative sediment starvation. *Water Resour. Res.*, *50*, 5158–5169. https://doi.org/10.1002/2013WR014651.Received

Kondolf, G. M., Schmitt, R. J. P., Carling, P., Darby, S., Arias, M., Bizzi, S., … Wild, T. (2018). Changing sediment budget of the Mekong : Cumulative threats and management strategies for a large river basin. *Science of the Total Environment*, *625*, 114–134. https://doi.org/10.1016/j.scitotenv.2017.11.361

Kong, D., Miao, C., Wu, J., Borthwick, A. G. L., Duan, Q., & Zhang, X. (2017). Environmental impact assessments of the Xiaolangdi Reservoir on the most hyperconcentrated laden river, Yellow River, China. *Environmental Science and Pollution Research*, *24*(5), 4337–4351. https://doi.org/10.1007/s11356-016-7975-4

Korfmacher, K. S. (2001). The politics of participation in watershed modeling. *Environmental Management*, *27*(2), 161–176. https://doi.org/10.1007/s002670010141

Laboratory, P. N. N. (2018). *DHSVM stream network generation scripts, GitHub repository*. Richland, Washington. Retrieved from https://github.com/pnnl/DHSVM-PNNL/tree/master/CreateStreamNetwork_PythonV

Lauer, J. W., Viparelli, E., & Piégay, H. (2016). Morphodynamics and sediment tracers in 1-D (MAST-1D): 1-D sediment transport that includes exchange with an off-channel sediment reservoir. *Advances in Water Resources*, *93*, 135–149. https://doi.org/10.1016/j.advwatres.2016.01.012

Lehner, B., Liermann, C. R., Revenga, C., Vörösmarty, C., Fekete, B., Crouzet, P., … Wisser, D.

(2011). High-resolution mapping of the world's reservoirs and dams for sustainable river-flow management. *Frontiers in Ecology and the Environment*, *9*(9), 494–502. https://doi.org/10.1890/100125

Leopold, L. B., & Maddock, T. J. (1953). *The Hydraulic geometry of stream channels and some physiographic implications*. Washington DC.

Lettenmaier, D. P. (2008). Have we dropped the ball on water resources research? *Journal of Water Resources Planning and Management*, *134*(6), 491–492. https://doi.org/10.1061/(ASCE)0733-9496(2008)134:6(491)

Li, L., Ni, J., Chang, F., Yue, Y., Frolova, N., Magritsky, D., … Walling, D. E. (2020). Global trends in water and sediment fluxes of the world's large rivers. *Science Bulletin*, *65*(1), 62–69. https://doi.org/10.1016/j.scib.2019.09.012

Livneh, B., Bohn, T. J., Pierce, D. W., Munoz-Arriola, F., Nijssen, B., Vose, R., … Brekke, L. (2015). A spatially comprehensive, hydrometeorological data set for Mexico, the U.S., and Southern Canada 1950-2013. *Scientific Data*, *2*, 1–12. https://doi.org/10.1038/sdata.2015.42

Livneh, B., Rosenberg, E. A., Lin, C., Nijssen, B., Mishra, V., Andreadis, K. M., … Lettenmaier, D. P. (2013). A long-term hydrologically based dataset of land surface fluxes and states for the conterminous United States: Update and extensions. *Journal of Climate*, *26*(23), 9384–9392. https://doi.org/10.1175/JCLI-D-12-00508.1

Loveland, T. R., Reed, B. C., Ohlen, D. O., Brown, J. F., Zhu, Z., Yang, L., & Merchant, J. W. (2000). Development of a global land cover characteristics database and IGBP DISCover from 1 km AVHRR data. *International Journal of Remote Sensing*, *21*(6–7), 1303–1330. https://doi.org/10.1080/014311600210191

Lu, X. X., Oeurng, C., Le, T. P. Q., & Thuy, D. T. (2015). Sediment budget as affected by construction of a sequence of dams in the lower Red River, Viet Nam. *Geomorphology*, *248*, 125–133. https://doi.org/10.1016/j.geomorph.2015.06.044

Magirl, C. S., Hilldale, R. C., Curran, C. A., Duda, J. J., Straub, T. D., Domanski, M., & Foreman, J. R. (2015). Large-scale dam removal on the Elwha River, Washington, USA: Fluvial sediment load. *Geomorphology*, *246*, 669–686. https://doi.org/10.1016/j.geomorph.2014.12.032

Mård, J., Di Baldassarre, G., & Mazzoleni, M. (2018). Nighttime light data reveal how flood protection shapes human proximity to rivers. *Science Advances*, *4*(8), 1–8.

https://doi.org/10.1126/sciadv.aar5779

Markert, K. N., Schmidt, C. M., Griffin, R. E., Flores, A. I., Poortinga, A., Saah, D. S., … Ganz, D. J. (2018). Historical and operational monitoring of surface sediments in the Lower Mekong Basin using Landsat and Google Earth Engine cloud computing. *Remote Sensing*, *10*(6), 1–19. https://doi.org/10.3390/rs10060909

McIntosh, B. S., Ascough, J. C., Twery, M., Chew, J., Elmahdi, A., Haase, D., … Voinov, A. (2011). Environmental decision support systems (EDSS) development - Challenges and best practices. *Environmental Modelling and Software*, *26*(12), 1389–1402. https://doi.org/10.1016/j.envsoft.2011.09.009

McLean, D. G., Vasquez, J. A., Oberhagemann, K., & Sarker, M. H. (2012). Padma River morphodynamics near Padma Bridge. In R. E. Murillo Munoz (Ed.), *River Flow 2012* (1st ed., pp. 741–747). London: Taylor & Francis Group.

McNamara, J. P., Ziegler, A. D., Wood, S. H., & Vogler, J. B. (2006). Channel head locations with respect to geomorphologic thresholds derived from a digital elevation model: A case study in northern Thailand. *Forest Ecology and Management*, *224*(1–2), 147–156. https://doi.org/10.1016/j.foreco.2005.12.014

Mekong River Commission (MRC). (2005). Overview of the hydrology of the Mekong Basin. Vientiane, Laos: MRC.

Mekong River Commission (MRC). (2011). Hydrological database. Vientiane, Laos: MRC.

Mekong River Commission (MRC). (2013). Improved environmental & socio-economic baseline information for hydropower planning (ISH11). Vientiane, Laos: MRC.

Minder, J. R., Mote, P. W., & Lundquist, J. D. (2010). Surface temperature lapse rates over complex terrain: Lessons from the Cascade Mountains. *Journal of Geophysical Research Atmospheres*, *115*(14), 1–13. https://doi.org/10.1029/2009JD013493

Mitchener, H., & Torfs, H. (1996). Erosion of mud/sand mixtures. *Coastal Engineering*, *29*(1–2), 1–25. https://doi.org/10.1016/S0378-3839(96)00002-6

Montgomery, D. R., & Brandon, M. T. (2002). Topographic controls on erosion rates in tectonically active mountain ranges. *Earth and Planetary Science Letters*, *201*(3–4), 481–489. https://doi.org/10.1016/S0012-821X(02)00725-2

Montgomery, D. R., & Dietrich, W. E. (1994). A physically based model for the topographic control on shallow landsliding. *Water Resources Research*, *30*(4), 1153–1171.

https://doi.org/10.1029/93WR02979

Montgomery, D. R., & Foufoula-Georgiou, E. (1993). Channel network source representation using digital elevation models. *Water Resources Research*, *29*(12), 3925–3934. https://doi.org/10.1029/93WR02463

Moriasi, D. N., Arnold, J. G., Liew, M. W. Van, Bingner, R. L., Harmel, R. D., & Veith, T. L. (2007). Model evaluation guidelines for systematic quantification of accuracy in watershed simulations, *50*(3), 885–900.

MRC (Mekong River Commission). (2017). *Mekong sediment from the Mekong River commission study*.

Nash, J. E., & Sutcliffe, J. V. (1970). River flow forecasting through conceptual models part I - A discussion of principles. *Journal of Hydrology*, *10*(3), 282–290. https://doi.org/10.1016/0022-1694(70)90255-6

National Research Council. (2000). *From Research to Operations in Weather Satellites and Numerical Weather Prediction: Crossing the Valley of Death*. Washington, DC: National Academies Press. https://doi.org/10.17226/9948

National Research Council. (2014). *Convergence is informed by research areas with broad scope*. *Convergence: Facilitating Transdisciplinary Integration of Life Sciences, Physical Sciences, Engineering, and Beyond*. https://doi.org/10.17226/18722

Neiman, P. J., Ralph, F. M., Wick, G. A., Lundquist, J. D., & Dettinger, M. D. (2008). Meteorological Characteristics and Overland Precipitation Impacts of Atmospheric Rivers Affecting the West Coast of North America Based on Eight Years of SSM/I Satellite Observations. *Journal of Hydrometeorology*, *9*(1), 22–47. https://doi.org/10.1175/2007JHM855.1

NOAA–Earth Observation Group. (2016). Version 4 DMSP-OLS nighttime lights time series.

OCHA ROAP. (2019, September 30). Bangladesh administrative level 0-4 boundary polygons, lines, points, tabular data, and live services - Humanitarian Data Exchange. Retrieved May 21, 2020, from https://data.humdata.org/dataset/administrative-boundaries-of-bangladesh-as-of-2015

Park, C. C. (1977). World-wide variations in hydraulic geometry exponents of stream channels: An analysis and some observations. *Journal of Hydrology*, *33*(1–2), 133–146. https://doi.org/10.1016/0022-1694(77)90103-2

Parker, G., & Klingeman, P. C. (1982). On why gravel bed streams are paved. *Water Resources Research*, *18*(5), 1409–1423. https://doi.org/10.1029/WR018i005p01409

Patil, S., Sivapalan, M., Hassan, M. A., Ye, S., Harman, C. J., & Xu, X. (2012). A network model for prediction and diagnosis of sediment dynamics at the watershed scale. *Journal of Geophysical Research: Earth Surface*, *117*(F4), n/a-n/a. https://doi.org/10.1029/2012JF002400

Pavelsky, T. M., & Smith, L. C. (2009). Remote sensing of suspended sediment concentration, flow velocity, and lake recharge in the Peace-Athabasca Delta, Canada. *Water Resources Research*, *45*(11), 1–16. https://doi.org/10.1029/2008WR007424

Pelto, M. (2018). Elwha River: Impact of ongoing glacier retreat. Dudley, MA. Retrieved from https://glaciers.nichols.edu/wp-content/uploads/2018/06/elwha-fact-sheet.pdf

Peterson, K. T., Sagan, V., Sidike, P., Cox, A. L., & Martinez, M. (2018). Suspended sediment concentration estimation from landsat imagery along the lower missouri and middle Mississippi Rivers using an extreme learning machine. *Remote Sensing*, *10*(10), 1503. https://doi.org/10.3390/rs10101503

Pfeiffer, A. M., & Finnegan, N. J. (2017). Basin-scale methods for predicting salmonid spawning habitat via grain size and riffle spacing, tested in a California coastal drainage. *Earth Surface Processes and Landforms*, *42*(6), 941–955. https://doi.org/10.1002/esp.4053

Phuong, J., Bandaragoda, C., Istanbulluoglu, E., Beveridge, C., Strauch, R., Setiawan, L., & Mooney, S. D. (2019). Automated retrieval, preprocessing, and visualization of gridded hydrometeorology data products for spatial-temporal exploratory analysis and intercomparison. *Environmental Modelling and Software*, *116*(January), 119–130. https://doi.org/10.1016/j.envsoft.2019.01.007

Piman, T., Cochrane, T. A., & Arias, M. E. (2016). Effect of Proposed Large Dams on Water Flows and Hydropower Production in the Sekong, Sesan and Srepok Rivers of the Mekong Basin. *River Research and Applications*, *32*(10), 2095–2108. https://doi.org/10.1002/rra.3045

Piman, Thanapon, Cochrane, T. A., Arias, M., Green, A., & Dat, N. D. (2013). Assessment of Flow Changes from Hydropower Development and Operations in Sekong, Sesan, and Srepok Rivers of the Mekong Basin. *Water Resources Planning and Management*, *139*, 723–732.

Piman, Thanapon, & Shrestha, M. (2017). *Case study on sediment in the Mekong River Basin : Current state and future trends*.

Prados, A. I., Carleton-hug, A., Gupta, P., Mehta, A., Blevins, B., Schmidt, C., … Kinsey, T. (2019). Impact of the ARSET Program on Use of Remote-Sensing Data. *International Journal of Geo-Information*, *8*(6), 261. https://doi.org/10.3390/ijgi8060261

Rahman, M., Dustegir, M., Karim, R., Haque, A., Nicholls, R. J., Darby, S. E., … Akter, M. (2018). Recent sediment flux to the Ganges-Brahmaputra-Meghna delta system. *Science of the Total Environment*, *643*, 1054–1064. https://doi.org/10.1016/j.scitotenv.2018.06.147

Rahman, M. M., Ahsan, Q., Haque, A., Rahman, M., Das, S., & Das, S. C. (2019, November 22). An innovative approach: Managing Brahmaputra-Jamuna River. *The Financial Express*. Retrieved from https://www.thefinancialexpress.com.bd/views/an-innovative-approach-1574432451

Randle, T. J., Bountry, J. A., Ritchie, A., & Wille, K. (2015). Large-scale dam removal on the Elwha River, Washington, USA: Erosion of reservoir sediment. *Geomorphology*, *246*, 709–728. https://doi.org/10.1016/j.geomorph.2014.12.045

Renard, K. G., Foster, G. R., Weesies, G. A., & Porter, J. P. (1991). RUSLE: Revised universal soil loss equation. *Journal of Soil and Water Conservation*, *46*(1), 30–33.

Rickenmann, D., & Recking, A. (2011). Evaluation of flow resistance in gravel-bed rivers through a large field data set. *Water Resources Research*, *47*(7). https://doi.org/10.1029/2010WR009793

Ritchie, J. C., Cooper, C. M., & Yongqing, J. (1987). Using landsat multispectral scanner data to estimate suspended sediments in Moon Lake, Mississippi. *Remote Sensing of Environment*, *23*(1), 65–81. https://doi.org/10.1016/0034-4257(87)90071-X

Salathé, E. P., Hamlet, A. F., Mass, C. F., Lee, S.-Y., Stumbaugh, M., & Steed, R. (2014). Estimates of Twenty-First-Century Flood Risk in the Pacific Northwest Based on Regional Climate Model Simulations. *Journal of Hydrometeorology*, *15*(5), 1881–1899. https://doi.org/10.1175/JHM-D-13-0137.1

Sandink, D., Simonovic, S. P., Schardong, A., & Srivastav, R. (2016). A decision support system for updating and incorporating climate change impacts into rainfall intensity-duration-frequency curves: Review of the stakeholder involvement process. *Environmental Modelling and Software*, *84*, 193–209. https://doi.org/10.1016/j.envsoft.2016.06.012

Sarker, M. H., Akter, J., & Ruknul, M. (2011). River bank protection measures in the Brahmaputra-Jamuna River: Bangladesh experience. *International Seminar on'River, Society and Sustainable Development, Dibrugarh University, India*, *121*(May), 1–14. https://doi.org/10.1002/2015JC011486.Received

Sarker, M. H., Huque, I., Alam, M., & Koudstaal, R. (2003). Rivers, chars and char dwellers of Bangladesh. *International Journal of River Basin Management*, *1*(1), 61–80. https://doi.org/10.1080/15715124.2003.9635193

Sarker, M. H., Thorne, C. R., Aktar, M. N., & Ferdous, M. R. (2014). Morpho-dynamics of the Brahmaputra-Jamuna River, Bangladesh. *Geomorphology*, *215*, 45–59. https://doi.org/10.1016/j.geomorph.2013.07.025

Sarkkula, J., Koponen, J., Lauri, H., & Virtanen, and M. (2010). MRC/ Information and knowledge management program detailed modelling support (DMS) project: Origin, fate and impacts of the Mekong sediments. *MRC/Information and Knowledge Management Program Detailed Modelling Support (DMS) Project: Origin, Fate and Impacts of the Mekong Sediments*. Vientiane, Laos: Mekong River Commission.

Schmitt, R. J. P., Bizzi, S., & Castelletti, A. (2016). Tracking multiple sediment cascades at the river network scale identifies controls and emerging patterns of sediment connectivity. *Water Resources Research*, *52*(5), 3941–3965. https://doi.org/10.1002/2015WR018097

Schmitt, R. J. P., Bizzi, S., Castelletti, A. F., & Kondolf, G. M. (2018a). Stochastic Modeling of Sediment Connectivity for Reconstructing Sand Fluxes and Origins in the Unmonitored Se Kong, Se San, and Sre Pok Tributaries of the Mekong River. *Journal of Geophysical Research: Earth Surface*, *123*, 2–25.

Schmitt, R. J. P., Bizzi, S., Castelletti, A. F., & Kondolf, G. M. (2018b). Stochastic Modeling of Sediment Connectivity for Reconstructing Sand Fluxes and Origins in the Unmonitored Se Kong, Se San, and Sre Pok Tributaries of the Mekong River. *Journal of Geophysical Research: Earth Surface*, *123*(1), 2–25. https://doi.org/10.1002/2016JF004105

Schmitt, R. J. P., Bizzi, S., Castelletti, A., & Kondolf, G. M. (2018c). Improved trade-offs of hydropower and sand connectivity by strategic dam planning in the Mekong. *Nature Sustainability*, *1*(2), 96–104. https://doi.org/10.1038/s41893-018-0022-3

Shajahan, A., & Reja, M. Y. (2012). Riverbank Erosion and Sustainable Planning Guidelines for Bangladesh with Emphasis on Padma River. *Journal of Habitat Engineering and Design*,

4(2), 145–156.

Shen, Z. Y., Gong, Y. W., Li, Y. H., Hong, Q., Xu, L., & Liu, R. M. (2009). A comparison of WEPP and SWAT for modeling soil erosion of the Zhangjiachong Watershed in the Three Gorges Reservoir Area. *Agricultural Water Management*, *96*(10), 1435–1442. https://doi.org/10.1016/j.agwat.2009.04.017

Skamarock, W. C., Klemp, J. B., Dudhi, J., Gill, D. O., Barker, D. M., Duda, M. G., … Powers, J. G. (2008). A Description of the Advanced Research WRF Version 3. *Technical Report*. Boulder, CO: University Corporation for Atmospheric Research. https://doi.org/10.5065/D6DZ069T

Small, C., Steckler, M., Seeber, L., Akhter, S. H., Goodbred, S., Mia, B., & Imam, B. (2009). Spectroscopy of sediments in the Ganges-Brahmaputra delta: Spectral effects of moisture, grain size and lithology. *Remote Sensing of Environment*, *113*(2), 342–361. https://doi.org/10.1016/j.rse.2008.10.009

Snyder, N. P., Nesheim, A. O., Wilkins, B. C., & Edmonds, D. A. (2013). Predicting grain size in gravel-bedded rivers using digital elevation models: Application to three maine watersheds. *Bulletin of the Geological Society of America*, *125*(1–2), 148–163. https://doi.org/10.1130/B30694.1

Soil Survey Staff, Natural Resources Conservation Service (NRCS), U. S. D. of A. (2016). Web soil survey. Washington, DC. Retrieved from http://websoilsurvey.nrcs.usda.gov/

Stark, C. P., & Passalacqua, P. (2014). A dynamical system model of eco-geomorphic response to landslide disturbance. *Water Resour. Res*, *50*, 8216–8226. https://doi.org/10.1002/2013WR014810

Strauch, R., Istanbulluoglu, E., & Riedel, J. (2019). A new approach to mapping landslide hazards: a probabilistic integration of empirical and process-based models in the North Cascades of Washington, U.S.A. *Natural Hazards and Earth System Sciences Discussions*, 1–29. https://doi.org/10.5194/nhess-2019-104

Strauch, R., Istanbulluoglu, E., Siddhartha Nudurupati, S., Bandaragoda, C., Gasparini, N. M., & Tucker, G. E. (2018). A hydroclimatological approach to predicting regional landslide probability using Landlab. *Earth Surface Dynamics*, *6*(1), 49–75. https://doi.org/10.5194/esurf-6-49-2018

Subramanian, V., & Ramanathan, A. L. (1996). Nature of Sediment Load in the Ganges-

Brahmaputra River Systems in India. In J. D. Milliman & J. D. Haq (Eds.), *Sea-Level Rise and Coastal Subsidence* (pp. 151–168). Dordrecht: Kluwer Academic Publishers. https://doi.org/10.1007/978-94-015-8719-8_8

Sudheer, K. P., Chaubey, I., & Garg, V. (2006). Lake water quality assessment from Landsat thematic mapper data using neural network: An approach to optimal band combination selection. *Journal of the American Water Resources Association*, *42*(6), 1683–1695. https://doi.org/10.1111/j.1752-1688.2006.tb06029.x

Suif, Z., Fleifle, A., Yoshimura, C., & Saavedra, O. (2016). Spatio-temporal patterns of soil erosion and suspended sediment dynamics in the Mekong River Basin. *Science of the Total Environment*, *568*, 933–945. https://doi.org/10.1016/j.scitotenv.2015.12.134

Syvitski, J. P. M. (2003). Supply and flux of sediment along hydrological pathways: Research for the 21st century. *Global and Planetary Change*, *39*(1–2), 1–11. https://doi.org/10.1016/S0921-8181(03)00008-0

Syvitski, J. P. M., & Kettner, A. (2011). Sediment flux and the anthropocene. *Philosophical Transactions of the Royal Society A: Mathematical, Physical and Engineering Sciences*, *369*(1938), 957–975. https://doi.org/10.1098/rsta.2010.0329

Syvitski, J. P. M., Vorosmarty, C. J., Kettner, A. J., & Green, P. (2005). Impact of Humans on the Flux of Terrestrial Sediment to the Global Coastal Ocean. *Science*, *308*(April), 376–381.

Thornton, P. E., & Running, S. W. (1999). An improved algorithm for estimating incident daily solar radiation from measurements of temperature, humidity, and precipitation. *Agricultural and Forest Meteorology*, *93*, 211–228. https://doi.org/10.1016/S0168-1923(98)00126-9

United Nations Office for Outer Space Affairs. (2018). European Global Navigation Satellite System and Copernicus: supporting the Sustainable Development Goals. Vienna. Retrieved from http://www.unoosa.org/res/oosadoc/data/documents/2018/stspace/stspace71_0_html/st_space_71E.pdf

United States Geological Survey (USGS). (2016). National Water Information System data available on the World Wide Web. Reston, VA: USGS. Retrieved from https://waterdata.usgs.gov/nwis/uv?site_no=12044900

United States Society on Dams. (2015). *Modeling Sediment Movement in Reservoirs*.

USGS. (2014). NLCD 2011 Land Cover (2011 edition). Sioux Falls, SD: U.S. Geological

Survey.

Vaughan, A. A., Belmont, P., Hawkins, C. P., & Wilcock, P. (2017). Near-Channel Versus Watershed Controls on Sediment Rating Curves. *Journal of Geophysical Research: Earth Surface*, *122*(10), 1901–1923. https://doi.org/10.1002/2016JF004180

Voinov, A., & Bousquet, F. (2010). Modelling with stakeholders. *Environmental Modelling and Software*, *25*(11), 1268–1281. https://doi.org/10.1016/j.envsoft.2010.03.007

Voinov, A., & Brown, E. J. (2008). Lessons for successful participatory watershed modeling : A perspective from modeling practitioners, *6*, 197–207. https://doi.org/10.1016/j.ecolmodel.2008.03.010

Volpe, V., Silvestri, S., & Marani, M. (2011). Remote sensing retrieval of suspended sediment concentration in shallow waters. *Remote Sensing of Environment*, *115*(1), 44–54. https://doi.org/10.1016/j.rse.2010.07.013

Vörösmarty, C. J., Meybeck, M., Fekete, B., Sharma, K., Green, P., & Syvitski, J. P. M. (2003). Anthropogenic sediment retention: Major global impact from registered river impoundments. *Global and Planetary Change*, *39*(1–2), 169–190. https://doi.org/10.1016/S0921-8181(03)00023-7

Wackerman, C., Hayden, A., & Jonik, J. (2017). Deriving spatial and temporal context for point measurements of suspended-sediment concentration using remote-sensing imagery in the Mekong Delta. *Continental Shelf Research*, *147*(September 2016), 231–245. https://doi.org/10.1016/j.csr.2017.08.007

Walling, D. E., & Fang, D. (2003). Recent trends in the suspended sediment loads of the world's rivers. *Global and Planetary Change*, *39*(1–2), 111–126. https://doi.org/10.1016/S0921-8181(03)00020-1

Walling, Desmond E. (2008). The changing sediment load of the Mekong River. AMBIO 37 (3): 150-157., *37*(3), 150–157.

Wang, W. C., & Dawdy, D. R. (2014). Flow resistance of gravel bed channels. *International Journal of Sediment Research*, *29*(1), 126–132. https://doi.org/10.1016/S1001-6279(14)60028-7

Warrick, J. A., Bountry, J. A., East, A. E., Magirl, C. S., Randle, T. J., Gelfenbaum, G., … Duda, J. J. (2015). Large-scale dam removal on the Elwha River, Washington, USA: Source-to-sink sediment budget and synthesis. *Geomorphology*, *246*, 729–750.

https://doi.org/10.1016/j.geomorph.2015.01.010

Warrick, J. A., Draut, A. E., McHenry, M. L., Miller, I. M., Magirl, C. S., Beirne, M. M., … Logan, J. B. (2011). Geomorphology of the Elwha River and its delta. *Coastal Habitats of the Elwha River—Biological and Physical Patterns and Processes Prior to Dam Removal*, 47–73. Retrieved from http://scholar.google.com/scholar?start=60&q=AND+stream+OR+river+%22dam+removal%22&hl=en&as_sdt=1,48&as_ylo=2011&as_yhi=2011#7

Water Land and Ecosystem (WLE). (2017). Dataset on the dams of the Irrawaddy, Mekong, Red and Salween River basins. Vientiane, Laos: CGIAR Research Program on Water, Land and Ecosystems—Greater Mekong. Retrieved from https://wle-mekong.cgiar.org/maps/.

Wei, X., Sauvage, S., Le, T. P. Q., Ouillon, S., Orange, D., Vinh, V. D., & Sanchez-Perez, J.-M. (2019). A Modeling Approach to Diagnose the Impacts of Global Changes on Discharge and Suspended Sediment Concentration within the Red River Basin. *Water*, *11*(5), 958. https://doi.org/10.3390/w11050958

Wigmosta, M. S., Vail, L. W., & Lettenmaier, D. P. (1994). A distributed hydrology-vegetation model for complex terrain. *Water Resources Research*. https://doi.org/10.1029/94WR00436

Wilcock, P. R. (1997). The components of fractional transport rate. *Water Resources Research*, *33*(1), 247–258. https://doi.org/10.1029/96WR02666

Wilcock, P. R., & Crowe, J. C. (2003). Surface-based Transport Model for Mixed-Size Sediment. *Journal of Hydraulic Engineering*, *129*(2), 120–128. https://doi.org/10.1061/?ASCE?0733-9429?2003?129:2?120? CE

Wilcock, P. R., & Kenworthy, S. T. (2002). A two-fraction model for the transport of sand/gravel mixtures. *Water Resources Research*, *38*(10), 12-1-12–12. https://doi.org/10.1029/2001WR000684

Wild, T., & Loucks, D. P. (2014). Managing flow, sediment, and hydropower regimes in the Sre Pok, Se San, and Se Kong Rivers of the Mekong basin. *Water Resour. Res.*, *50*, 5141–5157. https://doi.org/10.1002/2014WR015457

Wischmeier, W. H., & Smith, D. D. (1978). *Predicting rainfall erosion losses: A guide to conservation planning. U.S. Department of Agriculture, Agriculture Handbook number 537*. Washington DC: U.S. Government Printing Office.

Wohl, E., Bledsoe, B. P., Jacobson, R. B., Poff, N. L., Rathburn, S. L., Walters, D. M., &

Wilcox, A. C. (2015). The natural sediment regime in rivers: Broadening the foundation for ecosystem management. *BioScience*, *65*(4), 358–371. https://doi.org/10.1093/biosci/biv002

Xu, J., & Yan, Y. (2010). Effect of reservoir construction on suspended sediment load in a large river system: thresholds and complex response. *Earth Surface Processes and Landforms*, *35*(14), 1666–1673. https://doi.org/10.1002/esp.2006

Xu, T., Ma, T., Zhou, C., & Zhou, Y. (2014). Characterizing Spatio-Temporal Dynamics of Urbanization in China Using Time Series of DMSP/OLS Night Light Data. *Remote Sensing*, *6*(8), 7708–7731. https://doi.org/10.3390/rs6087708

Yao, X., Li, G., Xia, J., Ben, J., Cao, Q., Zhao, L., … Zhu, D. (2020). Enabling the big earth observation data via cloud computing and DGGS: Opportunities and challenges. *Remote Sensing*, *12*(1), 1–15. https://doi.org/10.3390/RS12010062

Yepez, S., Laraque, A., Martinez, J. M., De Sa, J., Carrera, J. M., Castellanos, B., … Lopez, J. L. (2018). Retrieval of suspended sediment concentrations using Landsat-8 OLI satellite images in the Orinoco River (Venezuela). *Comptes Rendus - Geoscience*, *350*(1–2), 20–30. https://doi.org/10.1016/j.crte.2017.08.004

Zarfl, C., Lumsdon, A. E., & Tockner, K. (2015). A global boom in hydropower dam construction. *Aquatic Sciences*, (77), 161–170. https://doi.org/10.1007/s00027-014-0377-0

Zhang, M., Dong, Q., Cui, T., Xue, C., & Zhang, S. (2014). Suspended sediment monitoring and assessment for Yellow River estuary from Landsat TM and ETM+ imagery. *Remote Sensing of Environment*, *146*, 136–147. https://doi.org/10.1016/j.rse.2013.09.033